

Two-Step Organo-Modification of Layered Silicates

MASTER THESIS

by

Rainer Puchleitner, BSc

Chair of Chemistry of Polymeric Materials Montanuniversität Leoben



Thesis Supervisor: Ass.Prof. Dipl.-Chem. Dr.rer.nat. Gisbert Rieß

Academic Advisor: Univ.-Prof. Mag.rer.nat. Dr.techn. Wolfgang Kern


Leoben, September 2011

Eidesstattliche Erklärung

Ich erkläre an Eides statt, dass ich diese Arbeit selbstständig verfasst, andere als die angegebenen Quellen und Hilfsmittel nicht benutzt und mich auch sonst keiner unerlaubten Hilfsmittel bedient habe.

20.08.2011

Datum



Unterschrift

Danksagung

Zuerst möchte ich Herrn Prof. Wolfgang Kern danken, der diese Arbeit möglich gemacht hat, und meinem Betreuer Herrn Dr. Gisbert Rieß, der mit stets mit Rat und Tat zur Seite gestanden ist. Darüber hinaus gilt mein Dank allen Mitarbeiterinnen und Mitarbeitern des Instituts für Chemie der Kunststoffe, die mir bei vielen Fragestellungen und Problemen eine große Hilfe waren, sowie Herrn Dr. Günther Maier und dem Materials Center Leoben für das Ermöglichen von SAXS sowie SEM Messungen. Zuletzt möchte ich mich noch bei Frau DI Hannelore Mattausch bedanken, die mir in vielerlei Hinsicht eine große Hilfe und eine stetige Wegbegleiterin im Laufe dieser Arbeit war.

Abstract

In this work sodium montmorillonites have been modified with fatty acids (oleic acid, undecylenic acid) and with various quaternary ammonium salts (ODTAB, HDTAB, etc.), to achieve a hydrophobic material character, to facilitate an incorporation and distribution of the layered silicate as filler material in a polyolefin, and make the use of a compatibilizer obsolete. To achieve that, two different modification methods were used. The fatty acids have been bound by polar interactions of the acid's carboxylic group and the hydroxy groups on the surface of the montmorillonite. In parallel an ion exchange was conducted and the sodium ions located in the interlayer space were substituted by quaternary ammonium salts. The combination of both modification processes led to a change in the material character that has been investigated with various characterization methods. The amount as well as the thermal stability of the adsorbed and intercalated surfactant molecules has been determined with thermogravimetric analysis (TGA). To verify the presence of the fatty acids and the ammonium salts on the surface and the interlayer space of the montmorillonite, Fourier transform infrared spectroscopy (FTIR) was used. Small-angle X-ray scattering (SAXS) and transmission electron microscopy (TEM) as well as Scanning electron microscopy (SEM) were used to determine physical properties such as the increase of the basal spacing after the modification process.

Keywords: Exfoliation; Intercalation; Montmorillonite; Layered Silicate; Organo modification; Fatty acid; Hydrophobization;

Kurzfassung

In dieser Arbeit wurden verschiedene Montmorillonit Typen mit Fettsäuren (Ölsäure, Undecylensäure) sowie mit verschiedenen quaternären Ammoniumsalzen (ODTAB, HDTAB) modifiziert, um einen hydrophoben Materialcharakter zu erhalten. Diese Modifikation hatte den Zweck das Einmischen und Verteilen der Schichtsilikate als Füllstoff in Polyolefinen ohne den Einsatz von Compatibilizern zu ermöglichen. Die Fettsäuren wurden durch polare Wechselwirkung auf der Oberfläche des Montmorillonites gebunden. Parallel dazu wurde ein Ionen Austausch der Natrium Ionen gegen quaternäre Ammoniumsalze durchgeführt. Die Kombination dieser beiden Modifikationsprozesse führte zu einer Änderung des Materialcharakters und wurde mit verschiedenen Charakterisierungsmethoden untersucht. Die Menge sowie die thermische Stabilität der adsorbierten und interkalierten Tenside wurden mit Hilfe von thermogravimetrischer Analyse (TGA) bestimmt. Um die Präsenz der Fettsäuren auf der Oberfläche und der Ammoniumsalze im Zwischenschichtraum nachzuweisen, wurde Infrarot Spektroskopie (FTIR) angewandt. Small-angle X-Ray (SAXS) Messungen sowie Transmissionselektronenmikroskopie (TEM) und Sekundärelektronenmikroskopie (SEM) Messungen wurden angewandt, um physikalische Eigenschaften wie die Änderung des Zwischenschichtabstandes vor und nach der Modifikation zu bestimmen.

List of abbreviations

CEC	Cation exchange capacity
MMT	Montmorillonite
TETAB	Tetraethylammonium bromide
HTAB	Hexyltrimethylammonium bromide
DDTAB	Dodecyltrimethylammonium bromide
HDTAB	Hexadecyltrimethylammonium bromide
ODTAB	Octadecyltrimethylammonium bromide
UA	Oleic acid
OA	Undecylenic acid
FT/IR	Fourier transform infrared spectroscopy
SAXS	Small-angle X-ray scattering
SEM	Scanning Electron Microscope
TEM	Transmission Electron Microscope
TGA	Thermogravimetric analysis

INDEX

Danksagung	i
Abstract	iii
Kurzfassung	iv
List of abbreviations	v
INDEX	vi
1 Introduction	1
1.1 Introduction	1
1.2 Motivation.....	2
1.3 Objectives	3
2 Theoretical Background	4
2.1 Layered silicates.....	4
2.1.1 Bentonite	4
2.1.2 Chemical Structure	4
2.1.3 Ion exchange.....	6
2.2 FT/IR-Spectroscopy	7
2.2.1 Wavelength range of FT/IR-Spectroscopy	7
2.2.2 Physical basis of IR-Spectroscopy.....	8
2.2.3 Principle of the Fourier Transform IR Spectroscopic method	9
2.2.4 Measurement principle of the Fourier Transform IR Spectroscopic method.....	10
2.3 Thermogravimetric Analysis (TGA).....	10
2.3.1 Measurement Setup	11
2.3.2 Evaluation principle	12
2.4 Small-Angle X-Ray Scattering (SAXS):	13
2.4.1 Instrumentation.....	14
2.4.2 Measurement principle	14
2.5 Scanning Electron Microscope (SEM)	15
3 Experimental	18
3.1 Experimental design, setup and procedure.....	18
3.1.1 Experimental design	19
3.1.2 Experimental setup.....	20
3.1.3 Experimental procedure.....	21
3.2 Analysis devices.....	22
3.2.1 Thermogravimetric Analyzer (TGA)	22
3.2.2 FT/IR-Spectrometer.....	23
3.2.3 Small Angle X-Ray Analyzer.....	24

3.3	Substances	25
3.3.1	Milos	25
3.3.2	Cloisite	25
3.3.3	Tetraethylammonium bromide (TEAB).....	25
3.3.4	Hexyltrimethylammonium bromide (HTAB).....	26
3.3.5	Dodecyltrimethylammonium bromide (DDTAB)	26
3.3.6	Hexadecyltrimethylammonium bromide (HDTAB).....	27
3.3.7	Octadecyltrimethylammonium bromide (ODTAB)	27
3.3.8	Cis-octadec-9-enoic (Oleic Acid (OA)).....	28
3.3.9	Undec-10-enoic acid (Undecylenic acid (UA))	28
3.4	TGA Evaluation	29
3.4.1	Sodium Montmorillonite	29
3.4.2	Surfactants	32
3.4.3	Evaluation of the one-step modified samples.....	39
3.4.1	Evaluation of the two-step modified samples	47
3.5	IR-Evaluation.....	59
3.5.1	Unmodified silicates.....	60
3.5.2	Surfactants	60
3.5.3	Cloisite Samples.....	64
3.5.4	Milos Samples	66
3.6	SAXS-Evaluation.....	67
3.7	SEM-Evaluation.....	69
3.7.1	Cloisite-MMT	69
3.7.2	Cloisite_ODTAB/OA	71
3.8	TEM-Evaluation.....	73
4	Discussion.....	75
4.1	Results TGA.....	75
4.2	Results FT/IR	76
4.2.1	Band assignment.....	76
4.3	Conclusion	77
4.4	Outline.....	80
5	Figures	81
6	Literatur	82

1 Introduction

1.1 Introduction

Na⁺-Montmorillonite is a layered silicate which belongs to the group of the 2:1 phyllosilicates. Its widespread use ranges from the use as adsorbent for hazardous pollutants ([Hocine, Boufatit et al. 2004](#)) to medical applications such as modified Montmorillonite which are used as vectors for gene delivery ([Lin, Chen et al. 2006](#)). The most important application of layered silicates for polymer chemistry, however, is its incorporation as filler material in a polymeric matrix. Montmorillonite filler materials can have a great impact on material properties such as the conductivity of polyaniline composites ([Bober, Steiskal et al. 2010](#)) or polymer electrolytes ([Moreno, Ana et al. 2010](#)), barrier properties for reduced permeability ([Fox, Ambuken et al. 2010](#)) and applications as flame retardant ([Huang, Li et al. 2011](#)). The main application of organo-clays in polymer processing is their use as reinforcing and toughening agents ([Jiang, Zhang et al. 2007](#)). The clay's incorporation without a modification is difficult in many cases due to the polar material properties of montmorillonite. Compatibilizers such as maleic anhydride must be used to create an interface between polymeric matrix and filler material ([Gallego, García-López et al. 2010](#)). To avoid the use of compatibilizer, montmorillonite particles can be organo-modified to exhibit apolar material properties by intercalation processes ([Avalos, Ortiz et al. 2009](#)) or by an in-situ polymerization ([Ma, Xu et al. 2003](#)).

Generally, as the name implies, layered silicates are ordered in multiple layers with varying distances.

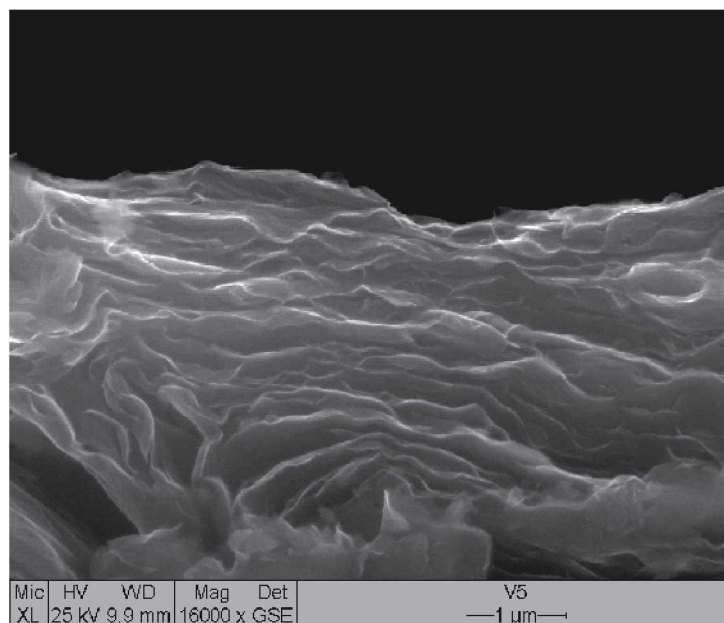


Fig.1.1: Densely packed layers of Milos montmorillonite (Provided by the Lehrstuhl für Aufbereitung und Veredlung, MUL © 2010)

To achieve a nano scaling character of the montmorillonite particles, a so called exfoliation process is necessary which simply means a separation of the densely packed layers by slipping from each other.

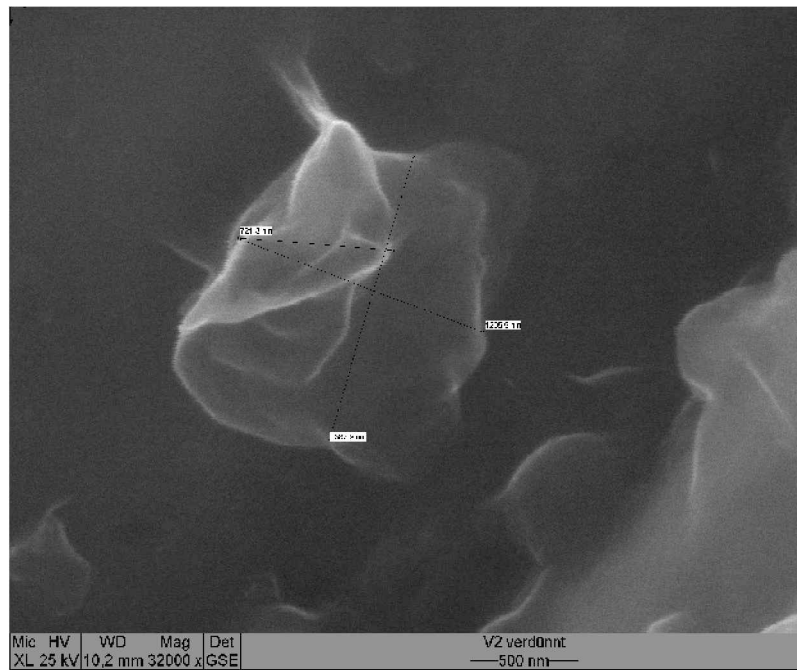


Fig. 1.2: Exfoliated Milos montmorillonite lamella (Provided by the Lehrstuhl für Aufbereitung und Veredlung, MUL © 2010)

There are several different ways to achieve or facilitate this process such as an in-situ polymerization of the clay material with a fitting monomer ([Choi and Chung 2004](#)). Another method is to increase the interlayer distance by inserting large spacer molecules in the interlayer space through an interlayer ion exchange ([Chu, Chiang et al. 2005](#); [Martin, Jimenez et al. 2009](#)).

1.2 Motivation

The modification of layered silicates and the manufacture of nano scaling filler materials as well as the intercalation process of quaternary ammonium salts has been the research objective of many studies. Also the adsorption of fatty acids on various surfaces among them montmorillonite, has been investigated extensively. Due to ([Khalil and Abdelhakim 2002](#)) pure fatty acids such as oleic acid do not penetrate the interlayer space of montmorillonite, but are adsorbed by hydrogen bonding on its surface. This suggests an investigation of a of both modification processes: an ion exchange with quaternary ammonium salts in parallel with a coating of the surface with fatty acids.

1.3 Objectives

In this work different goals have been pursued. The main target was to achieve a hydrophobization of an inorganic hydrophilic filler material (Sodium Montmorillonite), to obtain a material that can be incorporated and easily dispersed in a polyolefin without a compatibilizer for facilitated processing. Two different modification mechanisms were used to receive an “organo-clay” with hydrophobic material properties.

The second goal was to achieve a successful intercalation or even exfoliation of the layered silicate. Through an interlayer cation exchange different alkyl ammonium salts were inserted in the interlayer space of the montmorillonite and formed multilayer structures. Thereby the gallery spacing was altered, and a separation of the silicate layers was facilitated.

2 Theoretical Background

2.1 Layered silicates

Layered silicates are natural minerals and are the largest class of rock forming minerals. Silica and silicates by far constitute the largest part of the earth's crust and mantle and are a very important raw material in various industrial processes and products. They are also of great interest in applied science because of their application in medicine, pharmacy and - most notably for this work - the polymer processing industry.

2.1.1 Bentonite

Rock materials which contain a high percentage of montmorillonite are termed bentonite. These are most commonly formed by the in-situ alteration of volcanic ash or less common by the hydrothermal alteration of volcanic ash, ([Koo 2006](#)) and are therefore most commonly found in volcanic active regions. Bentonites have a micaceous habit and facile cleavage, high birefringence and a texture inherited from the volcanic ash ([Grim 1978](#)). There are different sorts of bentonite such as sodium, potassium, calcium or aluminum bentonite depending on the dominating element in the material. For industrial applications, especially the fabrication of organo-clays in the polymer industry, only calcium and sodium bentonites are of great importance. The largest and most important montmorillonite deposits are in the United States and South America. Calcium bentonite deposits are more common than sodium bentonite deposits and can be found in many countries in Europe and the United States ([Domínguez 2003](#)).

2.1.2 Chemical Structure

Montmorillonite named after Montmorillon in France, was first discovered in 1857 and is the main component of Bentonite. It is a 2:1 clay, meaning that it is built up by two silica tetrahedral layers interconnected by one alumina octahedral sheet. The general chemical formula for montmorillonite is $(\text{Na,Ca})_{0.33}(\text{Al,Mg})_2(\text{Si}_4\text{O}_{10})(\text{OH})_2 \cdot n\text{H}_2\text{O}$. Its structure is shown in Fig. 2.1.

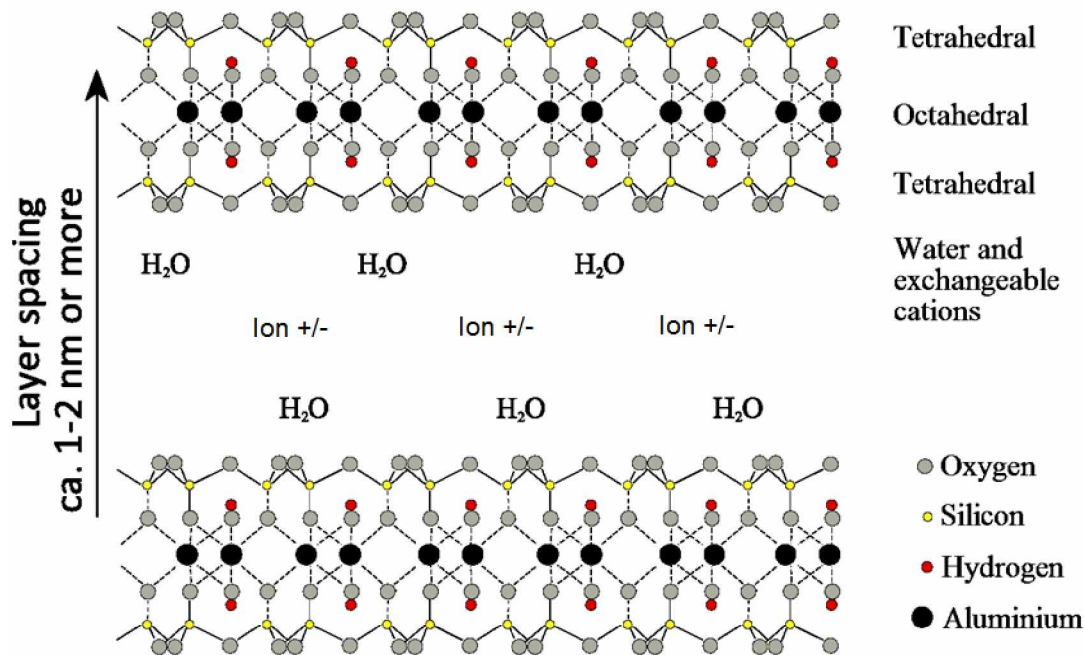


Fig. 2.1: Chemical structure of montmorillonite (9)

Naturally occurring clays exhibit isomorphous substitution of specific elements in the crystal structure of the montmorillonite. These substitutions can occur both in the tetrahedral and the octahedral layer. Iron or aluminum may replace silicon in the tetrahedral layer and other metals such as Mg, Cr, Zn or Li may substitute aluminum in the octahedral layer. As a result of the replacement of an atom with a higher valence by that of a lower valence a negative charge on the clay layers is created which must be balanced by a corresponding positive charge. This positive charge is contributed by interlayer cations. Those cations are located in the gallery or interlayer space and ensure a balanced clay (Kickelbick 2007).

The interlayer cations, which are present due to the substitution of Si^{4+} for the cations with lower valence like Al^{3+} , lead to a decreased electrostatic bonding of the crystal formations. In an aqueous surrounding or another hydrophilic substance, a hydration of the interlayer cations occurs, and the interlayer space swells. The volume increase can be up to 200% of the original volume. As a result of that the swelling of the montmorillonite can even lead to a fragmentation of the whole crystal in individual layers (Petzold 1991). This process is also called exfoliation, which means that the single fragments or platelets of the crystal are at least 7 nm apart and can be seen as independent fragments.

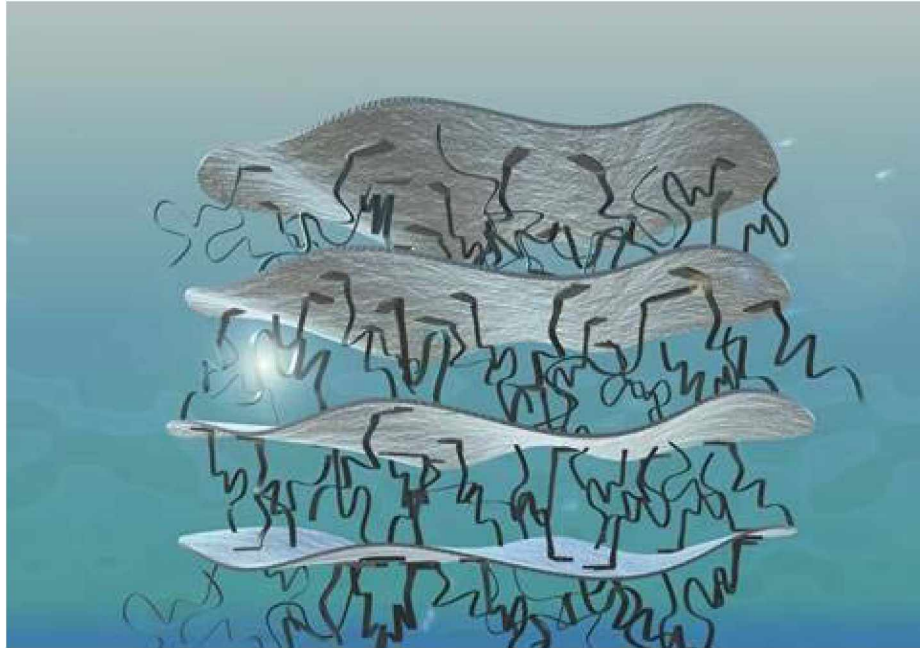


Fig. 2.2: Schematic figure of an exfoliated nano clay material in a polymeric matrix (10)

2.1.3 Ion exchange

One of the most important properties of layered silicates is the capability to perform ion exchange. An ion exchange is a hydrochemical process where ions from a solvent are incorporated in a sorbent and the equivalent amount of ions is released. If those ions are positively charged it is considered to be a cation exchange, if the ions are negatively charged an anion exchange.

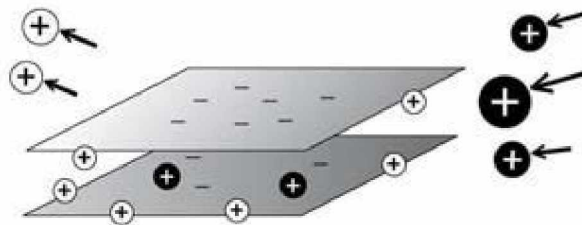


Fig. 2.3: Schematic figure of an ion exchange process (11)

The ion exchange is completely reversible and the extent of this process strongly depends on the properties of the involved materials. The cation exchange capacity (CEC) states the amount of exchangeable cations of a material and is defined as the maximum quantity of

cations, at a given pH-value, that are available for an exchange. The CEC is expressed as milliequivalent of hydrogen per 100 g (meq+/100g) and are approximately at 70-100 meq+/100g at a pH of 7 for montmorillonite. Formally the equivalent is defined as the amount of a specific substance that will react or supply one mole of hydrogen ions.

2.2 FT/IR-Spectroscopy

Fourier transform infrared spectroscopy (FT/IR) is an optical-physical method for recording absorption spectra of chemical compounds in the infrared spectral region. It is a very powerful tool for identification and characterization of polymers and their structure and therefore one of the most used tools for the study of polymers. It combines the advantages of a rapid and sensitive sampling technique with an easy operation of the equipment ([Koenig 1999](#)).

2.2.1 Wavelength range of FT/IR-Spectroscopy

Due to its historical development the wavelength is usually not stated in infrared spectroscopy. Instead the wavenumber is used, which is defined as the reciprocal wavelength (cm^{-1}) and states the number of wavelengths per unit distance ($1 / \lambda$ where λ is the wavelength). Beyond that, this unit also has the advantage of being linear with energy. From a spectroscopic point of view three different wavelength-, wavenumber ranges respectively, can be divided. The near-IR range (NIR, wavenumber 12800-3333 cm^{-1}) the far-IR range (FIR, 33-333 cm^{-1}) and the mid-infrared range (MIR, 3333-333 cm^{-1}).

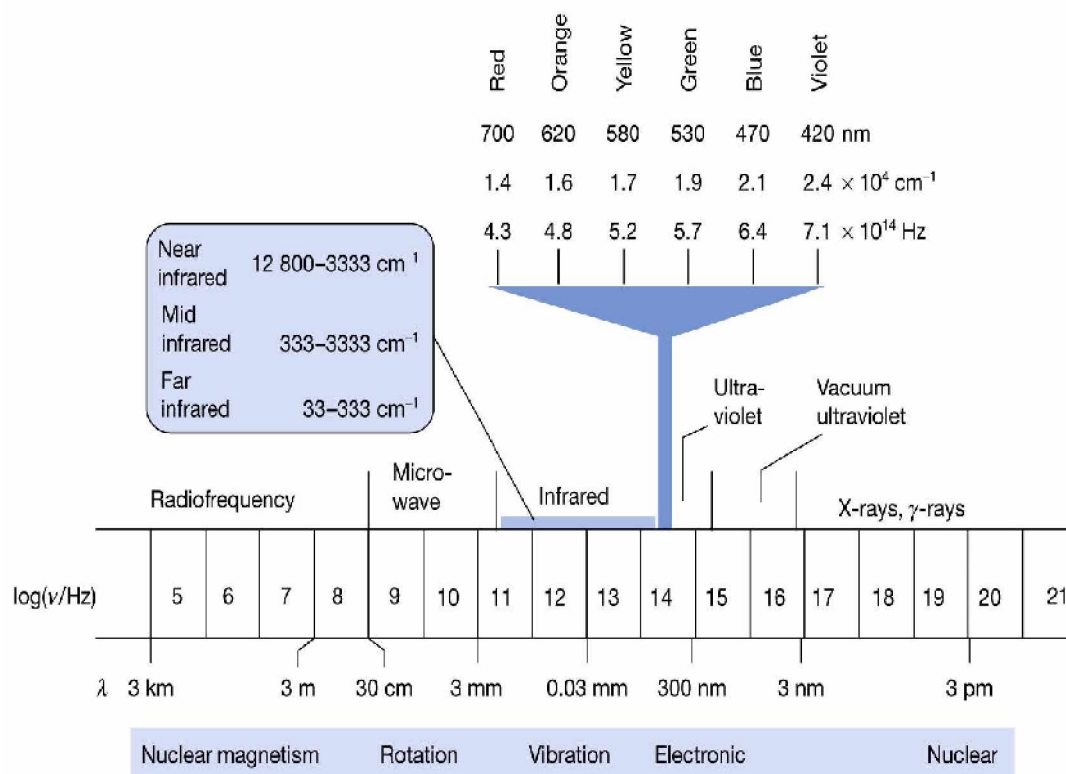


Fig. 2.4: Electromagnetic spectrum with a special marking of the three infrared ranges (1)

The infrared spectroscopy in the mid-infrared range is used in the chemical analysis as an easily accessible method, to determine the presence and concentration respectively of organic infrared active substances and their functional groups.

2.2.2 Physical basis of IR-Spectroscopy

Substances or molecules exhibiting an electromagnetic dipole and therefore an electric dipole moment absorb electromagnetic waves at a specific wavenumber. Such molecules are referred to as “infrared active” for their absorption properties in the infrared range. The interactions of electromagnetic waves with dipoles in molecules can be associated with vibrations and rotations, due to the relative movement of the atoms in a molecule to each other. A diatomic molecule would exhibit only the compression and stretching of its bond and that would therefore account for one degree of vibrational freedom. Polyatomic molecules have $3N$ degrees of freedom whereby N represents the amount of atoms present in the molecule. The different vibration modes of molecules (in total $3N-6$) are pictured in Fig. 2.6 (Koenig 1999).

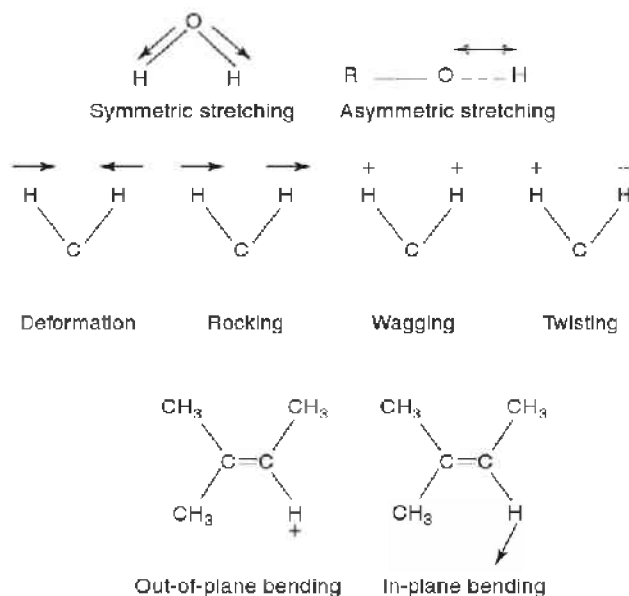


Fig. 2.5: Examples for different vibration modes(2)

2.2.3 Principle of the Fourier Transform IR Spectroscopic method

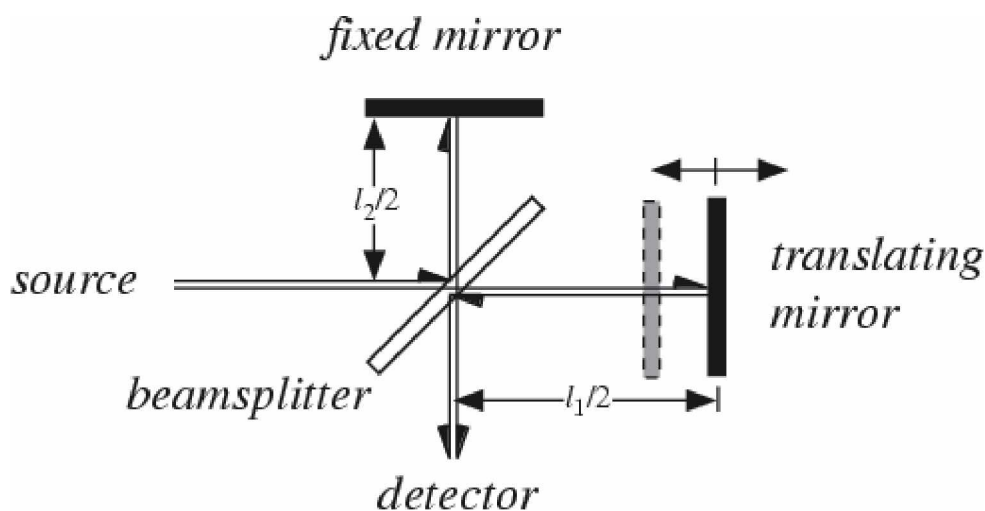


Fig. 2.5: Schematic figure of the basic parts of a Michelson Interferometer(3)

A Michelson interferometer, pictured in Fig. 2.5, is the basic module of a FT/IR-spectrometer. It consists of two perpendicular arms of which one contains a stationary mirror and the other one a movable highly polished mirror. The arms are bisected by a beam splitter which divides the beam by partial reflection and transmission (Paus 2007). After being reflected from their respective mirror the beams are recombined and reflected to the detector. Depending on the difference of the length of the optical path constructive or destructive interference can be observed. Constructive interference occurs when the two paths differ by a whole number of wavelengths and results in a strong signal at the detector. When the paths differ by one and a half wavelengths, destructive interference occurs and only a weak signal at the detector

can be monitored([Saptari 2004](#)). To obtain an interferogram, the spectrometer generates the spectrum of its source radiation by modulating the radiation in the time domain through interference. So the interferogram is a modulated radiation signal as a function of the displacement of the moving mirror. This analog signal is recorded at a photo detector and transformed to a digital signal. To receive the actual spectrum from the digital raw data the application of a mathematical algorithm is needed. The digital data is Fourier transformed using the fast Fourier transform algorithm and thus the spectrum is obtained ([Hatakeyama 1994](#)).

2.2.4 Measurement principle of the Fourier Transform IR Spectroscopic method

Infrared spectra can be pictured in form of absorption-or transmission spectra, while generally the depiction in form of the transmission spectrum is used. The transmission spectra show amplitudes due to the low transparency of the test substance against infrared radiation of specific wavelengths. In case of a transmission spectrum these amplitudes, so called peaks, contribute negative maxima on the vertical axis, while in an absorption spectrum positive peaks are shown.

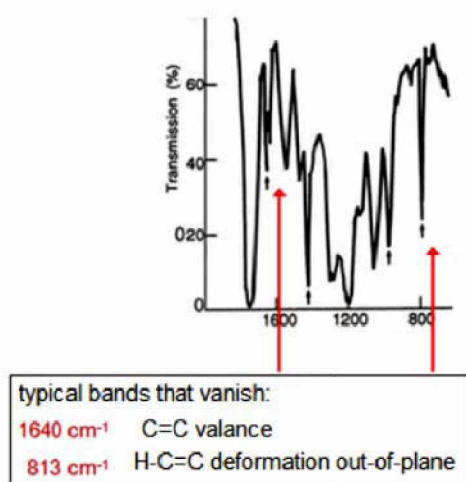


Fig. 2.6: Example for a typical infrared spectrum of an organic compound(7)

2.3 Thermogravimetric Analysis (TGA)

The thermogravimetric analysis is a method used to examine the mass change of a sample as a function of the temperature. It is a method that requires a high degree of precision in the measurement of the weight, temperature and the temperature change. Various thermal induced processes can be investigated with TGA: desorption, absorption, sublimation, vaporization, oxidation, reduction and decomposition. It is an appropriate method to investigate and characterize thermal decomposition and degradation of polymeric materials

under various conditions. Due to the multitude of influencing factors TGA curves are not to be seen as fingerprint curves and strongly depend on the experimental parameters such as atmospheric condition in the sample chamber, pressure in the sample chamber, sample mass volume and shape, sample holder setup and the scanning ([Hatakeyama 1994](#)).

2.3.1 Measurement Setup

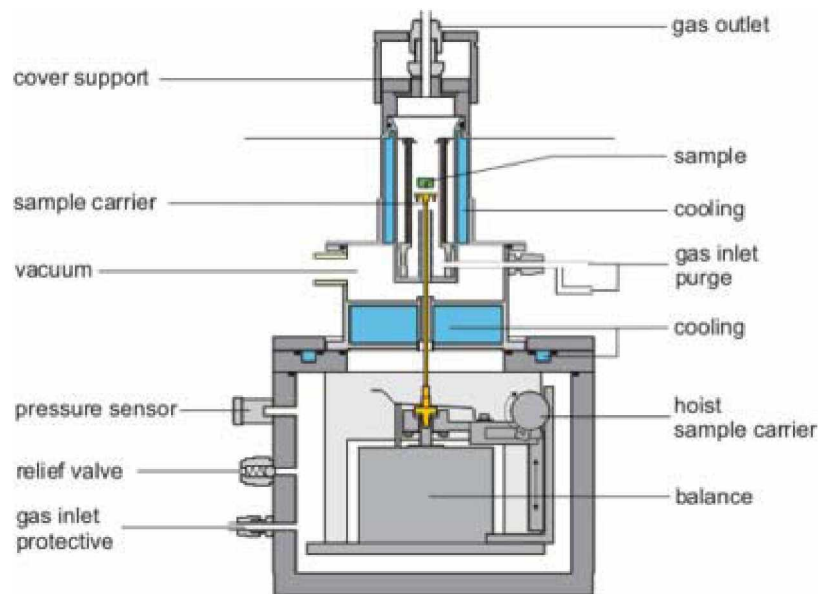


Fig. 2.7: General structure of a TGA device (8)

A TGA analyzer basically consists of a high-precision balance with a sample holder, usually in form of a crucible. The weight changes occurring during the measurements are electromagnetically or electromechanically compensated by the balance. That compensation signal determines the mass of the sample as a function of the temperature and the time. Various designs for the microbalance and the crucible are available. The microbalance can be designed as beam, cantilever, spring or torsion wire. The shape and the material of the crucible can also affect the measurements. To inhibit any reactions between the crucible and the sample, the crucibles are usually made from platinum, quartz or aluminum, but there are also other materials available for special purposes such as ceramics. The crucible must transfer the energy uniformly to the sample. Due to that the heat conduction and of course the thermal stability of the crucible material, at least 100°K higher than the program temperature, are of importance. The sample holder is placed in the furnace. In order to achieve a uniform hot zone many different configurations of the furnace are available to minimize the temperature gradient in horizontal, vertical and radial direction. Those gradients can have a strong influence on the atmosphere in the furnace chamber and subsequently on the heat flow in the crucible and the sample ([Hatakeyama 1994](#)).

2.3.2 Evaluation principle

The mass change can be determined absolute as a loss of absolute weight in [mg] or as a percentage of the original weight of the sample. In this work the latter was chosen for easy comparison between the samples. The evaluation principle shown in Fig. 2.8 was chosen due to the possibility to differentiate exactly between various weight loss steps that occur closely one after another.

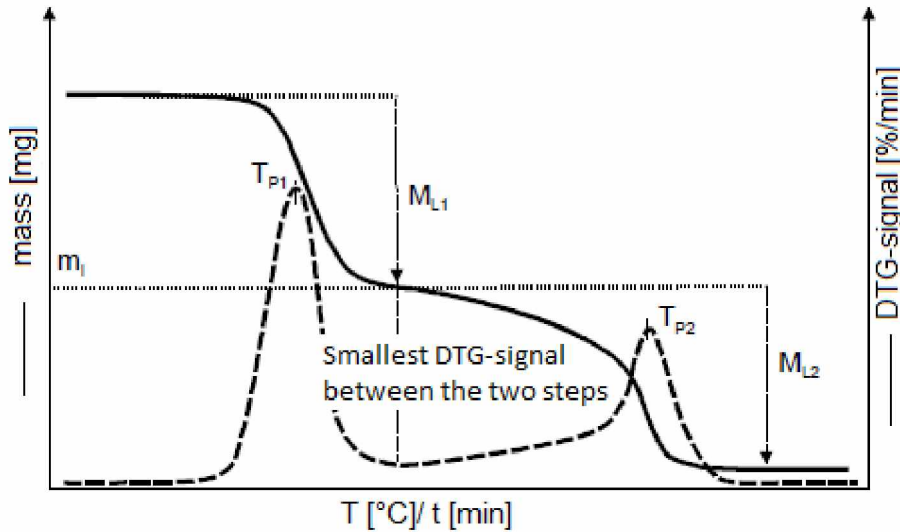


Fig. 2.8: Evaluation principle of two mass loss steps with the DTG-signal(5)

- M_{L1}first mass loss
- M_{L2}second mass loss
- T_{P1}Peak temperature of the DTG-curve (M_{L1})
- T_{P2}Peak temperature of the DTG curve (M_{L2})

To differentiate between mass loss one and mass loss two the minimum of the DTG-curve between the two maxima is chosen. After this separation the isolated mass loss steps can be determined according to the principle in Fig. 2.9 and according to formula 2.1.

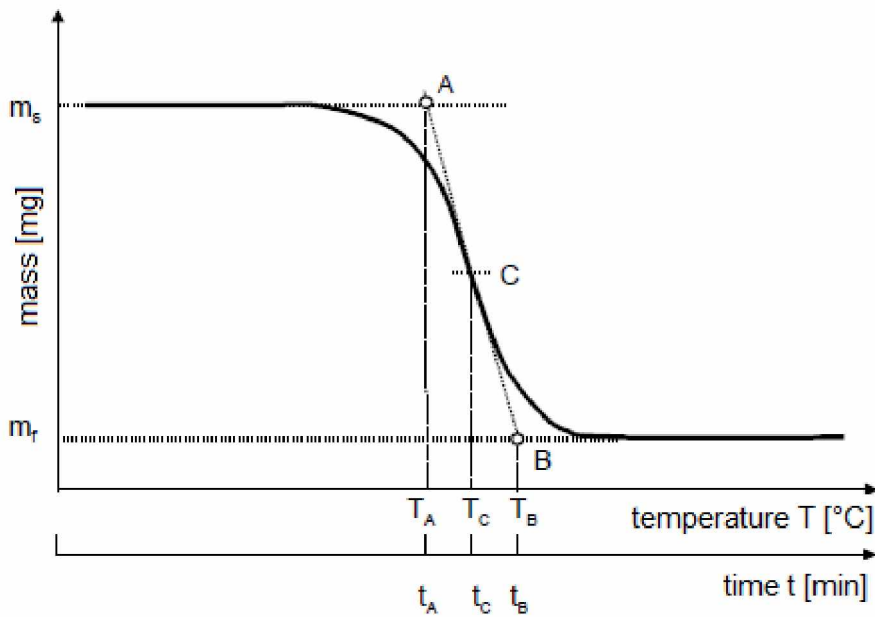


Fig. 2.9: Determination of the weight loss of a single mass loss step (5)

For.2.1:
$$M_L = \frac{m_S - m_F}{m_S} \cdot 100 [\%]$$

- A starting point
- B end point
- C center point
- T_A/t_A temperature/time at the start
- T_B/t_B temperature/time at the end
- T_C/t_C temperature/time at the central point
- m_S starting mass / mass before heating
- m_F end mass / mass after the heating process

2.4 Small-Angle X-Ray Scattering (SAXS):

Small-angle X-ray scattering is a technique which is used to characterize the structural properties of solid and fluid materials by elastic scattering of X-rays with a wavelength of 0,1-0,2 nm by a sample which exhibits inhomogeneities in the nanometer range. By probing inhomogeneities of the electron density of a material with more than one phase, information of various material parameters can be derived such as the shape or size of macromolecules, crystal orientations and the determination of nanoparticle pore and size distributions. Furthermore, the structures of colloids, liquid crystals, micro emulsions and, most important, polymers can be characterized. Provided that the particles have the same size properties like

their shape and structure or surface to volume ratio can be examined. The appearance of small-angle X-ray scattering is typical for particles with a diameter of approximately 50 nm.

2.4.1 Instrumentation

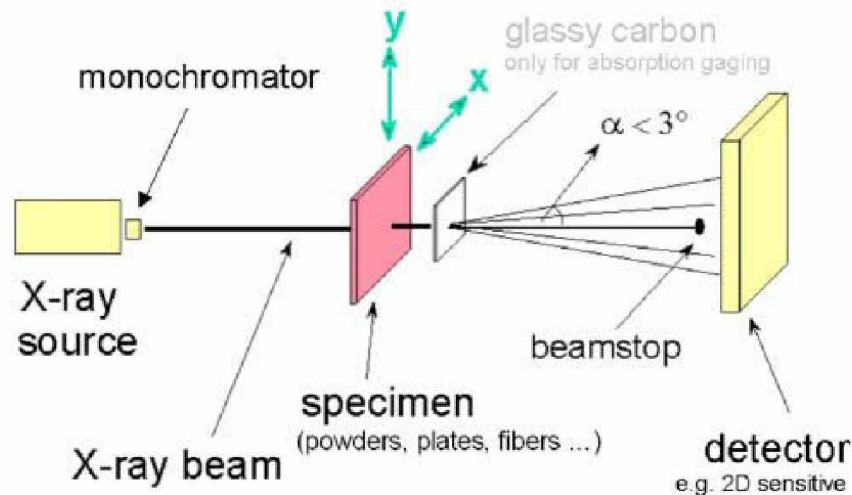


Fig. 2.10: Schematic figure of the composition of a SAXS apparatus(4)

In a Small-angle X-Ray scattering instrument a monochromatic beam of X-rays passes through a sample which is mounted in the instrument. The majority of the X-rays simply passes the sample without interactions but some of them are scattered. Those scattered X-rays form a scattering pattern which is recognized by a detector. This detector is most commonly located behind the sample perpendicular to the direction of the primary beam which initially hit the sample. To obtain the scattering pattern which contains the desired information of the sample properties, the weak scattered intensity must be separated from the strong main beam. To do that SAXS instruments are equipped with Point-collimation or Line-collimation instruments. These instruments produce light rays that are nearly parallel and spread much slower during their propagations compared to non collimated rays. The principle is either to direct the beam through pinholes to shape the X-ray beam to a small circular spot (Point-collimation) that hits the sample, or to confine the beam only in one dimension so that the beam profile is shaped to a narrow line (line collimation) on the sample surface.

2.4.2 Measurement principle

The evaluation of SAXS data is different for dilute monodisperse, polydisperse and concentrated systems. The dilute monodisperse system is the simplest case to observe. This system assumes a very dilute system of scatters without interparticle interaction. For such a

system the scattered intensity could be defined as $I(q) = 4\pi \int p(r) \frac{\sin(qr)}{qr} dr$ with

$$q = \left(\frac{4\pi}{\lambda}\right) \sin\left(\frac{\theta}{2}\right). \quad p(r) = \Delta \rho^2 (r) * r^2$$

which is the pair distance distribution function. The height of this value is proportional to the amount of scattered intensities that are found for one particle inside the interval or $r + dr$. This function correlates with the shape of the particles. For a symmetric function the particles can be assumed to have a spherical shape. The factor ρ in this formula is related to a density distribution of the particles ([Singh 2005](#)).

q Scattering vector

λ wavelength

r certain distance within a sample

$p(r)$ distance distribution function

2.5 Scanning Electron Microscope (SEM)

A Scanning Electron Microscope is an electron microscope that guides an electron beam in a raster scan pattern over the surface of a sample and uses interactions of the electrons and the sample surface to generate a micrograph of the object. That is how various properties, like the topography, composition and electrical conductivity of the sample, can be determined. There is a variety of signals that can be produced by the SEM including secondary electrons, backscattered electrons, characteristic X-rays, cathodoluminescence, the specimen current and transmitted electrons. Usually not all of these detectors are integrated in a SEM.

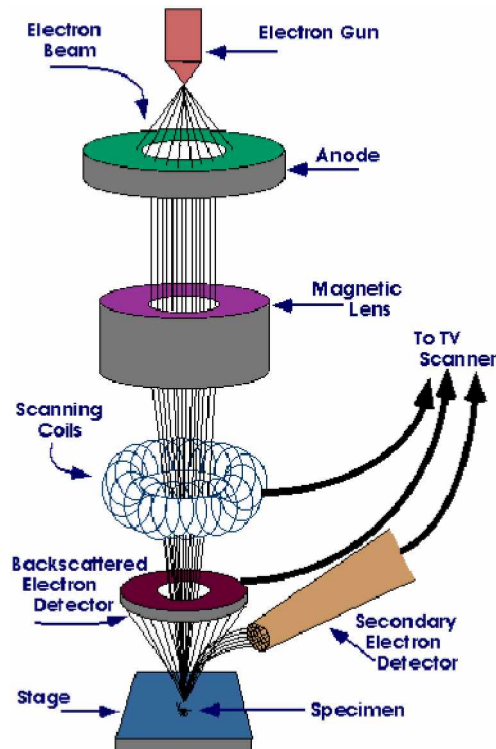


Fig. 2.11: Functional principle of a SEM(6)

Functional principle:

An average SEM uses an electron gun to emit the electron beam. This electron gun is usually fitted with a Tungsten filament cathode bent like a hairpin or a LaB₆ crystal due to its high heat resistance. This filament is heated to emit electrons, which are then accelerated in an electric field with 0.5-40 keV. Other devices use a field emission gun that operates with high voltage to generate a “tunnel effect” to generate electrons. It can be distinguished between the cold field emission where the tunnel effect is generated only by the applied voltage, and the thermal field emission where a Schottky-cathode is slightly heated to generate the electrons. A higher field emission can be generated through the thermally supported method. It generates higher radiation intensity, and therefore a better picture quality can be obtained.

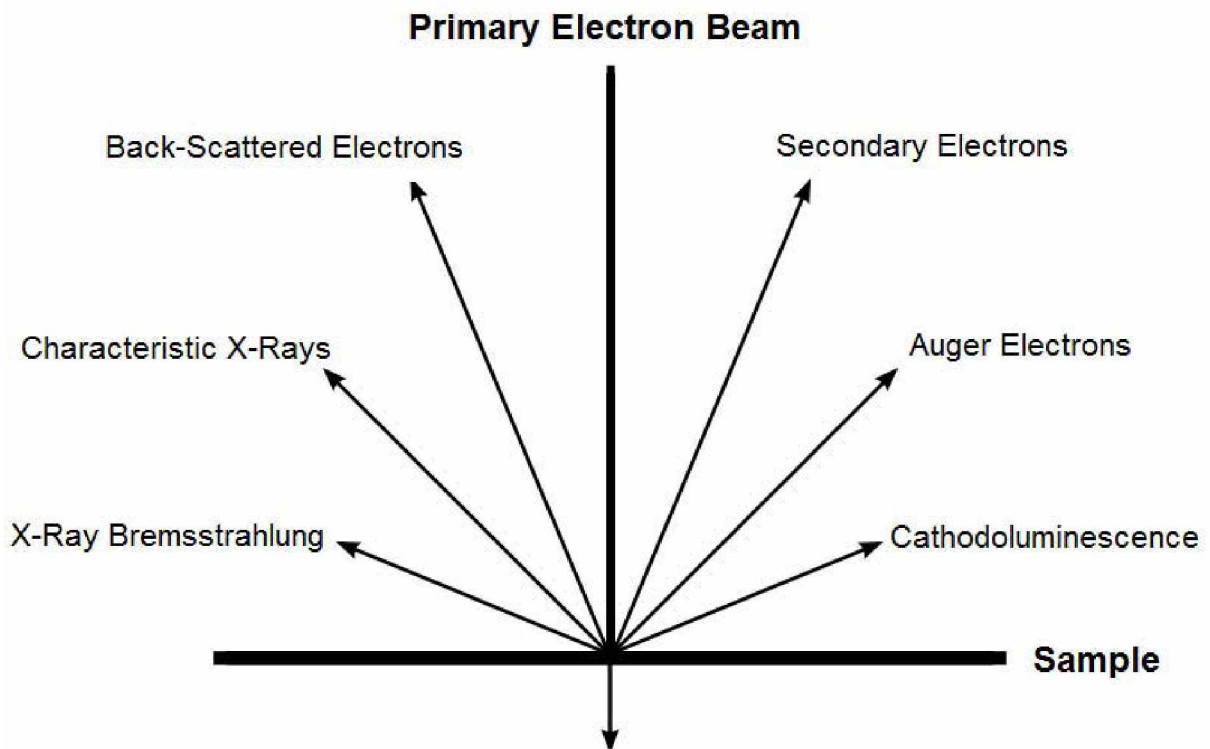


Fig. 2.12: Various detection modes of SEM

The SEM is based on the principle of scanning the sample surface in a specific pattern. The electron beam with an energy range between 0.5 to 40 keV is focused to a spot on the surface by a condenser lens and covers usually an area of 0.5-5 nm. Following the raster pattern the electron beam is guided over the sample surface and the resulting interactions are detected. The different detection modes are shown in Fig. 2.12.

3 Experimental

3.1 Experimental design, setup and procedure

Several different ammonium salts and fatty acids have been used to examine the influence of surfactants on the material properties of montmorillonite. The two different types of sodium montmorillonite were provided and preprocessed by “Lehrstuhl für Aufbereitung und Veredelung”.

The first step of the experimental design was the modification of the layered silicates with five different quaternary ammonium salts at 100% of the CEC of the montmorillonite to examine the intercalation and exfoliation behavior. The goal was to gain information on the influence of the different lengths of the alkyl tails on the material properties and especially the loading rate of the surfactants after the modification to choose two salts for further investigations. Those tests have been carried out according to the experimental setup described in chapter 3.1.2.

The second stage of the experimental design was the modification with two different surfactants, each added with 20% of the theoretical CEC of the montmorillonite. The surfactants were a combination of a fatty acid and an ammonium salt. For these tests the ammonium salts with the best intercalation properties according to the first series of test were chosen. The tests have been carried out according to the experimental setup described in 3.1.2.

To examine the modified layered silicates described above, various characterization methods have been used (TGA, FT/IR-Spectroscopy, SAXS-Measurements, SEM). In this way valuable insights in the physical and chemical processes of the material were obtained.

3.1.1 Experimental design

To examine the influence of quaternary ammonium salts on the properties of montmorillonite, experiments according to table Tab. 3.1 were carried out.

Tab. 3.1: Combinations of Cloisite-MMT with the cationic surfactants. (*Cloisite-MMT has 10% solid content)

	Cloisite* [g]	TEAB [g]	HTAB [g]	DDTAB [g]	HDTAB[g]	ODTAB [g]
Cloisite_TEAB	54,5	13,265	0	0	0	0
Cloisite_HDTAB	54,5	0	0	0	23	0
Cloisite_ODTAB	54,5	0	0	0	0	24,77
Cloisite_DDTAB	54,5	0	0	19,47	0	0
Cloisite_HTAB	54,5	0	14,16	0	0	0

To examine the influence of quaternary ammonium salts in combination with fatty acids on the spacing of montmorillonite, experiments according to Tab. 3.2 were carried out.

Tab. 3.2: Combinations of Milos-MMT and Cloisite-MMT with OA; UA; HDTAB and ODTAB (*Milos has a solid content of 5%; Cloisite has a solid content of 10%)

	Milos/Cloisite* [g]	OA [g]	UA [g]	HDTAB [g]	ODTAB [g]
Milos_HDTAB/UA	202		4,64	9,94	
Milos_ODTAB/UA	202		4,64		10,7
Milos_HDTAB/OA	202	7,11		9,94	
Milos_ODTAB/OA	202	7,11			10,7
Cloisite_HDTAB/UA	109		4,64	9,94	
Cloisite_ODTAB/UA	109		4,64		10,7
Cloisite_HDTAB/OA	109	7,11		9,94	
Cloisite_ODTAB/OA	109	7,11			10,7

3.1.2 Experimental setup

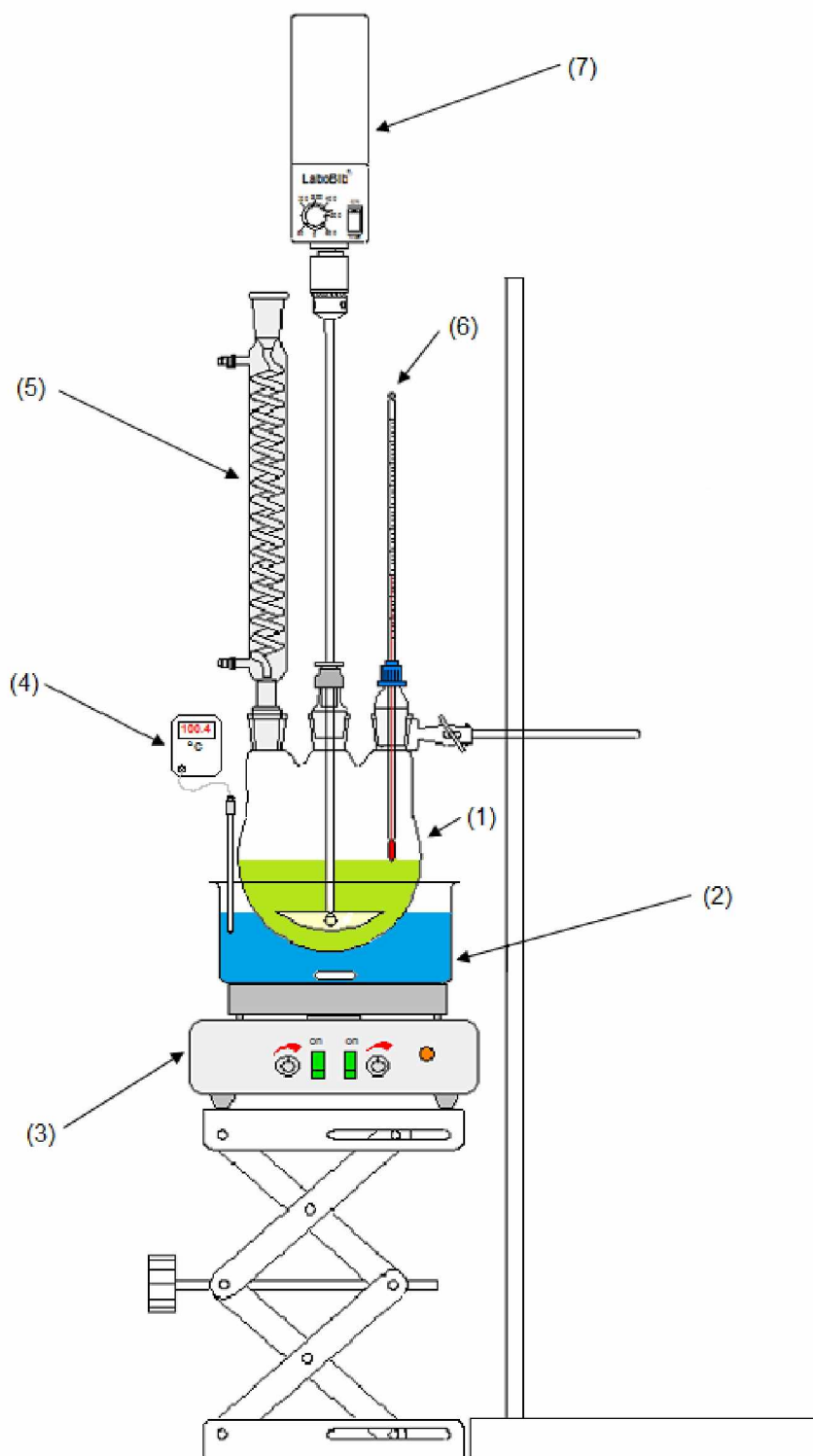


Fig. 3.1: Experimental setup used for the modification of the layered silicates.

For all of the montmorillonite ion exchange reactions the same experimental setup was used. The reaction vessel (1) was placed in a silicon oil bath (2) that was heated and stirred by a magnetic heater and stirrer (3) to provide a homogenous heat transition from the bath in the

vessel. The temperature of the bath was controlled by a thermocouple (4) that was placed in the oil bath. The reaction vessel was a three-necked flask to provide enough space for a KPG-driven stirrer, a thermometer and an attached reflux condenser (5). The thermometer (6) was needed to control the temperature inside the flask and to find a matching heating temperature for the oil bath. Due to the changing viscosity of the reaction mixture because of the swelling of the montmorillonite a rotating magnet did not provide the needed torque and through-mixing. This is why a KPG-driven PTFE-stirrer (7) was used. The temperature of 100°C of the reaction mixture caused the volatile solvent being condensed with an attached reflux condenser to counteract superheating.

3.1.3 Experimental procedure

Modification procedure with 100% CEC

The montmorillonite was provided as an aqueous, stable dispersion with 10% solid content for Cloisite. That solution was further diluted with distilled water and afterwards rigorously stirred with a disperser tool for 2 hours to undo any initial sedimentation, and to facilitate the subsequent intercalation. The dispersion was induced in a 1000mL flask with an attached reflux condenser and heated to 100°C. The intercalation agent with an amount of 100% of the cation exchange capacity was added to dispersion. This suspension was rigorously stirred for 3 hours at 100°C. Then the suspension was washed with an ethanol/water solution to cleanse the montmorillonite from any surfactant that was not bound or adsorbed and filtrated in a Büchner funnel.

Modification with 40% CEC:

The montmorillonite was provided as an aqueous, stable dispersion with 10% solid content for Cloisite and 5% for Milos. That solution was further diluted with distilled water, and afterwards rigorously stirred with a disperser tool for 2 hours to undo any initial sedimentation and to facilitate the subsequent exfoliation. The dispersion was induced in a 1000mL flask with an attached reflux condenser, and heated to 100°C. The first surfactant with an amount of 20% of the cation exchange capacity was added to dispersion. This suspension was rigorously stirred for 3 hours at 100°C. Then the second surfactant agent with an amount of 20% of the cation exchange capacity was added and the suspension was stirred for another 3 hours at 100°C. The suspension was cooled down to room temperature and left unchanged for 3 hours. Then the suspension was washed with an ethanol/water solution to cleanse the montmorillonite from any surfactant that was not bound or adsorbed and filtrated in a Büchner funnel.

3.2 Analysis devices

3.2.1 Thermogravimetric Analyzer (TGA)



Fig. 3.2: Perkin Elmer TGA 7 Thermogravimetric Analyzer

Specifications:

Balance Sensitivity: 0.1 μg

Balance Accuracy..... Better than 0.1%

Weighting precision: up to 10 ppm

Sample Capacity: up to 50 micro liters

Temperature Range: ambient to 1000°C

Heating and cooling rates:..... 0.1 to 200°C/min in 0.1°C increments

Cool down times:..... 1000°C to 50°C in less than 15 min.

Sample type: solids; liquids; powders; films; fibers

Atmosphere: static or dynamic including nitrogen,

..... Argon, carbon dioxide, air, oxygen

Reduced pressure: operation to 10^{-4} torr optional

Temperature sensor: chromel-alumel thermocouple

Cooling method: forced air cooling

3.2.2 FT/IR-Spectrometer



Fig. 3.3: FTIR-IR-Spectrometer, Spectrum One, Perkin-Elmer, Waltham, USA-Massachusetts(12)

Specifications:

PerkinElmer Spectrum One FT-IR spectrometer

Operation modes:in ratio, single-beam or interferogram mode

Data collection range:7800 to 370 cm^{-1} with a best resolution of 0.5 cm^{-1}

Detectors: DTGS (deuterated triglycine sulphate); LiTaO_3 (lithium tantalite);

3.2.3 Small Angle X-Ray Analyzer



Fig. 3.4: Bruker NanoSTAR (Bruker AXS, Karlsruhe, Germany) small angle X-ray scattering (SAXS) equipment

X-ray source: IS, Maximum power 0.03 kW

Flux density at sample 1.7×10^7 cps/mm²

Detector:

VANTEC-2000 TM

Patented MikroGap

technology detector, high spatial resolution with increased dynamic range

real time data collection and display

max. 2048 × 2048 pixel frame

14 × 14 cm active area

Resolution of the instrument:

Detector sample distance (variable) 270 mm
 q-min 0,04 (Å⁻¹)
 Particle size 150 (Å)

3.3 Substances

3.3.1 Milos

Solid Content: 10%
 CEC: 125 meq/100g
 Appearance: light brown compound
 Provided by the „Lehrstuhl für Aufbereitung und Veredlung, Montanuniversität Leoben“

3.3.2 Cloisite

Solid Content: 5%
 CEC: 125 meq/100g
 Appearance: dark brown compound
 Provided by the „Lehrstuhl für Aufbereitung und Veredlung, Montanuniversität Leoben“

3.3.3 Tetraethylammoniumbromide (TEAB)

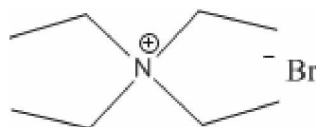


Fig. 3.5: Structural formula of TEAB

Chemical formula: (C₂H₅)₄NBr
 Molecular weight 210.6 g/mol
 Appearance at room temperature crystalline
 Color colorless

Melting point..... 285°C
Solubility in water at room temperature 2795 g/L

3.3.4 Hexyltrimethylammoniumbromide (HTAB)

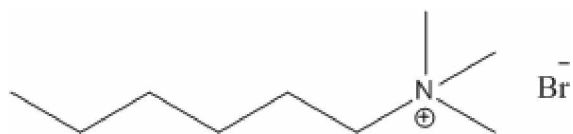


Fig. 3.6: Structural formula of HTAB

Chemical formula $C_9H_{22}N Br$
Molecular weight 224.18 g/mol
Appearance at room temperature crystalline
Color colorless
Melting point..... 185°C
Solubility in water rat room temperature unknown

3.3.5 Dodecyltrimethylammoniumbromide (DDTAB)

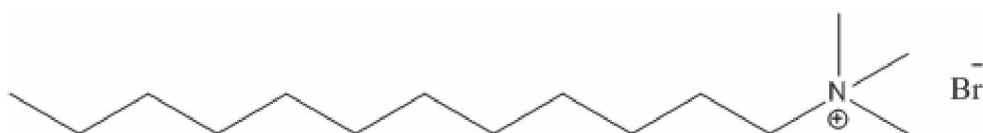


Fig. 3.7: Structural formula of DDTAB

Chemical formula $C_{15}H_{34}NBr$
Molecular weight 308.34 g/mol
Appearance at room temperature crystalline
Color colorless
Melting point..... 246°C
Solubility in water at room temperature 30.8 g/l

3.3.6 Hexadecyltrimethylammoniumbromide (HDTAB)

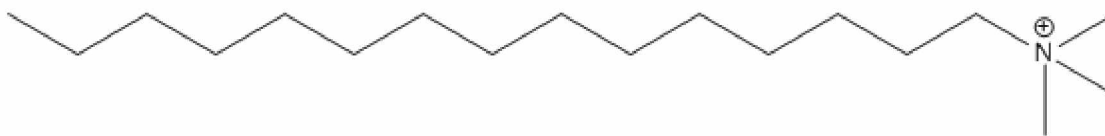


Fig. 3.8: Structural formula of HDTAB

Chemical formula:	$C_{19}H_{42}NBr$
Molecular weight	364.45 g/mol
Appearance at room temperature	crystalline
Color	colorless
Melting point.....	248 – 251 °C
Solubility in water at room temperature	36.4 g/l

3.3.7 Octadecyltrimethylammoniumbromide (ODTAB)

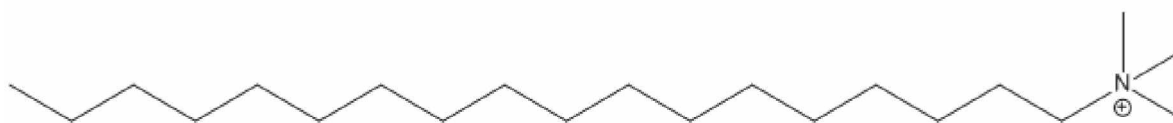


Fig. 3.9: Structural formula of OTTAB

Chemical Formula:	$C_{21}H_{46}N Br$
Molecular weight	392.5 g/mol
Appearance at room temperature	crystalline
Color	colorless
Melting point.....	250°C
Solubility in water at room temperature	unknown

3.3.8 Cis-octadec-9-enoic (Oleic Acid (OA))

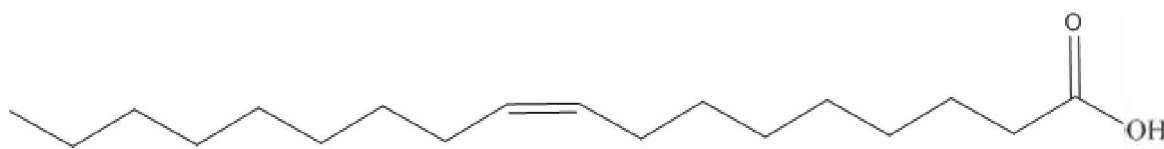


Fig. 3.10: Structural formula of oleic acid

Chemical formula:	$C_{18}H_{34}O_2$
Molecular weight	282.46 g/mol
Appearance at room temperature	liquid
Color	colorless
Melting point.....	17°C
Boiling point.....	360°C
Solubility in water at room temperature	insoluble in water

3.3.9 Undec-10-enoic acid (Undecylenic acid (UA))

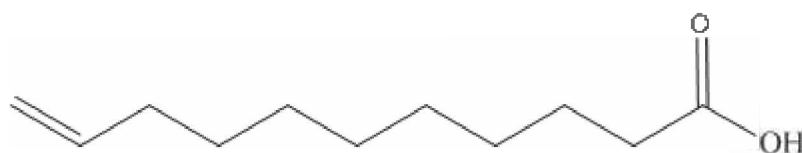


Fig. 3.11: Structural formula of undecylenic acid

Formula:	$C_{11}H_{20}O_2$
Molecular weight	182.27
Appearance at room temperature	solid
Color	colorless
Melting point.....	25-27°
Boiling point.....	275°C
Solubility in water at room temperature	0.74g/l

3.4 TGA Evaluation

To determine the exact amount of bound surfactant (quaternary ammonium salts and fatty acids) the modified layered silicate were subjected to thermal analysis. After the modification process the montmorillonite has been subjected to several washing and filtration procedures, to ensure that it had been cleansed from any unbound residues. After the filtration and cleaning process the montmorillonite was dried for several hours in a compartment dryer at 90°C to eliminate the remaining moisture. 15-20 mg of the dried silicate were used as sample for the thermogravimetric tests to derive information regarding the amount of interlayer water and in particular the amount of intercalated or adsorbed surfactant. In addition to the modified montmorillonite the raw silicate and the pure surfactant were tested to be able to assign the mass losses at specific temperatures to the specific surfactant. To verify a successful modification the alteration of the temperature curve from the unmodified to the modified montmorillonite was evaluated. To separate the decomposition temperatures of the surfactants within and on the clay the percentage of the weight loss and the derivative weight loss were examined.

In addition to the raw experimental data chapter 3.4 includes first results and assumptions regarding the effects of the modification process. For a better clarity these assumptions and results will be discussed in detail in chapter 4.1.

3.4.1 Sodium Montmorillonite

To determine the mass loss, in particular the organic mass loss, of the modified layered silicates it is necessary to know the mass loss curve of the unmodified montmorillonite. This is why both raw materials (Milos and Cloisite) were tested in their unmodified state. The mass loss of unmodified montmorillonite between ambient temperature and 900°C can be explained by three different effects. During the heating process below a temperature of 100°C silicate materials, especially montmorillonites, are known to undergo a weight loss caused by desorption of water ([Bray et. al. 1999](#)). Due to the drying step during the preprocessing and the sample preparation this desorption peak is of minor importance in the coming evaluation. The second process ranges up to a temperature ~360°C and is a dehydration process which has already been closely investigated by ([Koster van Groos et. al. 1984](#)). According to this work the water dehydrates in two stages. First the voluminous weakly bound water evaporates, then the water molecules which are strongly bound and located in the inner hydration shell evaporate as well. The exact amount of bound water depends on the interlayer cations and is characteristic of each type of montmorillonite. The third mass loss process is the dehydroxylation of the montmorillonite ([Bray et. al. 2000](#)). It starts at approximately 600°C. The structural OH groups of the octahedral layers form water molecules and evaporate. This is the last mass loss process that can be observed because of the temperature limit of the used TGA device of 900°C.

3.4.1.1 Cloisite

The unmodified montmorillonite had a solid content of 10% in its condition as received and was dried in a compartment dryer at 90°C until a constant weight had been reached. The solid material received that way was ground to dust with an agate mortar. The powder was weighed in. The sample weight used amounted to approximately 15 mg.

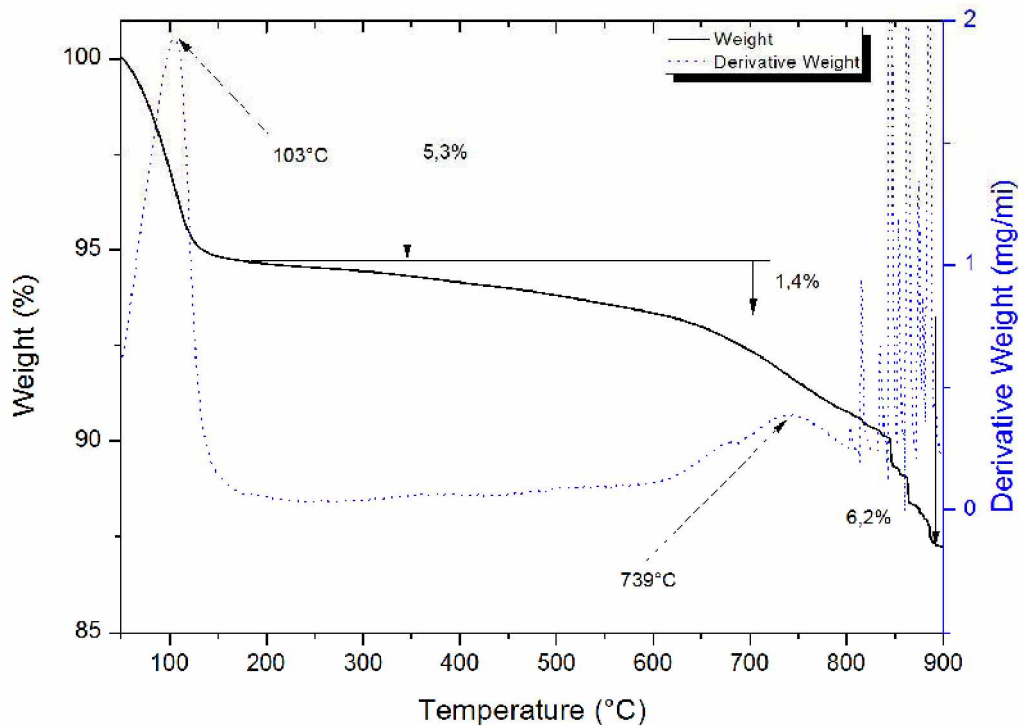


Fig. 3.12: Weight loss and derivative weight loss of the unmodified Cloisite bentonite

The mass loss of the Cloisite's type unmodified montmorillonite took place in three stages. The first mass loss could be observed between 90 and 191°C and had its maximum weight loss at 103°C. That rapid loss of weight is caused by a combination of dehydration and desorption of adsorbed water. The next area between 191 and 614°C shows a slight but constant decrease of weight and marks the end of the dehydration process. At approximately 600°C the dehydroxylation starts. The OH groups of the octahedral layers form water molecules and evaporate. This can be considered the structural degradation of the montmorillonite, and also marks the end of the measurement range.

3.4.1.2 Milos

For the sample preparation of the Milos montmorillonite the same procedure as for the Cloisitemontmorillonite was used. The drying of the silicate took somewhat longer because the solid content of the montmorillonite in its as-received condition was lower than that of the Cloisite montmorillonite suspension.

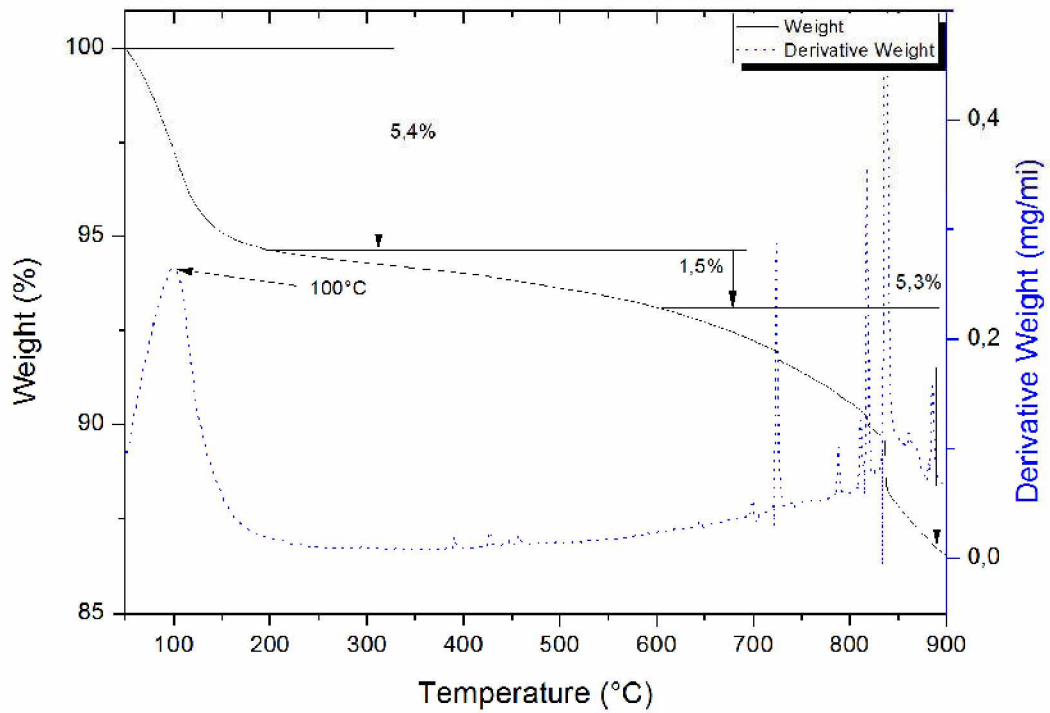


Fig. 3.13: Weight loss and derivative weight loss of the unmodified Milos bentonite

The shape of the mass loss curve of the Milos and Cloisite type is quite similar. The first weight loss also occurs between 90 and 200°C and is caused by dehydration and desorption of water molecules. This first weight loss step is followed by a constant weight loss up to approximately 600°C. After this threshold a more rapid weight loss can be observed due to dehydroxylation up to 900°C.

3.4.1.3 Comparison of Cloisite and Milos

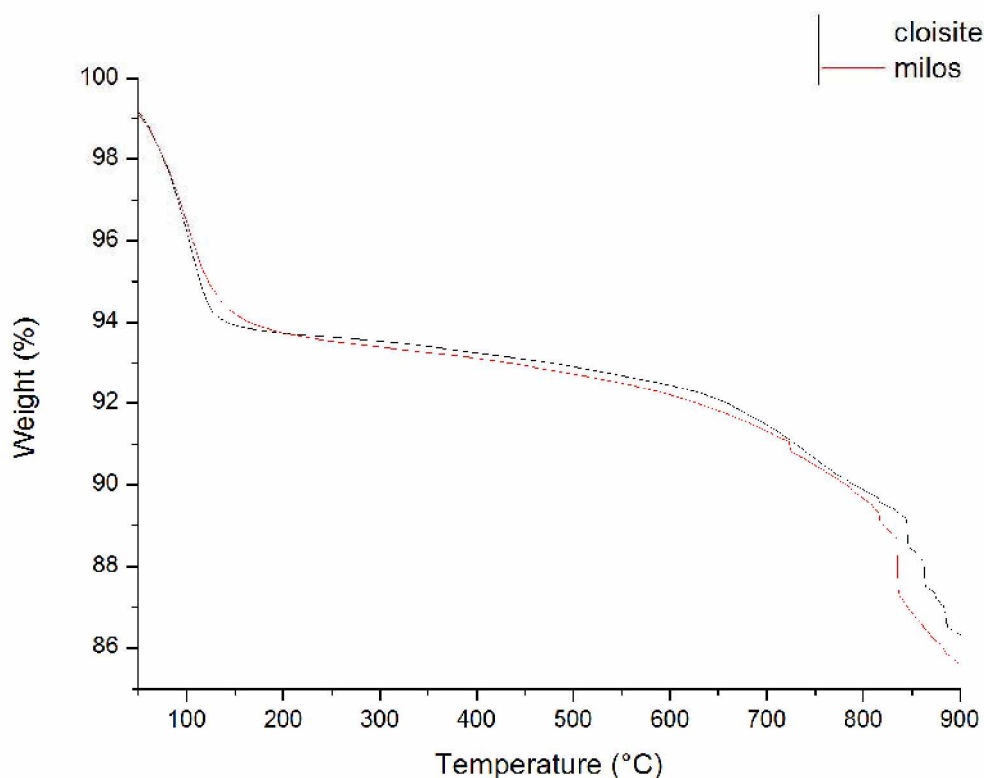


Fig. 3.14: Comparison of the thermal degradation of Cloisite-MMT and Milos-MMT

The direct comparison of the two montmorillonite types shows that there are no considerable thermally detectable differences between the two silicate branches. The curve shapes are very similar. The initial decrease may be slightly stronger for the Cloisite bentonite but due to the imprecision of the TGA device this difference cannot be considered as significant.

3.4.2 Surfactants

To bring the thermally induced weight losses of the modified montmorillonite in relation to the used surfactants, the pure surfactants have been tested to determine the decomposition temperatures. Every surfactant was tested in a temperature range of 100-900°C with a heating rate of 20°C/min. The percental weight loss and the derivation of the weight loss were recorded over the sample temperature.

3.4.2.1 Dodecyltrimethylammonium bromide (DDTAB)

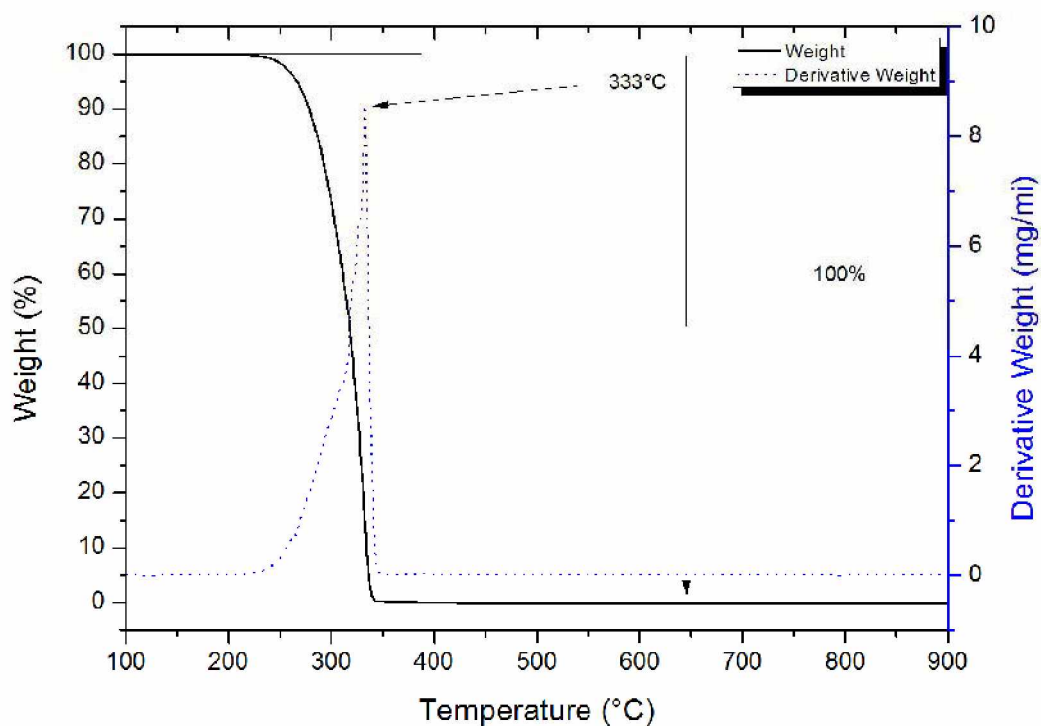


Fig. 3.15: Weight loss and derivative weight loss of pure DDTAB

15 mg of pure DDTAB were weighed in and heated over a temperature range from 100 to 900°C with a heating rate of 20°C/min under nitrogen atmosphere. The melting point of this substance is at 246°C according to the data sheet. The temperature of the maximum weight loss lies at 333°C. 100% of the substance is decomposed at a temperature of 346°C.

3.4.2.2 Tetraethyltrimethylammonium bromide (TEAB)

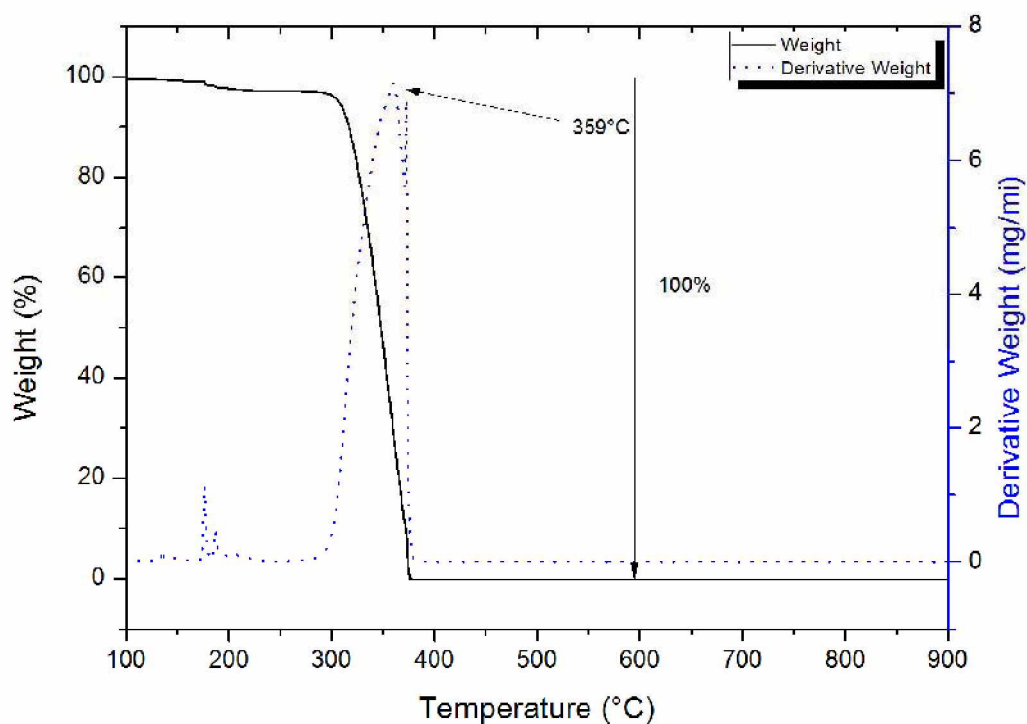


Fig. 3.16: Weight loss and derivative weight loss of pure TEAB

15 mg of pure TEAB were weighed in and heated over a temperature range from 100 to 900°C with a heating rate of 20°C/min under nitrogen atmosphere. The temperature of the maximum weight loss lies at 359°C. 100% of the substance is decomposed at a temperature of 378°C.

3.4.2.3 Oleic acid (OA)

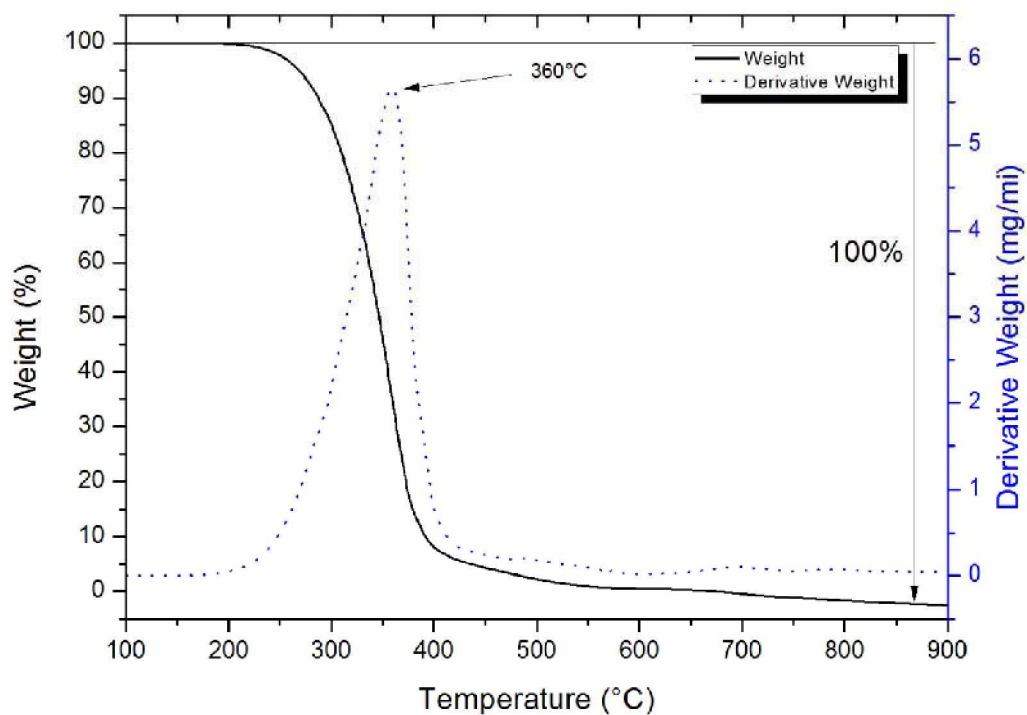


Fig. 3.17: Weight loss and derivative weight loss of pure oleic acid

15 mg of pure oleic acid were weighed in and heated over a temperature range from 100 to 900°C with a heating rate of 20°C/min under nitrogen atmosphere. The boiling point of that substance is at 360°C according to the data sheet. The temperature of the maximum weight loss lies at 360°C. The substance decomposes completely within the measurement range.

3.4.2.4 Undecylenicacid (UA)

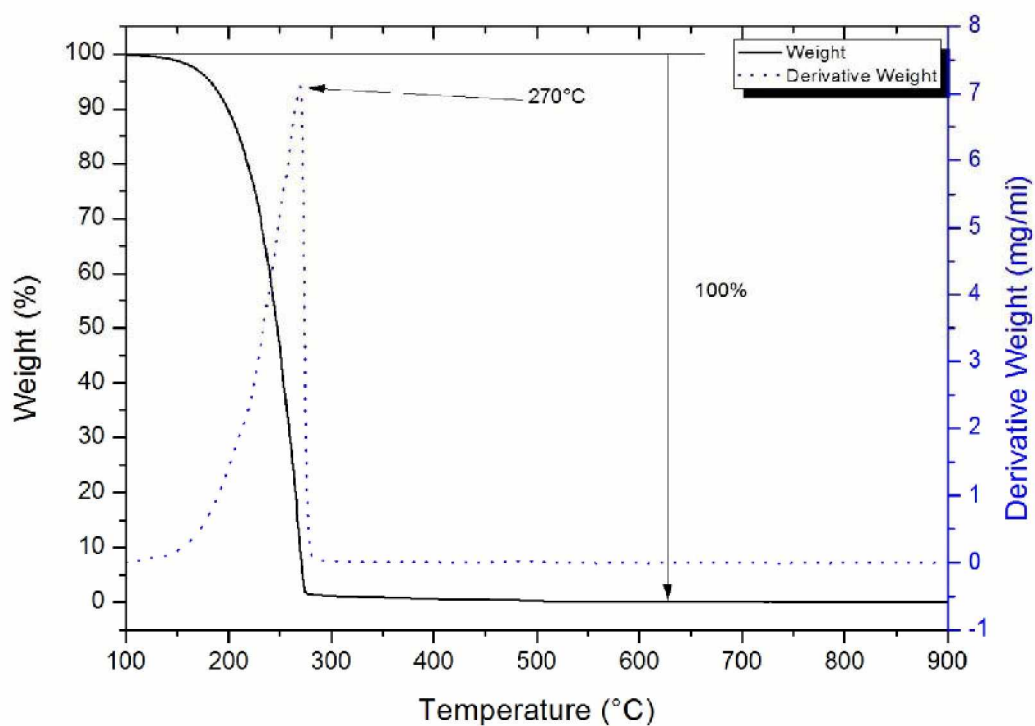


Fig. 3.18: Weight loss and derivative weight loss of pure undecylenic acid

15 mg of pure undecylenic acid was weighed in and heated over a temperature range from 100 to 900°C with a heating rate of 20°C/min under nitrogen atmosphere. The boiling point of that substance is at 275°C according to the data sheet. The temperature of the maximum weight loss lies at 270°C. The substance decomposes completely within the measurement range.

3.4.2.5 Hexadecyltrimethylammoniumbromide (HDTAB)

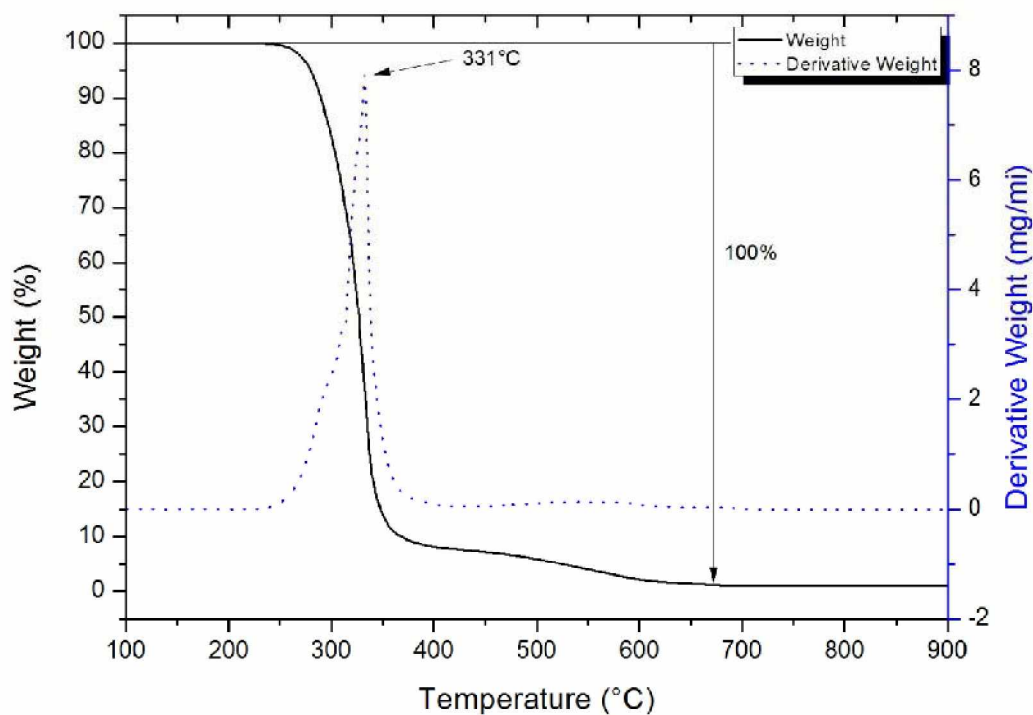


Fig. 3.19: Weight loss and derivative weight loss of pure HDTAB

15 mg of pure HDTAB were weighed in and heated over a temperature range from 100 to 900°C with a heating rate of 20°C/min under nitrogen atmosphere. The temperature of the maximum weight loss lies at 331°C. The substance decomposes completely within the measurement range.

3.4.2.6 Octadecyltrimethylammoniumbromide (ODTAB)

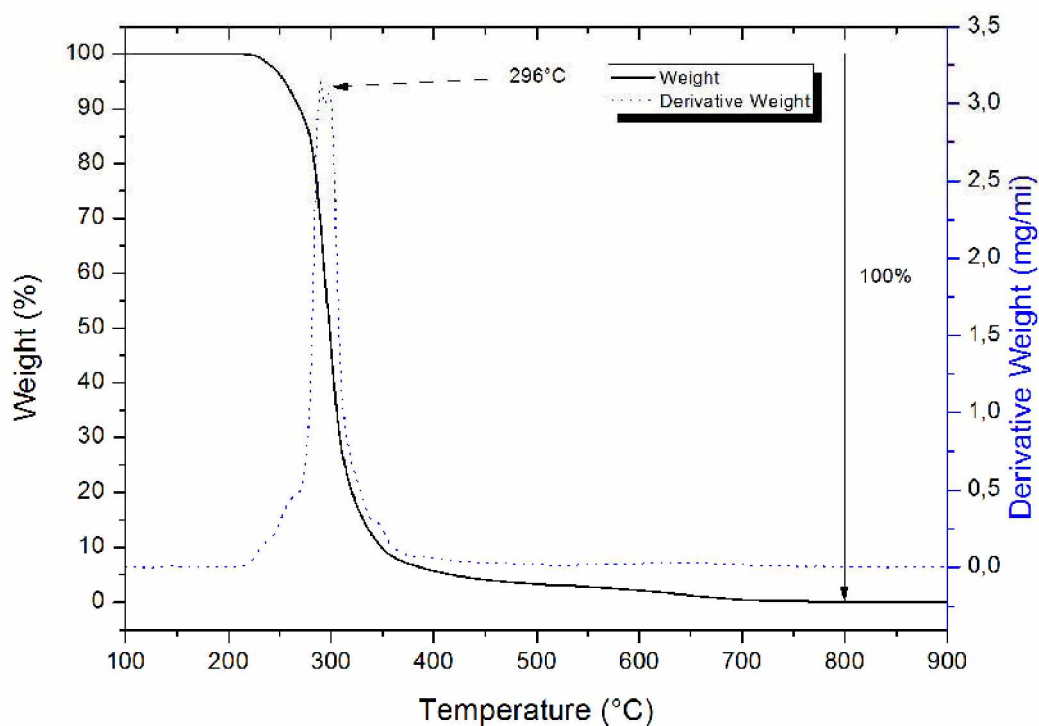


Fig. 3.20: Weight loss and derivative weight loss of pure ODTAB

15 mg of pure ODTAB were weighed in and heated over a temperature range from 100 to 900°C with a heating rate of 20°C/min under nitrogen atmosphere. The temperature of the maximum weight loss lies at 296°C. The substance decomposes completely within the measurement range.

3.4.2.7 Hexyltrimethylammoniumbromide (HTAB)

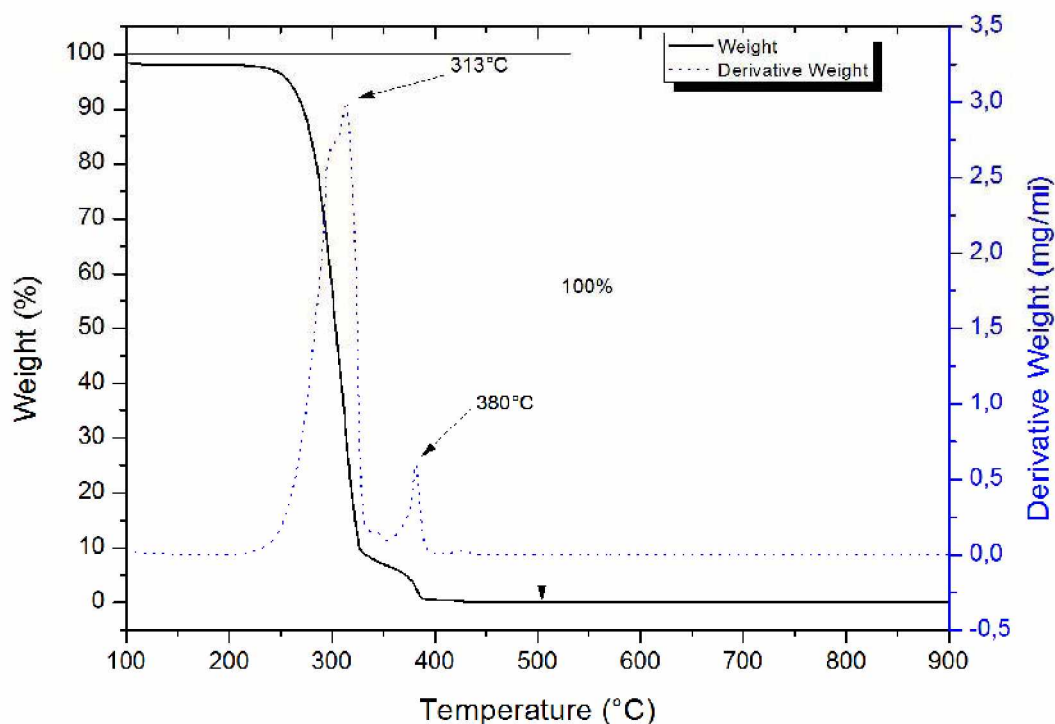


Fig. 3.21: Weight loss and derivative weight loss of pure HTAB

15 mg of pure HTAB were weighed in and heated over a temperature range from 100 to 900°C with a heating rate of 20°C/min under nitrogen atmosphere. This substance exhibits a double peak. The temperature of the maximum weight loss lies at 313°C and the second decomposition peak is at a temperature of 380°C. The substance decomposes completely within the measurement range.

3.4.3 Evaluation of the one-step modified samples

To examine the montmorillonite's intercalation and exfoliation behavior, experiments with montmorillonite of the type Cloisite and five different alkyl ammonium salts were carried out. The goal of these tests was to determine two salts with good intercalation properties for the further test series. The tests were conducted according to the experimental design in chapter 3.1.1, setup in chapter 3.1.2 and the procedure in 3.1.3.

3.4.3.1 Cloisite_TEAB

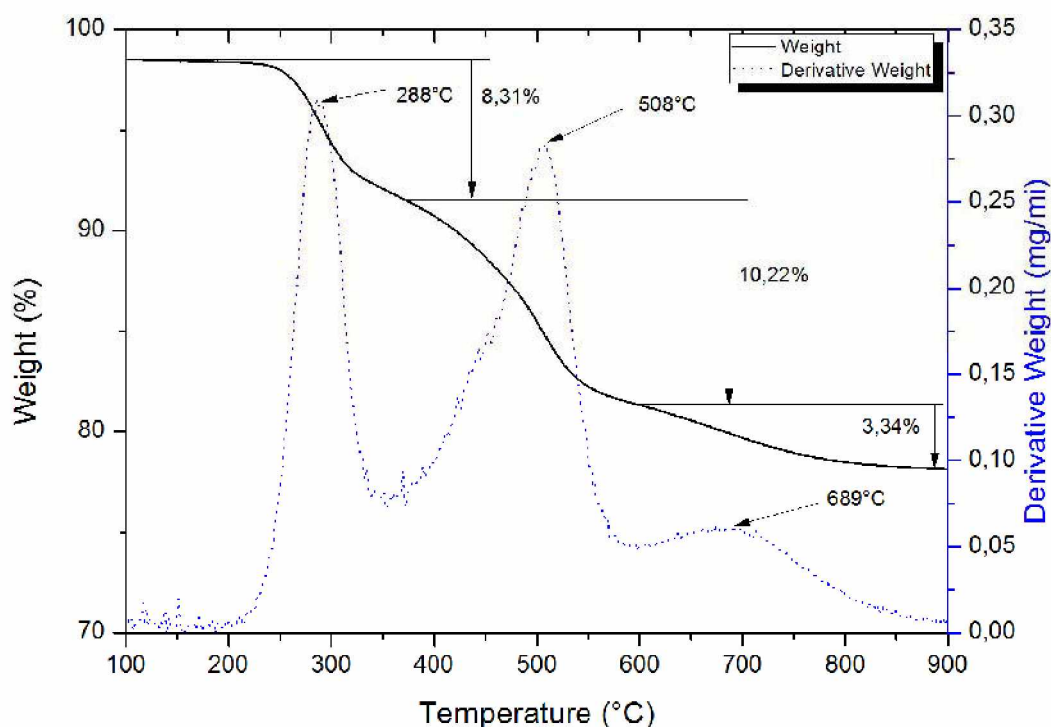


Fig. 3.22: Weight loss and derivative weight loss of Cloisite-MMT modified with TEAB

The montmorillonite of the type Cloisite was modified with tetraethylammonium bromide. The entire mass loss amounts to 22%. The mass loss is divided in three steps. The first step ranges from 100°C to 366°C and has its maximum decrease at a temperature of 288°C. That mass loss of 8.3% can be attributed to the decomposition of the pure surfactant. The second mass loss takes place in an interval from 366 to 591°C with a maximum at 508°C. The mass loss in that interval is related to the decomposition of the intercalated surfactant and amounts to 10.2%. The third mass loss ranges from 591 to 900°C with a maximum at 689°C. It can be attributed to the dehydroxylation of the montmorillonite, and contributes 3.3% to the weight loss.

Tab. 3.3: Mass loss steps, mass loss maxima and mass loss expressed as percentage of the absolute sample weight of Cloisite-MMT modified with TEAB

	Temperature Range [°C]	Peak maximum[°C]	Weight loss [%]
Peak 1	100-366	288	8,3%
Peak 2	366-591	508	10,2%
Peak 3	591-900	689	3,3

3.4.3.2 Cloisite_HDTAB

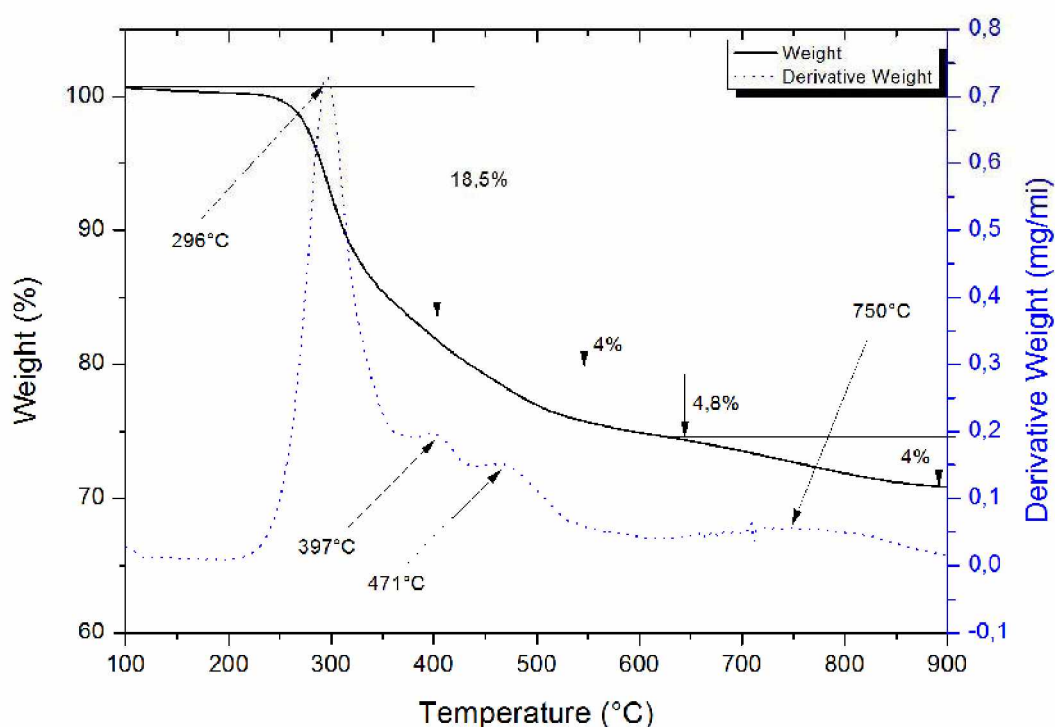


Fig. 3.23: Weight loss and derivative weight loss of Cloisite-MMT modified with HTAB

The montmorillonite of the type Cloisite has been modified with hexyltrimethylammoniumbromide. The entire weight loss amounts to 31.2% and takes place in four steps. The first and most significant weight loss takes place between 100 and 377°C and has its maximum at 296°C. This first peak can be attributed to the decomposition of the surfactant and contributes 18.5% to the weight loss. The second peak at 397°C can also be assigned to the decomposition of the surfactant. The shoulder at 471 °C represents the decomposition of the intercalated surfactants. The remaining weight loss is caused by dehydroxylation.

Tab. 3.4: Mass loss steps, mass loss maxima and mass loss expressed as percentage of the absolute sample weight of Cloisite-MMT modified with HTAB

	Temperature Range [°C]	Peak maximum [°C]	Weight loss [%]
Peak 1	100-377	296	18,5%
Peak 2	377-445	397	4%
Peak 3	445-616	471	4,8%
Peak 4	616-900	750	4%

3.4.3.3 Cloisite_DDTAB

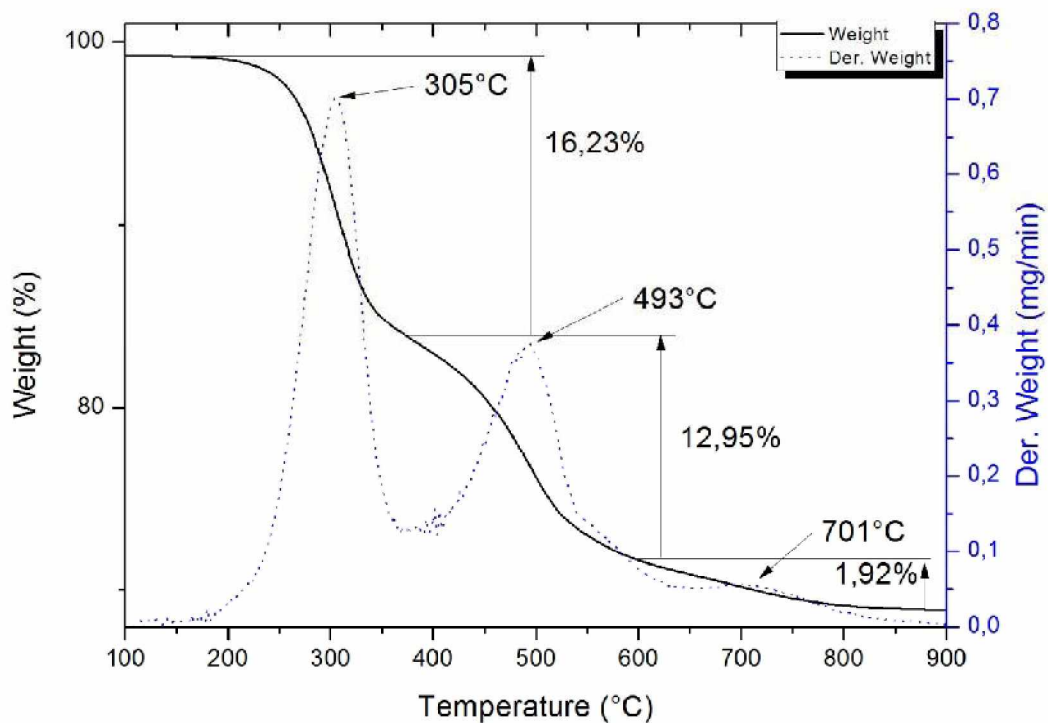


Fig. 3.24: Weight loss and derivative weight loss of Cloisite-MMT modified with DDTAB

The montmorillonite of the type Cloisite has been modified with dodecyltrimethylammonium bromide. The entire weight loss amounts to 31.1% and takes place in three steps. The first and most significant weight loss takes place between 100 to 378°C with a peak maximum at 305°C. It amounts to 16.2% and can be attributed to the decomposition of pure surfactant.

The second weight loss with an amount of 13% and a maximum at 493°C can be attributed to the decomposition of the intercalated surfactants. The last peak emerges due to the dehydroxylation of the montmorillonite between 652 and 900°C with a maximum at 701°C and amounts to 1.9%.

Tab. 3.5: Mass loss steps, mass loss maxima and percental mass loss of the absolute sample weight of Cloisite-MMT modified with DDTAB

	Temperature Range [°C]	Peak maximum [°C]	Weight loss [%]
Peak 1	100-378	305	16,2
Peak 2	378-652	493	13
Peak 3	652-900	701	1,9

3.4.3.4 Cloisite_HDTAB

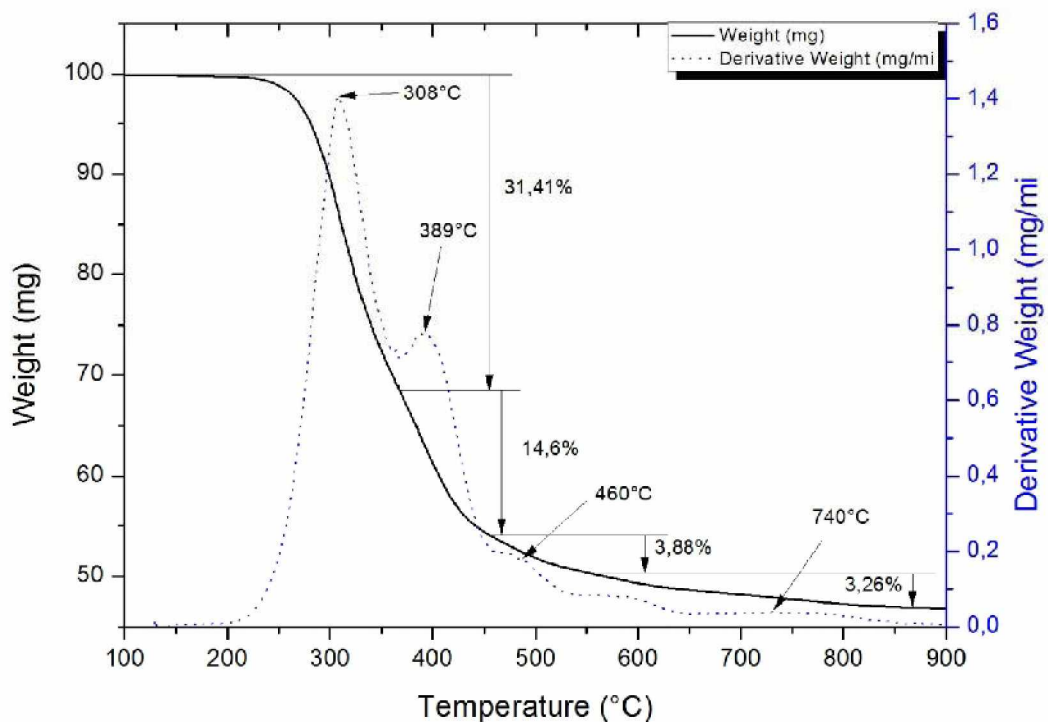


Fig. 3.25: Weight loss and derivative weight loss of Cloisite-MMT modified with HDTAB

The montmorillonite of the type Cloisite was modified with hexadecyltrimethylammoniumbromide. The entire weight loss amounts to 53.6% and takes

place in four steps. The first step has a temperature range of 100 to 366°C with a maximum mass decrease at 308°C. The corresponding weight loss amounts to 31.4% and can be attributed to the decomposition of the surfactant. The second peak with a maximum of 389°C and the weight loss of 14.6% partially overlaps with the first peak and can also be assigned to the decomposition of the surfactant. The third peak at 460°C represents the decomposition of the intercalated surfactant molecules. And partially overlaps with the second peak, so the exact amount of the intercalated molecules can't be determined precisely but tends to be significantly higher than 3.9%. The last weight loss is caused by the dehydroxylation process of the montmorillonite.

Tab. 3.6: Mass loss steps, mass loss maxima and mass loss expressed as percentage of the absolute sample weight of Cloisite-MMT modified with HDTAB

	Temperature Range [°C]	Peak maximum [°C]	Weight loss [%]
Peak 1	100-366	308	31,4
Peak 2	366-457	389	14,6
Peak 3	457-563	460	3,9
Peak 4	563-900	740	3,3

3.4.3.5 Cloisite_ODTAB

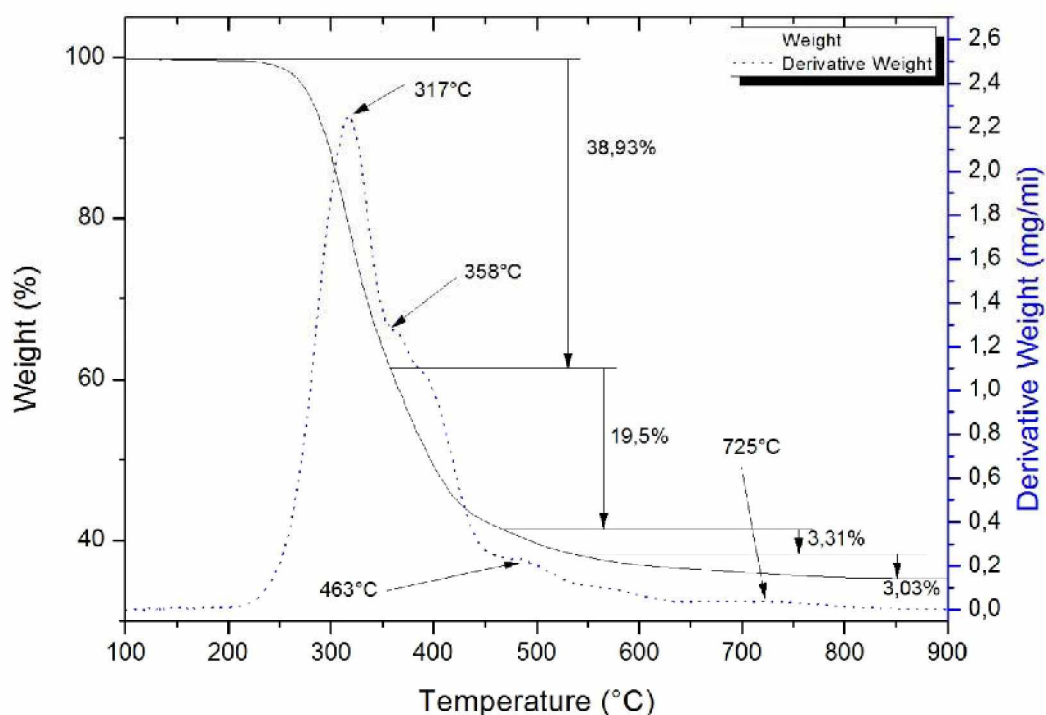


Fig. 3.26: Weight loss and derivative weight loss of Cloisite-MMT modified with OTAB

The montmorillonite of the type Cloisite has been modified with octadecyltrimethylammonium bromide. The entire weight loss amounts to 64.8% and takes place in four stages. The curve shape is very similar to the curve shape of the HDTAB-MMT sample, but the subdivision is more difficult. The first weight loss amounts to 38.9% and ranges from 100-358°C with a maximum at 317°C. It can be attributed to the decomposition of the surfactant. The shoulder at 358°C is the maximum of the second weight loss and is difficult to separate from the first peak because of the strong overlap of the broad first peak with the narrow second one. The second peak can also be assigned to the decomposition of the surfactant. The third peak at 463°C exhibits the decomposition of the intercalated surfactant molecules up to a temperature of 538°C. Further weight losses are caused by dehydroxylation.

Tab. 3.7: Mass loss steps, mass loss maxima and mass loss expressed as percentage of the absolute sample weight of Cloisite-MMT modified with OTAB

	Temperature Range [°C]	Peak maximum [°C]	Weight loss [%]
Peak 1	100-358	317	38,93
Peak 2	358-463	358	19,5

Peak 3	463-538	463	3,31
Peak 4	538-900	725	3,03

3.4.3.6 Comparison of the 100% CEC samples

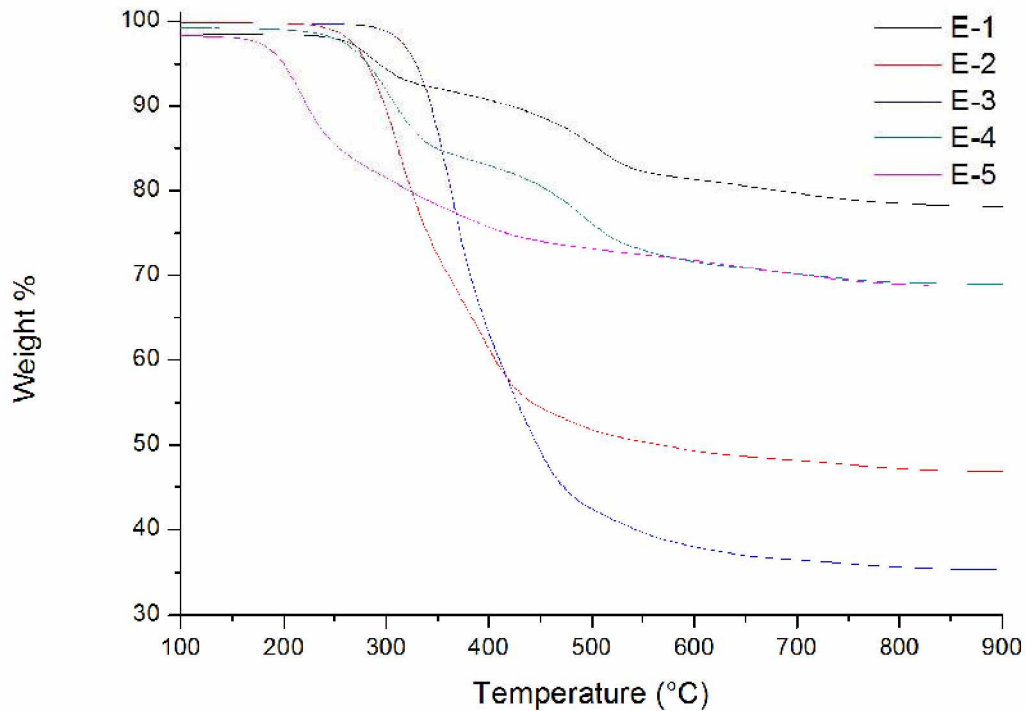


Fig. 3.27: Comparison of the thermal degradation of the ammonium salt modified Cloisite-MMT samples

In comparison to the unmodified montmorillonite the first two peaks of the mass loss curve between 100 and 200°C have either vanished or are only very weak. This observation can be explained by the hydrophobization of the montmorillonite. The affinity of the montmorillonite to adsorb water was lowered through the change of its surface polarity, which is conditioned through the exchange of the hydrophilic sodium ions against the hydrophobic alkyl ammonium ions. That also explains the absence of the weight loss through the hydrate shells of the sodium ions in the tested samples of the modified montmorillonite.

The unmodified montmorillonite does not exhibit any substantial thermally induced changes in a temperature range from 200 to 600°C. Therefore, all observed temperature losses in that area can be attributed to the decomposition of the surfactants. The decomposition of the surfactants occurred in all samples at at least two different temperatures. That indicated at least two different types of bonding of the surfactant.

The total weight losses range from 22.0 to 64.8%. A trend can be observed: surfactants with longer alkyl units such as ODTAB and HDTAB have higher loading percentages than the surfactants with lower alkyl remainders like TEAB, DDTAB and HTAB.

Three different decomposition processes were observed for some of the samples. The decomposition of the intercalated surfactant, surfactant adsorbed between montmorillonite pores and or adsorbed through its counter ion, and surfactant molecules that were bound through apolar interactions on the intercalated surfactant molecules. These mechanisms will be closely investigated in chapter 4.

The peaks above 600°C were also observed for the unmodified montmorillonite and document the weight loss due to dehydroxylation of the structural Hydroxyl groups of the montmorillonite.

In addition to the absolute weight loss the molar amount of surfactant bound to the montmorillonite has been evaluated.

Tab. 3.8: Comparison of the molecules surfactant bound per gram of montmorillonite for the samples Cloisite_TEAB, Cloisite_HDTAB, Cloisite_ODTAB, Cloisite_DDTAB and Cloisite_HDTAB

Sample	Cloisite_ TETAB	Cloisite_ HDTAB	Cloisite_ ODTAB	Cloisite_ DDTAB	Cloisite_ HTAB
Surfactant molecules [mmol]/ montmorillonite[g]	1,15	2,89	4,45	1,51	1,68

Tab. 3.8 shows a general trend regarding the amount of surfactant molecules bound to the montmorillonite: It is higher for surfactants with longer alkyl tails. This could be attributed to the higher apolar interactions between the longer alkyl chains. Consequently, HDTAB and ODTAB were chosen for further investigations and the two step modification.

3.4.1 Evaluation of the two-step modified samples

The following samples were each modified with two different surfactants. To examine the loading rate and all interactions between the surfactants, thermogravimetric measurements were carried out. The tests were conducted according to the experimental design in chapter 3.1.1, setup in chapter 3.1.2 and procedure in 3.1.3.

3.4.1.1 Cloisite_HDTAB/UA

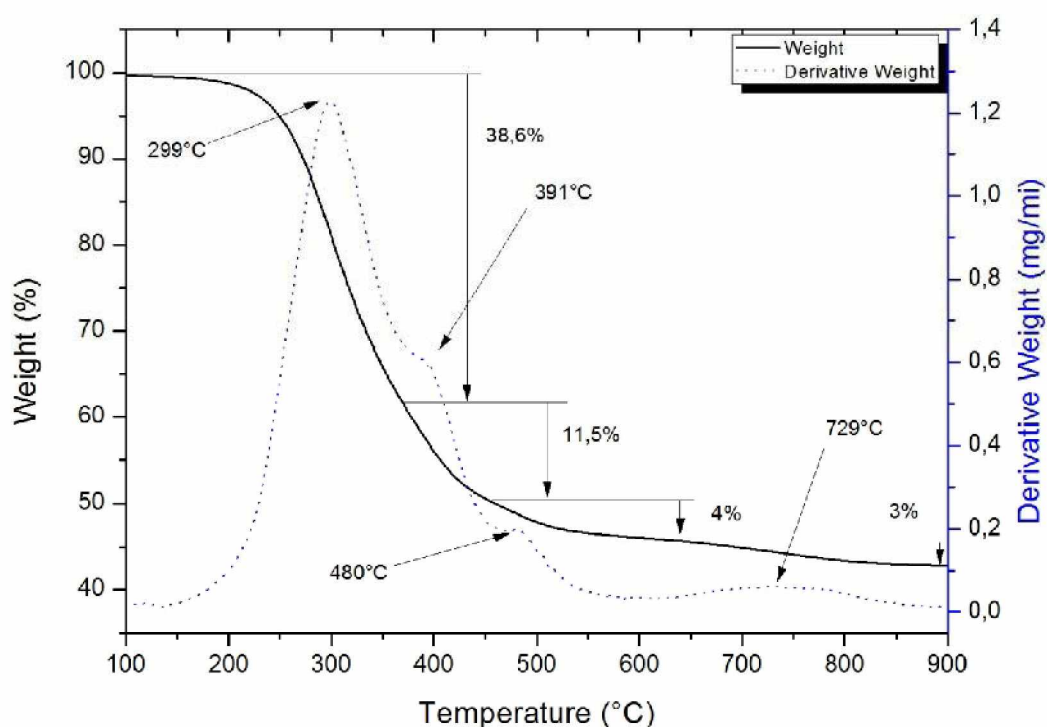


Fig. 3.28: Weight loss and derivative weight loss of Cloisite-MMT modified with HDTAB and UA

The montmorillonite of the type Cloisite has been modified with surfactants equal to 40% of its CEC. The amount surfactant added has been equally divided per mole between the quaternary ammonium salt HDTAB and the fatty acid UA. The entire weight loss during the measurement amounts to 57.1% and takes place in four steps. The first and most significant mass loss takes place between 100 and 370°C with a maximum mass loss at 299°C. The shoulder with the maximum at 391°C marks the second weight loss with a mass loss of 11.5% of the total sample weight. The third mass loss ranges from 460 to 620°C and has its maximum at 480°C. This step contributes 4% to the overall weight loss. The last weight loss ranges from 620 to 900°C with a maximum at 729°C and is related to the dehydroxylation of the montmorillonite.

Tab. 3.9: Mass loss steps, mass loss maxima and percental mass loss of the absolute sample weight of Cloisite-MMT modified with HDTAB and UA

	Temperature Range [°C]	Peak maximum [°C]	Weight loss [%]
Peak 1	100-370	299	38,6
Peak 2	370-460	391	11,5
Peak 3	460-620	480	4
Peak 4	620-900	729	3

3.4.1.2 Cloisite_ODTAB/UA

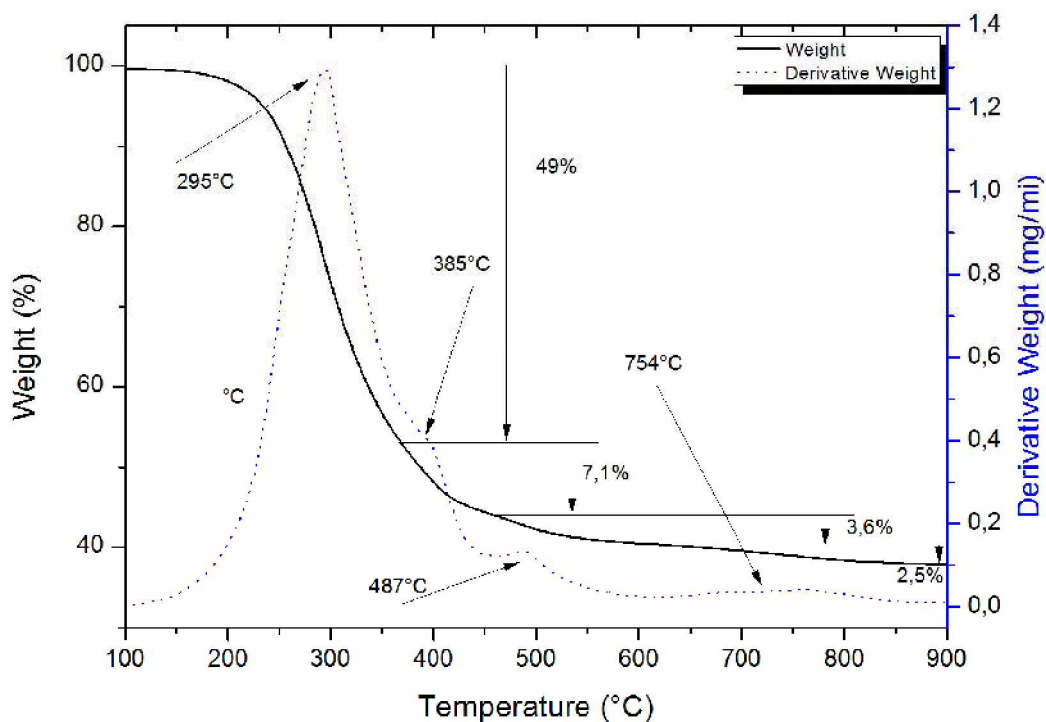


Fig. 3.29: Weight loss and derivative weight loss of Cloisite-MMT modified with ODTAB and UA

The montmorillonite of the type Cloisite was modified with surfactants equal to 40% of its CEC. The amount surfactant added was equally divided per mole between the quaternary ammonium salt ODTAB and the fatty acid UA. The entire weight loss during the measurement amounts to 63.7% and takes place in four steps. The first mass loss step takes place between 100 and 380°C with a maximum at 295°C and amounts to 49% of the sample weight. The second weight loss amounts to 7.1% and has its maximum at 385°C. The third weight loss ranges from 460°C to 617°C and amounts to 3.6% with a maximum at 487°C.

The fourth and last weight loss step with 2.5% has its maximum at 754°C and ranges from 617 to 900°C.

Tab. 3.10: Mass loss steps, mass loss maxima and mass loss expressed as percentage of the absolute sample weight of Cloisite-MMT modified with ODTAB and UA

	Temperature Range [°C]	Peak maximum [°C]	Weight loss [%]
Peak 1	100-380	295	49,0
Peak 2	380-460	385	7,1
Peak 3	460-617	487	3,6
Peak 4	617-900	754	2,5

3.4.1.3 Cloisite_HDTAB/OA

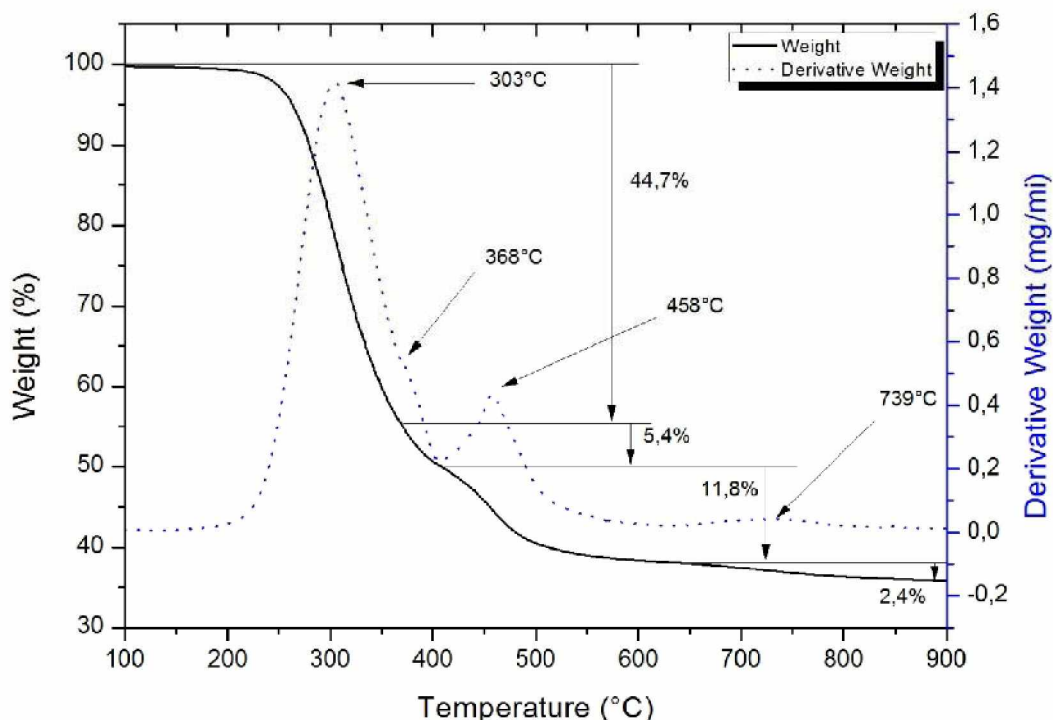


Fig. 3.30: Weight loss and derivative weight loss of Cloisite-MMT modified with HDTAB and OA

The montmorillonite of the type Cloisite has been modified with surfactants equal to 40% of its CEC. The amount surfactant added has been equally divided per mole between the quaternary ammonium salt HDTAB and the fatty acid OA. The entire weight loss during the

measurement amounts to 64.3% and takes place in four steps. The first step ranges from 100 to 368°C with a maximum at 303°C and amounts to 44.7% of the sample weight. The second mass loss peak is nearly completely overlapped by the first one and ranges between 368 and 409°C with a maximum at 368°C and a weight loss of 5.4%. The third weight loss exhibits a good resolved peak between 409 and 633°C with a maximum at 458°C and a weight loss of 11.8%. The last weight loss with a maximum at 739°C amounts to 2.4% and takes place between 633 and 900°C.

Tab. 3.11: Mass loss steps, mass loss maxima and percental mass loss of the absolute sample weight of Cloisite-MMT modified with HDTAB and OA

	Temperature Range [°C]	Peak maximum [°C]	Weight loss [%]
Peak 1	100-368	303	44,7
Peak 2	368-409	368	5,4
Peak 3	409-633	458	11,8
Peak 4	633-900	739	2,4

3.4.1.4 Cloisite_ODTAB/OA

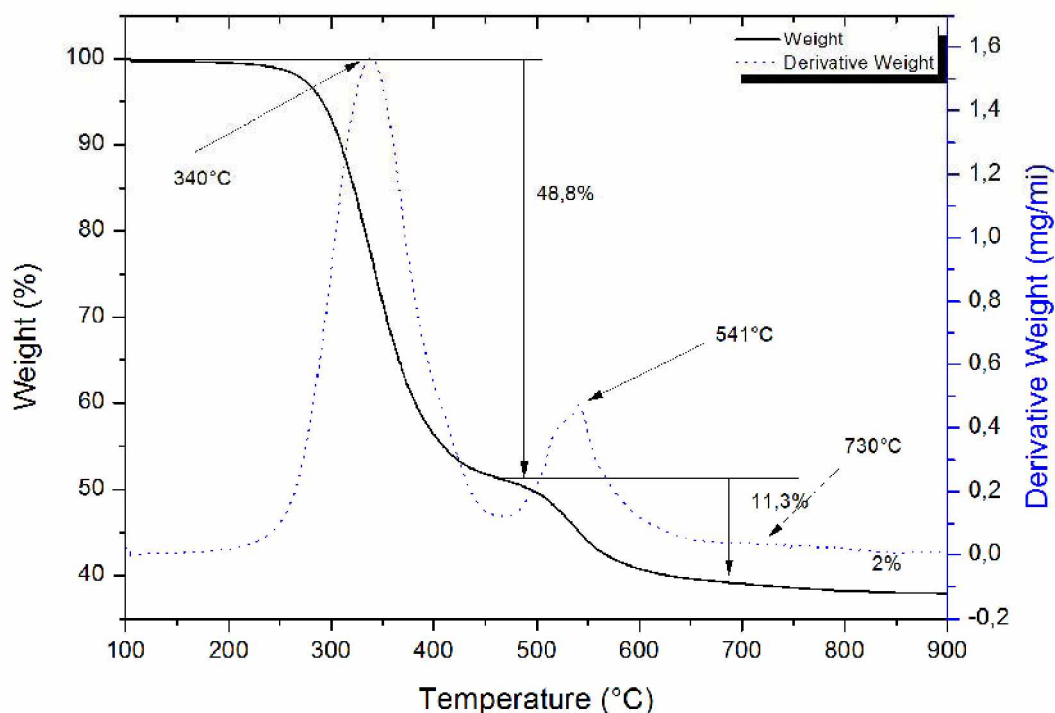


Fig. 3.31: Weight loss and derivative weight loss of Cloisite-MMT modified with ODTAB and OA

The montmorillonite of the type Cloisite was modified with surfactants equal to 40% of its CEC. The amount surfactant added was equally divided per mole between the quaternary ammonium salt ODTAB and the fatty acid OA. The entire weight loss during the measurement amounts to 62.1% and takes place in three steps. The first mass loss ranges from 100 to 460°C with a maximum at 340°C and amounts to 48.8% of the sample weight. The second mass loss also exhibits a well resolved peak in the temperature range of 460 to 630°C with a maximum at 541°C and a weight loss of 11.3%. The last weight loss amounts to 2%, has its maximum at 760°C and ranges between 630 and 900°C.

Tab. 3.12: Mass loss steps, mass loss maxima and mass loss expressed as percentage of the absolute sample weight of Cloisite-MMT modified with ODTAB and OA

	Temperature Range [°C]	Peak maximum [°C]	Weight loss [%]
Peak 1	100-460	340	48,8
Peak 2	460-630	541	11,3
Peak 3	630-900	760	2%

3.4.1.5 Comparison of the Cloisite samples

Tab. 3.13: List of the modified Cloisite-MMT mass loss peak maxima related to the decomposition of surfactants

	Peak 1 [°C]	Peak 2 [°C]	Peak 3 [°C]
Cloisite_HDTAB/UA	299	391	480
Cloisite_ODTAB/UA	295	385	487
Cloisite_HDTAB/OA	303	368	458
Cloisite_ODTAB/OA	340	/	541

The first observations to be made is the missing dehydration peak in the temperature range up to 200°C. This is a valuable indicator for the successful organo-modification of the montmorillonite and the subsequent hydrophobization of the clay material, but is also a result of the drying during sample preparation.

The first weight loss step (Peak 1) occurs in all samples over a temperature of approximately 150°C and can be assigned to both, the decomposition of the quaternary ammonium salt molecules that were adsorbed in pores and between montmorillonite particles or were adsorbed on the surface with their counterion and the fatty acids. The absolute amount of these weight losses ranges from 38 to 49% of the total weight of the samples. Due to the fact that the decomposition temperatures of all four pure surfactants are in a range of only 70°K, a direct differentiation is not possible, though shifts of the peak maxima of the decomposition temperatures of the organic surfactants are an indicator for different decomposition processes within the sample. Major differences can be observed concerning the location of the first decomposition peak of samples that were modified with ODTAB and the fatty acids. The position of the first peak shifted from 295°C to 340°C, and is related to the joint decomposition of non intercalated HDTAB molecules and fatty acid molecules. This decisive difference could not be observed for samples which were modified with HDTAB and fatty acids. The equivalent peak shift for the samples modified with HDTAB amounts only 4°C and is therefore far smaller. That indicates that there is an interaction between the ODTAB surfactants and the fatty acids that is weaker or not present for HDTAB and fatty acids.

The second weight loss (Peak 2) that can be observed, amounts to 5.4-11.5% and is related to the decomposition of ammonium salt molecules bound by apolar interactions to the intercalated and ion exchanged ammonium salt molecules. These molecules form a multilayer structure between the clay layers and decompose at a lower temperature than their intercalated counterparts. The exact location of the second decomposition peak maximum and the related mass loss were difficult to determine as a result to the overlapping of the first and the second peak. Generally well resolved shoulders with maxima between 369 and 391°C could be observed. For Cloisite_ODTAB/OA the second peak was completely overlapped by the broad first peak with a maximum of 340°C.

The third and last weight loss (Peak 3) related to organic decomposition can be assigned to the decomposition of the intercalated ammonium salt molecules. The peaks are well resolved and maxima were located between 458 and 541°C. This weight loss reflects the essential amount of intercalated surfactant. If the weight loss is normalized only on the organic weight loss, the weight loss percentages of the intercalated surfactants range between 7,4 and 11,9% for undecylenic acid modified Cloisite-MMTs, and 18,9 and 19,0% for oleic acid modified Cloisite-MMTs. This indicates that the oleic acid has an influence on the amount of intercalated surfactant.

3.4.1.6 Milos_HDTAB/UA

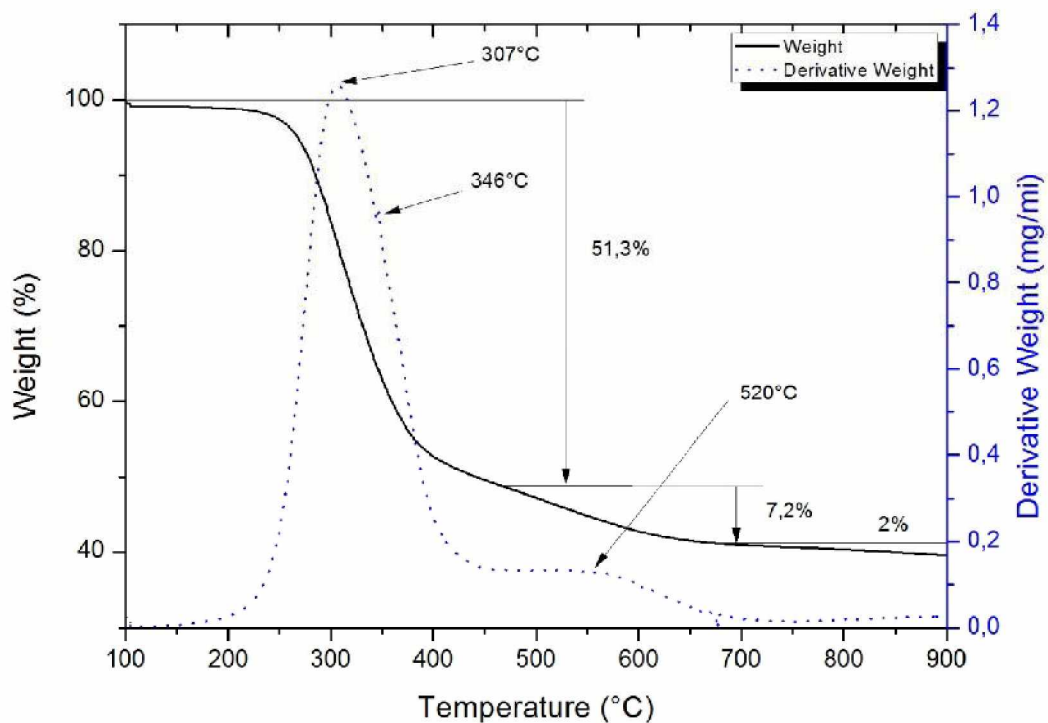


Fig. 3.32: Weight loss and derivative weight loss of Milos-MMT modified with HDTAB and UA

The montmorillonite of the type Milos was modified with surfactants equal to 40% of its CEC. The amount surfactant added was equally divided per mole between the quaternary ammonium salt HDTAB and the fatty acid UA. The entire weight loss during the measurement amounts to 60.5% and takes place in four steps. The first and most significant mass loss takes place between 100 and 467°C with a maximum mass loss at 307°C. It also exhibits an overlapped peak at 346°C. The weight loss in that area amounts to 51.3% and can be attributed to the decomposition of both surfactants. The second peak can be attributed to the decomposition of the intercalated surfactant and amounts to 7.2% of the total weight.

Tab. 3.14: Mass loss steps, mass loss maxima and mass loss expressed as percentage of the absolute sample weight of Milos-MMT modified with HDTAB and UA

	Temperature Range [°C]	Peak maximum [°C]	Weight loss [%]
Peak 1	100-467	307	51.3
Peak 2	467-650	520	7.2
Peak 3	650-900	/	2

3.4.1.7 Milos_ODTAB/UA

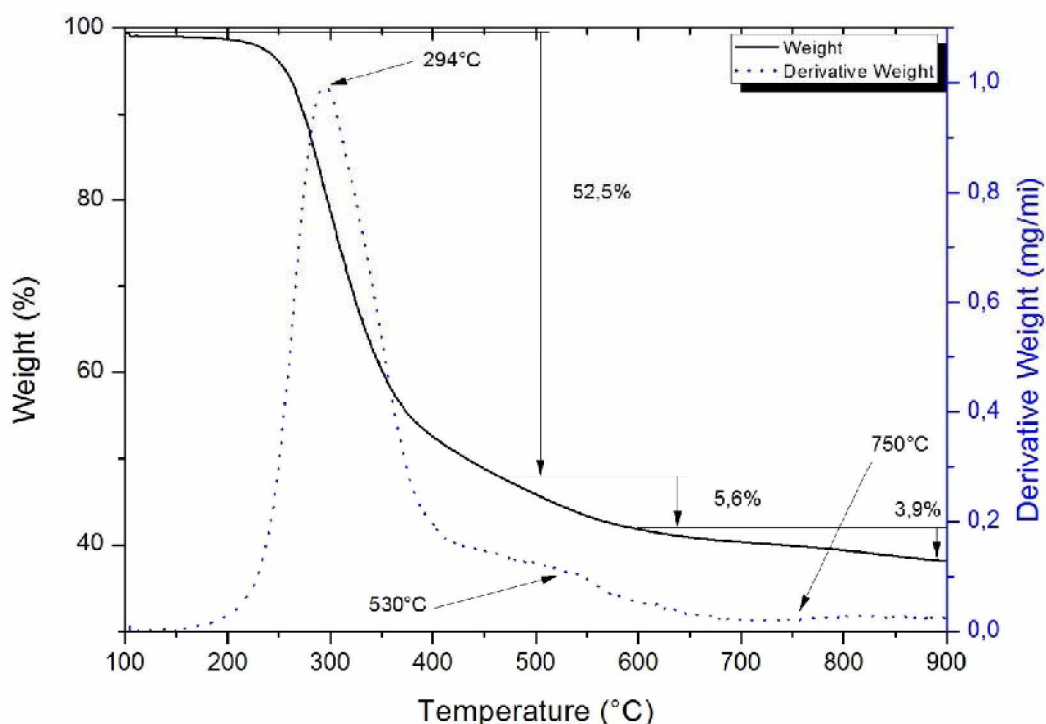


Fig. 3.33: Weight loss and derivative weight loss of Milos-MMT modified with ODTAB and UA

The montmorillonite of the type Milos was modified with surfactants equal to 40% of its CEC. The amount surfactant added was equally divided per mole between the quaternary ammonium salt ODTAB and the fatty acid UA. The entire weight loss during the measurement amounts 61.9% and takes place in three steps. The first and most significant mass loss takes place between 100 and 471°C with a maximum mass loss at 294°C. The second weight loss ranges between 471 and 620°C with a maximum at 530°C and amounts

6.1% of the total weight loss. The last weight loss from 620 to 900°C amounts 3.3% with a maximum at 750°C.

Tab. 3.15: Mass loss steps, mass loss maxima and percental mass loss of the absolute sample weight of Cloisite-MMT modified with ODTAB and UA

	Temperature Range [°C]	Peak maximum [°C]	Weight loss [%]
Peak 1	100-471	294	52.5
Peak 2	471-620	530	6.1
Peak 3	620-900	750	3,3

3.4.1.8 Milos_HDTAB/OA

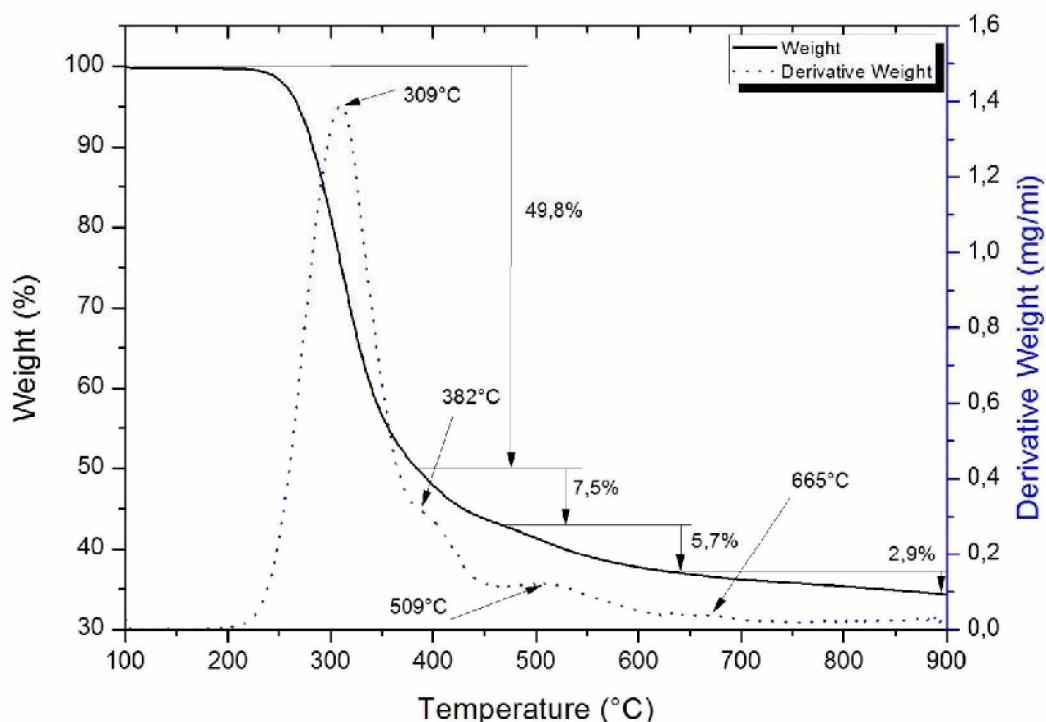


Fig. 3.34: Weight loss and derivative weight loss of Milos-MMT modified with HDTAB and OA

The montmorillonite of the type Milos was modified with surfactants equal to 40% of its CEC. The amount surfactant added was equally divided per mole between the quaternary ammonium salt HDTAB and the fatty acid OA. The entire weight loss amounts 65.8% and takes place in four steps. The first weight loss amounts 49.8% and takes place between 100 and 382°C with a maximum at 309°C. The second weight loss is partially overlapped and can

be enclosed in the range between 382 and 471 with a maximum at 382°C and an amount of 7.7% weight loss. The third weight loss between 471 and 633°C has its maximum at 509°C and amounts 5.7%. The weight loss in the range of 633 to 900°C can be attributed to the dehydroxylation of the montmorillonite and amounts 2.9%.

Tab. 3.16: Mass loss steps, mass loss maxima and percental mass loss of the absolute sample weight of Cloisite-MMT modified with HDTAB and OA

	Temperature Range [°C]	Peak maximum [°C]	Weight loss [%]
Peak 1	100-382	309	49,8
Peak 2	382-471	382	7,5
Peak 3	471-633	509	5,7
Peak 4	633-900	665	2,9

3.4.1.9 Milos_ODTAB/OA

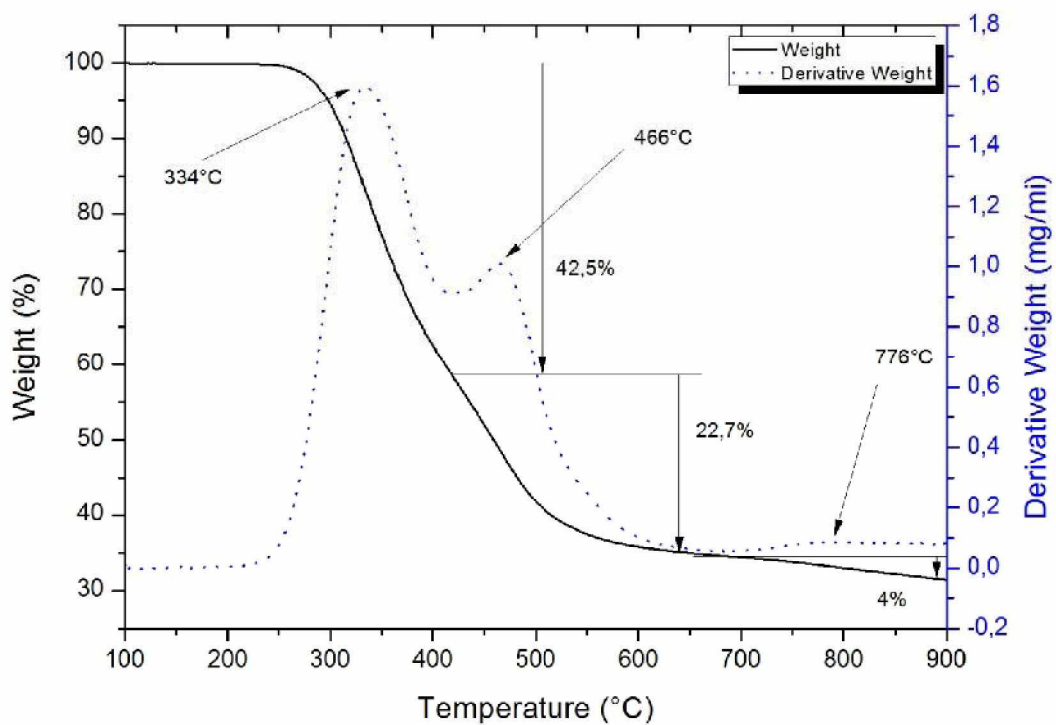


Fig. 3.35: Weight loss and derivative weight loss of Milos-MMT modified with ODTAB and OA

The montmorillonite of the type Milos was modified with surfactants equal to 40% of its CEC. The amount surfactant added was equally divided per mole between the quaternary ammonium salt ODTAB and the fatty acid OA. The entire weight loss amounts 69.3% and takes place in three steps. The weight loss between 100 and 423°C amounts 42.5% and has its maximum at 334°C. The second peak with a maximum at 466°C and a range of 423 to 667°C is partially overlapped by this first weight loss. The weight loss of the second peak amounts 22.7%. The third weight loss lies between 667 and 900°C with a maximum at 776°C and amounts 4% of the total weight.

Tab. 3.17: Mass loss steps, mass loss maxima and mass loss expressed as percentage of the absolute sample weight of Cloisite-MMT modified with ODTAB and OA

	Temperature Range [°C]	Peak maximum [°C]	Weight loss [%]
Peak 1	100-423	334	42,5
Peak 2	423-667	466	22,7
Peak 3	667-900	776	4

3.4.1.10 Comparison of the Milos Samples

Like for the Cloisite-MMT samples the first peak related to the desorption and dehydration of water molecules is missing, which is an indication for a successful hydrophobization and interlayer cation exchange. The first mass loss is caused by the decomposition of both surfactants. The location of the peak maximum is in a 15°C temperature range for all samples except Milos_ODTAB/OA, which reflects the strong effect found for samples modified with ODTAB/OA. The samples modified with undecylenic acid exhibit slightly lower peak maxima and the decomposition process starts at 150°C whereas the samples that were modified with oleic acid showed no weight loss under a temperature of 200°C.

For the samples modified with undecylenic acid the signal of the expected second decomposition peak was considerably weak or even not present, when in fact the samples modified with oleic acid showed a mass loss in this range. This could indicate that the affinity of oleic acid of forming multilayer structures in the interlayer space is higher than that of undecylenic acid.

For three of four samples the decomposition peak maximum for the intercalated surfactant was in the range of 509 to 533°C and amounted 5 to 7% of the total weight. The sample modified with ODTAB and OA varied extensively from the other samples. The peak maximum of the very broad peak was located at 466°C. This is a much lower rate compared to the other samples and leads to the conclusion that we deal with a joint peak consisting of the signal of the intercalated surfactant and molecules that are bound by apolar interactions.

This variance caused by the combination of those specific surfactants has also been observed for the Cloisite samples.

3.5 IR-Evaluation

The FTIR experiments were conducted to gain an understanding of the chemical and physical changes through an ion exchange. The spectra of the unmodified montmorillonite as well as the spectra of the surfactants were closely investigated. To detect any changes resulting from the modification process the spectra of the unmodified montmorillonite were compared to the spectra of the modified clay.

For the manufacturing of the specimens different methods of the FT/IR measurements were tested to find an appropriate process. First the pure clay was measured but the test results were not satisfying due to the high water content and the low transmission through the specimen. Good results could be received by grinding the clay, that had been dried for 2h at 95°C, to dust and admixing it in potassium bromide and pressing it under exclusion of air to platelets. Ultimately a third method was chosen due to the very good results and the easy handling. The modified montmorillonite was dispersed in a water/ethanol mixture by sonication and was then applied on calcium fluoride platelets by spin coating. Afterwards this sample preparation method was used for all the samples to exclude any inhomogeneities in the sample preparation. The specimens were measured immediately after the spin coating to avoid a readsorption of water.

3.5.1 Unmodified silicates

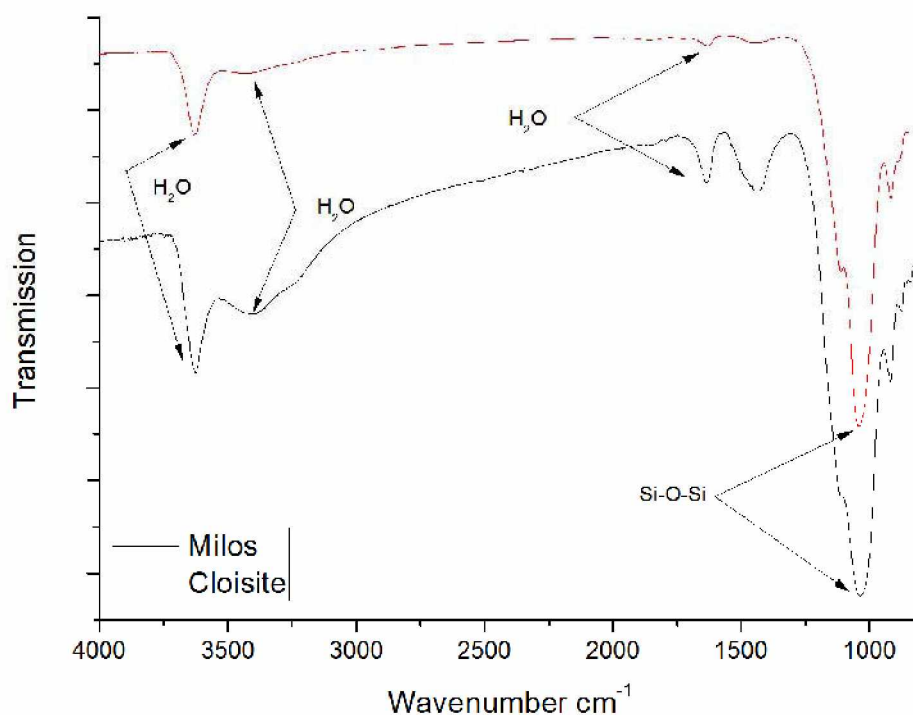


Fig. 3.36: Infrared spectrum of Cloisite-MMT and Milos-MMT

Fig. 3.36 shows the IR spectrum of Cloisite and Milos. The well resolved band at 3630cm^{-1} can be attributed to the vibration of firmly bound hydrate water and the broad band at 3334cm^{-1} can be assigned to the asymmetric stretching vibration of weakly bound H-O-H which is present in a hydrogen bonded state. The small peak at 1631cm^{-1} is related to the hydrate water bound by the sodium ions. This peak is of utmost importance for the ion exchange process due its correlation with the amount of sodium ions present in the montmorillonite. The broad peak at 1042cm^{-1} and the shoulder at 1114cm^{-1} can be assigned to the in plane and out of plane Si-O-Si stretch vibration.

3.5.2 Surfactants

Characteristic bands of the surfactants had to be identified for the evaluation of the modified samples. Infrared spectra of all surfactants were taken and analyzed to extract single characteristic bands for each surfactant substance. The references for the band identification can be found in chapter 4.2.1.1 and 4.2.1.2.

3.5.2.1 Fatty acids (OA, UA)

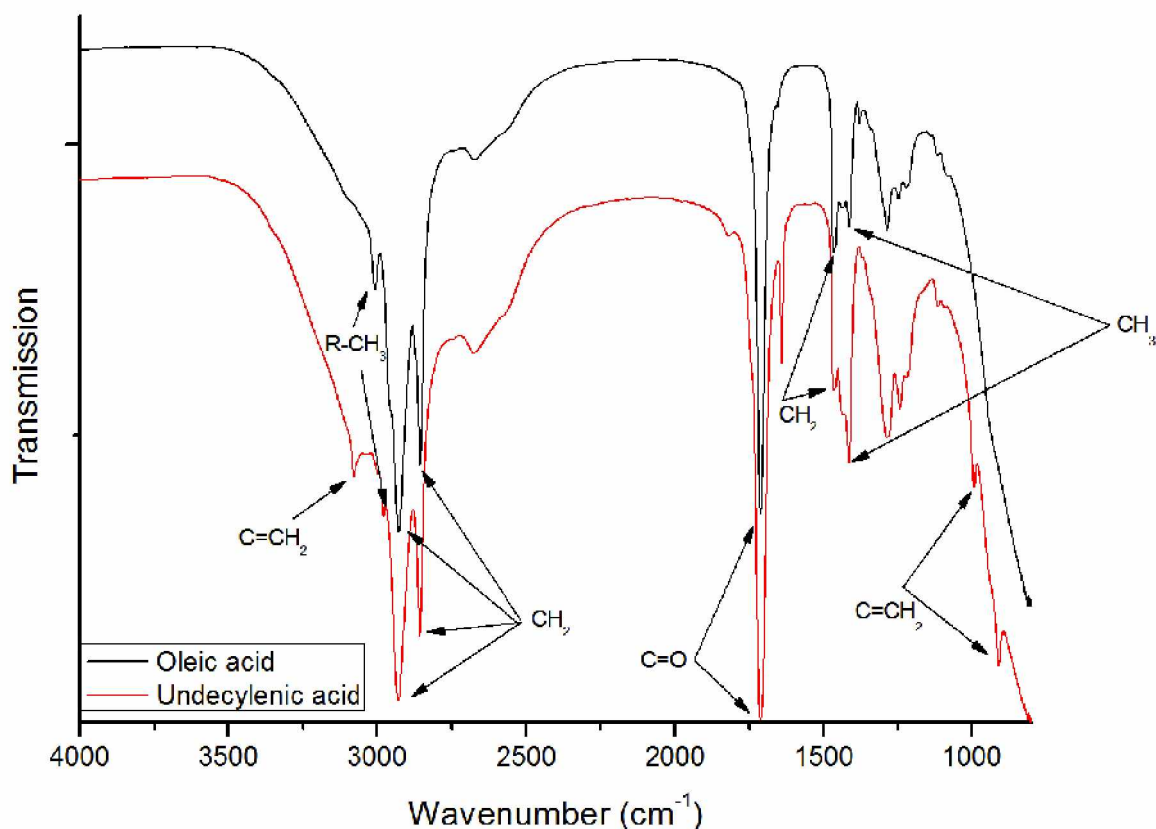


Fig. 3.37: Infrared spectra of oleic acid and undecylenic acid with assignment of the characteristic bands to the chemical groups

Both fatty acids exhibit bands in a region between 3100 and 2800 cm^{-1} . The peak occurring at a wavenumber of 3077 cm^{-1} was only found for undecylenic acid and can be attributed to the stretching vibration of the terminal vinyl group of undecylenic acid. In contrast to that the $\text{CH}_3\text{-R}$ end group of oleic acid exhibits a peak at 3006 cm^{-1} for the symmetric stretching vibration. The bands at $\sim 2922 \text{cm}^{-1}$ and $\sim 2854 \text{cm}^{-1}$ occur for both samples and can be attributed to the asymmetric and symmetric stretching band of the CH_2 groups. The narrow and strong peak at 1711 cm^{-1} is also characteristic of both samples and belongs to the C=O stretching band of the carboxyl group of the fatty acid. This band will be used to prove the presence of the fatty acids on the montmorillonite surface. While the bands at 1465 cm^{-1} belong to the symmetric bending of the CH_2 groups, the doublet at ~ 1285 and $\sim 1242 \text{cm}^{-1}$ belongs to a combination of C-O stretch and C-H bending vibration. Undecylenic acid exhibits two bands at 991 and 909 cm^{-1} , which are not present for oleic acid. These bands can be attributed to the vibrations of the -C=CH_2 group of undecylenic acid.

Tab. 3.18: Identification and listing of the bands found for oleic acid and undecylenic acid in Fig. 3.37.

undecylenic acid [cm ⁻¹]	oleic acid [cm ⁻¹]	Assignment
3077		C=CH ₂ stretching
	3006	CH ₃ -R symmetric stretching band
2976	2954	CH ₃ -R asymmetric stretching band
2927	2926	CH ₂ asymmetric stretching band
2856	2855	CH ₂ symmetric stretching band
1711	1711	C=O stretching band
1465	1465	CH ₂ symmetric bending
1287	1285	C-O stretch and C-H bend
1242	1246	C-O stretch and C-H bend
	991	-C=CH ₂
	909	-C=CH ₂

3.5.2.2 Ammonium Salts (HDTAB, ODTAB)

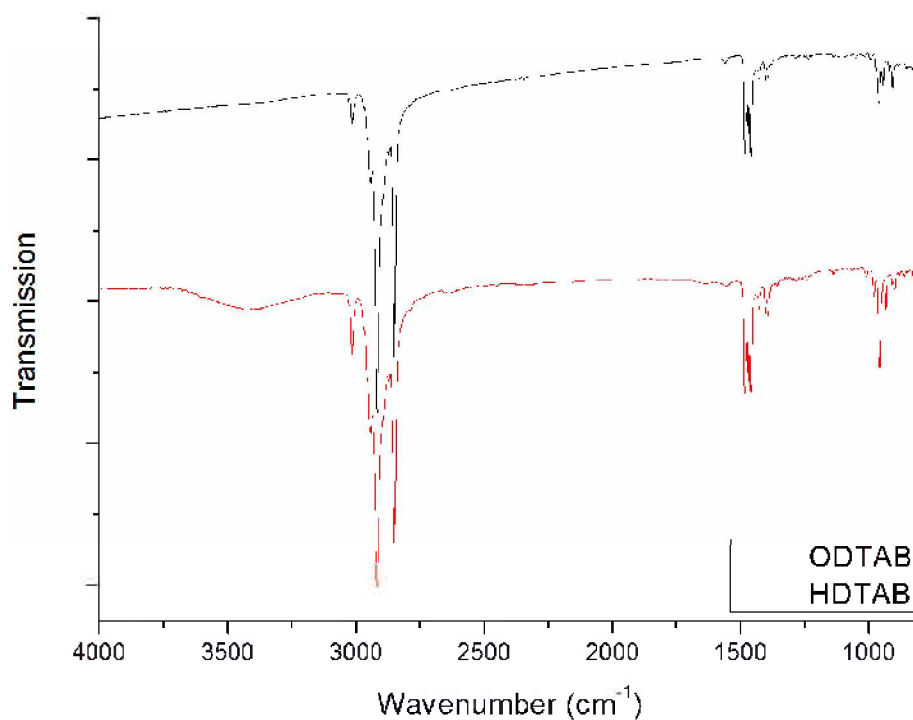


Fig. 3.38: Infrared spectra of HDTAB and ODTAB with assignment of the characteristic bands to the chemical groups

Due to the chemical similarities of the two surfactants a precise differentiation between the two ammonium salts is difficult, but also unnecessary because they are not applied on the same montmorillonite samples and therefore a joint band determination is possible. The band at $\sim 3018\text{ cm}^{-1}$, on the one hand, can be assigned to the symmetric stretch vibration of R-CH₃ and the band at 2953 cm^{-1} , on the other hand, can be assigned to the asymmetric stretching vibration. The two narrow and well resolved peaks at 2921 and 2851 cm^{-1} can be attributed to the asymmetric and symmetric stretching vibration of the CH₂ groups of the methylene tails of the ammonium molecules. The band at 1487 and 1407 cm^{-1} are the asymmetric and symmetric bending vibrations of the CH₃ groups attached to the Nitrogen atom. The signal that occurs because of the vibrations of the -N(CH₃)₃ group was used to verify the presence of the ammonium salts in the montmorillonite because those peaks are characteristic of the ammonium salt and are not present in the FT/IR spectra of the fatty acids. The doublet at 1472 and 1431 cm^{-1} can be assigned to the CH₂ group's bending vibrations. The bands below a wavenumber of 1000 cm^{-1} were not evaluated due to their minor importance for the characterization and due to the strong overlapping of the Si-O-Si vibrations in that region.

Tab. 3.19: Identification and listing of the bands found for HDTAB and ODTAB in Fig. 3.38.

HDTAB [cm ⁻¹]	ODTAB [cm ⁻¹]	Assignment
3016	3018	CH ₃ -R asymmetric stretching band
2943	2944	CH ₃ -R asymmetric stretching band
2917	2918	CH ₂ asymmetric stretching band
2871	2871	CH ₃ -R symmetric stretching band
2849	2849	CH ₂ symmetric stretching band
1487	1487	asymmetric bending CH ₃ of -N(CH ₃) ₃
1472	1472	bending CH ₂ doublet
1462	1463	bending CH ₃ doublet
1431	1431	asymmetric bending CH ₃ -R
1407	1407	symmetric bending CH ₃ of -N(CH ₃) ₃

3.5.3 Cloisite Samples

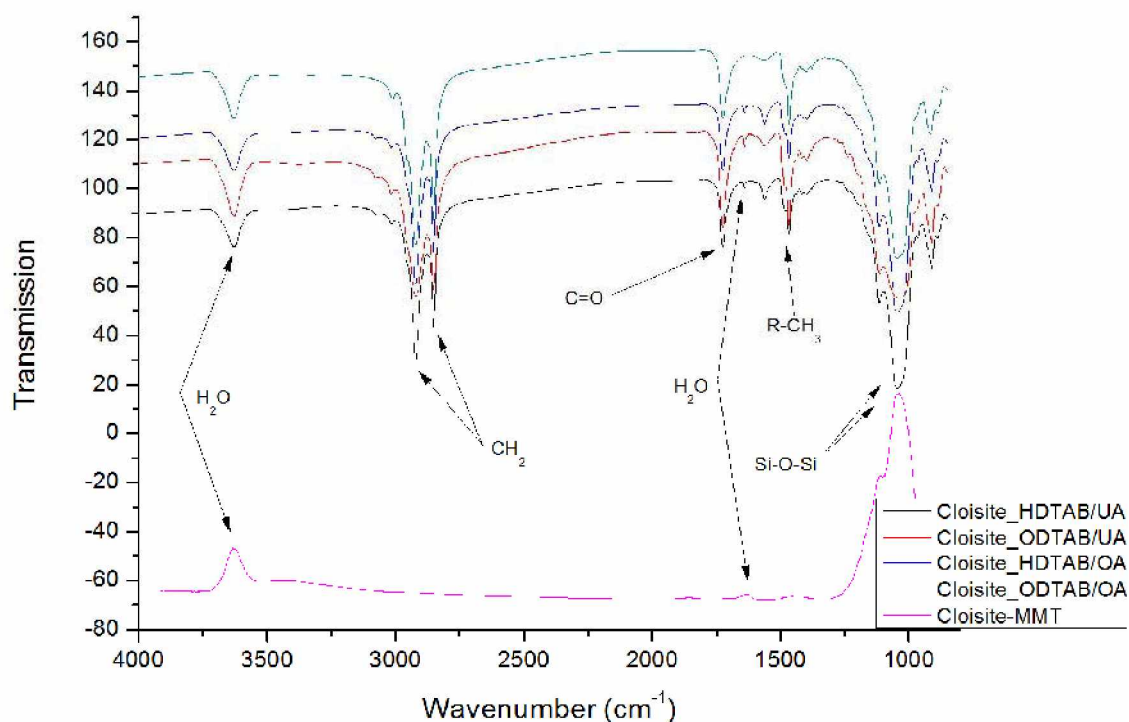


Fig. 3.39: Infrared spectra of unmodified Cloisite-MMT compared to Cloisite_HDTAB/UA, Cloisite_ODTAB/UA, Cloisite_HDTAB/OA and Cloisite_ODTAB/OA with assignment of the characteristic bands to the chemical groups

In Fig. 3.39 all FT/IR spectra obtained from modified Cloisite montmorillonite samples as well as a spectrum of the unmodified Cloisite montmorillonite are compared. All bands in the organo-modified clay, which were not exhibited by Cloisite montmorillonite, can be attributed to the surfactants. The presence of the fatty acids after the modification can be confirmed because of the presence of the C=O peak at 1711 cm^{-1} . The location of this peak has shifted from 1711 cm^{-1} for the pure fatty acids to 1726 cm^{-1} in the montmorillonite surface. The shoulder at 1485 cm^{-1} may be attributed to the $-\text{N}(\text{CH}_3)_3$ groups' presence. All bands related to CH₂ and CH₃ symmetric asymmetric bending and stretching vibrations also confirm the presence of both surfactants in the montmorillonite. One significant change could be observed in the intensity of the H₂O peak related to the hydrate water bound by the Sodium ions at a wavenumber of 1631 cm^{-1} . For three of four samples a decrease of the intensity of this peak was observed. For Cloisite_ODTAB/OA the peak was no more discernible.

Tab. 3.20: Identification and listing of the bands found for Cloisite-MMT, Cloisite_HDTAB/UA, Cloisite_ODTAB/UA, Cloisite_HDTAB/OA and Cloisite_ODTAB/OA (The detailed discussion of the bands found for these samples can be found in chapter 4.2)

Cloisite-MMT [cm ⁻¹]	Cloisite_HDTAB/UA [cm ⁻¹]	Cloisite_ODTAB/UA [cm ⁻¹]	Cloisite_HDTAB/OA [cm ⁻¹]	Cloisite_ODTAB/OA [cm ⁻¹]	Band assignment
3630	3628	3627	3629	3628	(H-O-H)
3434	3445	3377	3386	3386	(H-O-H) hydrogen bonded
	3017	3017	3014	3011	C-H stretching
	2955	2955	2955	2953	$\delta_{AS}(CH_3-R)$
	2921	2920	2921	2921	$\delta_{AS}(CH_2)$
	2850	2850	2852	2851	$\vartheta_S(CH_2)$
	1725	1725	1725	1725	C=O
1631	1641	1642	1634	/	ϑ_S (H-O-H) of Na bound Water
	1483	1484	1483	1483	$\vartheta_S(C-H)$ of $(CH_3)_4N^+$
	1468	1467	1467	1468	$\delta_{AS}(CH_2)$
	1378	1379	1378	1378	$\delta_S(CH_3-R)$
1114	1117	1117	1117	1117	Out of plane Si-O-Si stretching
1042	1045	1043	1046	1046	In plane Si-O-Si stretching
917	911	912	914	916	(OH) liberation of Al ₂ -OH
884	887	887	886	888	(OH) liberation of AlFe-OH
850	844	845	843	844	(OH) liberation of AlMg-OH

3.5.4 Milos Samples

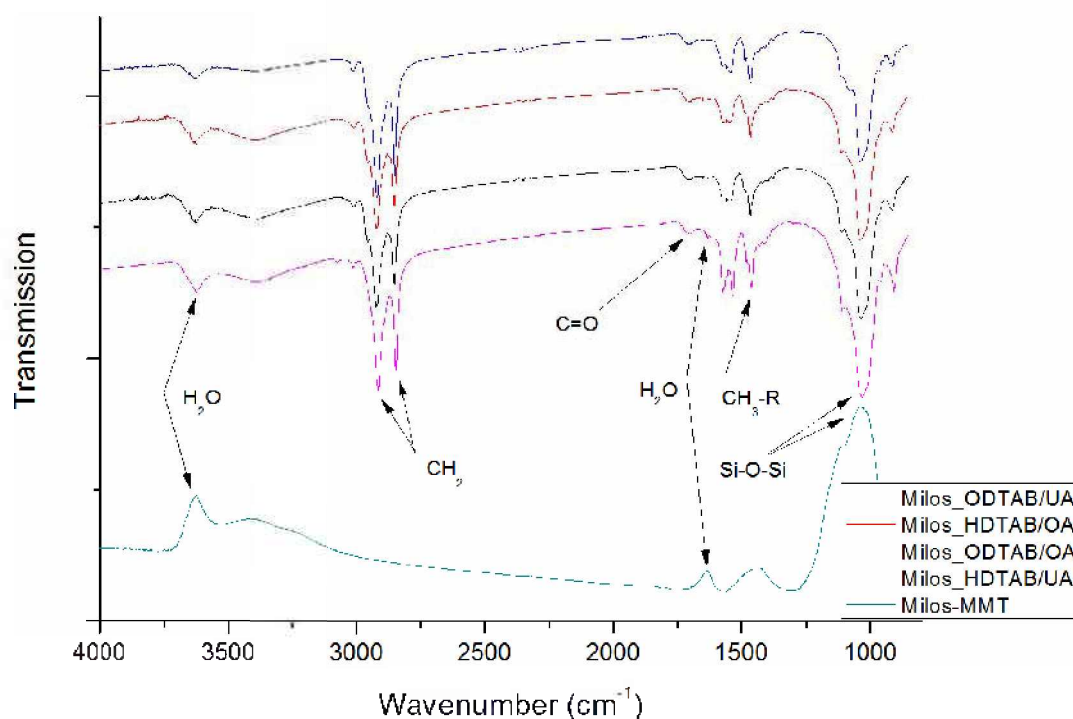


Fig. 3.40: Infrared spectra of Sodium-MMT compared to Milos_HDTAB/OA, Milos_ODTAB/OA, Milos_HDTAB/OA and Milos_ODTAB/OA with assignment of the characteristic bands to the chemical groups

In Fig. 3.39 all IR spectra obtained from modified Milos montmorillonite samples as well as a spectrum of the unmodified Milos montmorillonite are compared. All bands in the organo-modified clay that were not present in the Milos montmorillonite can be attributed to the surfactants. The presence of the fatty acids after the modification can be confirmed because of the evolution of the C=O peak at 1703 cm⁻¹. The location of this peak has shifted from 1711 cm⁻¹ for the pure fatty acids to 1703 cm⁻¹ in the montmorillonite surface. The shoulder at 1481 cm⁻¹ may be attributed to the presence of the -N(CH₃)₃ groups. All bands related to CH₂ and CH₃ symmetric asymmetric bending and stretching vibrations also confirm the presence of both surfactants in the montmorillonite. One significant change could be observed in the intensity of the H₂O peak related to the hydrate water bound by the Sodium ions at a wavenumber of 1635 cm⁻¹. For three of four samples a decrease of their intensity was observed. For Milos_ODTAB/OA the peak was no more discernible.

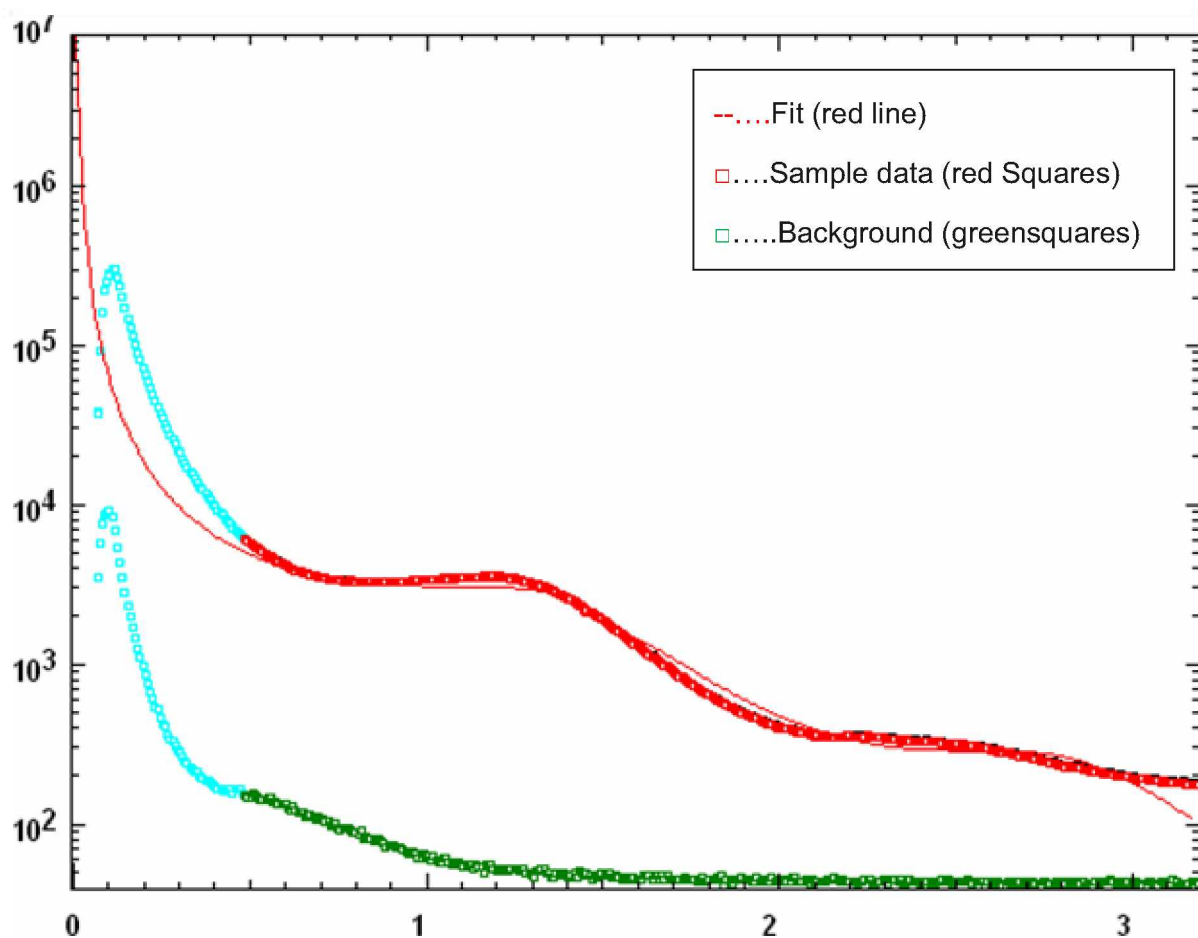
Tab. 3.21 Identification and listing of the bands found for Milos-MMT, Milos_HDTAB/UA, Milos_ODTAB/UA, Milos_HDTAB/OA and Milos_ODTAB/OA (The detailed discussion of the bands received for these samples can be found in chapter 4.2

Milos-MMT [cm ⁻¹]	Milos_HDTAB/UA [cm ⁻¹]	Milos_ODTAB/UA [cm ⁻¹]	Milos_HDTAB/OA [cm ⁻¹]	Milos_ODTAB/OA [cm ⁻¹]	Band assignment
3631	3619	3637	3630	3627	(H-O-H)
3415	3381	3397	3399	3400	(H-O-H) hydrogen bonded
	3019	3008	3008	3013	C-H stretching
	2955	2955	2955	2956	$\delta_{AS}(CH_3-R)$
	2913	2920	2920	2918	$\delta_{AS}(CH_2)$
	2845	2851	2852	2849	$\vartheta_S(CH_2)$
	1704	1702	1703	1700	C=O
1645	1636	1635	1634	/	ϑ_S (H-O-H) of Na bound Water
	1481	1482	1480	1486	$\vartheta_S(C-H)$ of $(CH_3)_4N^+$
	1461	1466	1467	1462	$\delta_{AS}(CH_2)$
1114	1117	1112	1112	1112	Out of plane Si-O-Si stretching
1038	1045	1038	1038	1038	In plane Si-O-Si stretching
907	911	915	916	912	(OH) liberation of Al ₂ -OH
885	881	885	887	890	(OH) liberation of AlFe-OH
854	850	855	852	856	(OH) liberation of AlMg-OH

3.6 SAXS-Evaluation

The small angle X-ray measurements were performed to determine the change in the spacing (a) of the montmorillonite. To verify a successful intercalation the interlayer distance of the unmodified Sodium-MMT was measured (MCL; Dr. Günther Maier) and compared to the values for the modified montmorillonite samples.

For the sample preparation the modified montmorillonite samples were dispersed in deionized water and afterwards sonicated for 5 minutes to ensure a good dispersion of the particles. Afterwards droplets of the dispersion were placed on a multisampleholder and measured. The measurements as well as the evaluation were conducted on the MCL (Materials Center Leoben).



3.41: The scattered intensity (I) is plotted against the scattering vector (q) for Cloisite_ODTAB/UA sample.

Sample	Solvent	Spacing a [nm]
Milos_HDTAB/UA	H ₂ O	4,67
Milos_ODTAB/UA	H ₂ O	4,6
Milos_HDTAB/OA	H ₂ O	5
Milos_ODTAB/OA	H ₂ O	5,93

For the Milos-MMT samples a general trend could be observed: The basal spacing for samples treated with oleic acid was significantly higher than for samples treated with undecylenic acid. The highest interlayer distance could be observed for a combination of oleic acid and ODTAB.

Sample	Solvent	Spacing a [nm]
Cloisite_HDTAB/UA	H ₂ O	4,47
Cloisite_ODTAB/UA	H ₂ O	4,39
Cloisite_HDTAB/OA	H ₂ O	4,82
Cloisite_ODTAB/OA	H ₂ O	5,68

The trend observed for the Milos-MMT samples can be verified by evaluation of the Cloisite-MMT data. The $d(001)$ spacing for Cloisite-MMT samples is also higher for oleic acid modified samples and the highest values were also found for a surfactant combination of oleic acid and ODTAB.

3.7 SEM-Evaluation

To gain insight in the morphology of the montmorillonite SEM measurements were conducted at the Materials Center Leoben in cooperation with Dr. Günther Maier. The SEM micrographs are only used to demonstrate the significant difference between the modified and the unmodified montmorillonite samples and can only be seen as a qualitative representation of the morphology of the samples in a small area.

The samples were prepared as follows: The montmorillonite was dispersed in deionized water and sonicated. The dispersion was drop-coated on a silicon monocrystal and dried in a compartment drier under vacuum.

3.7.1 Cloisite-MMT

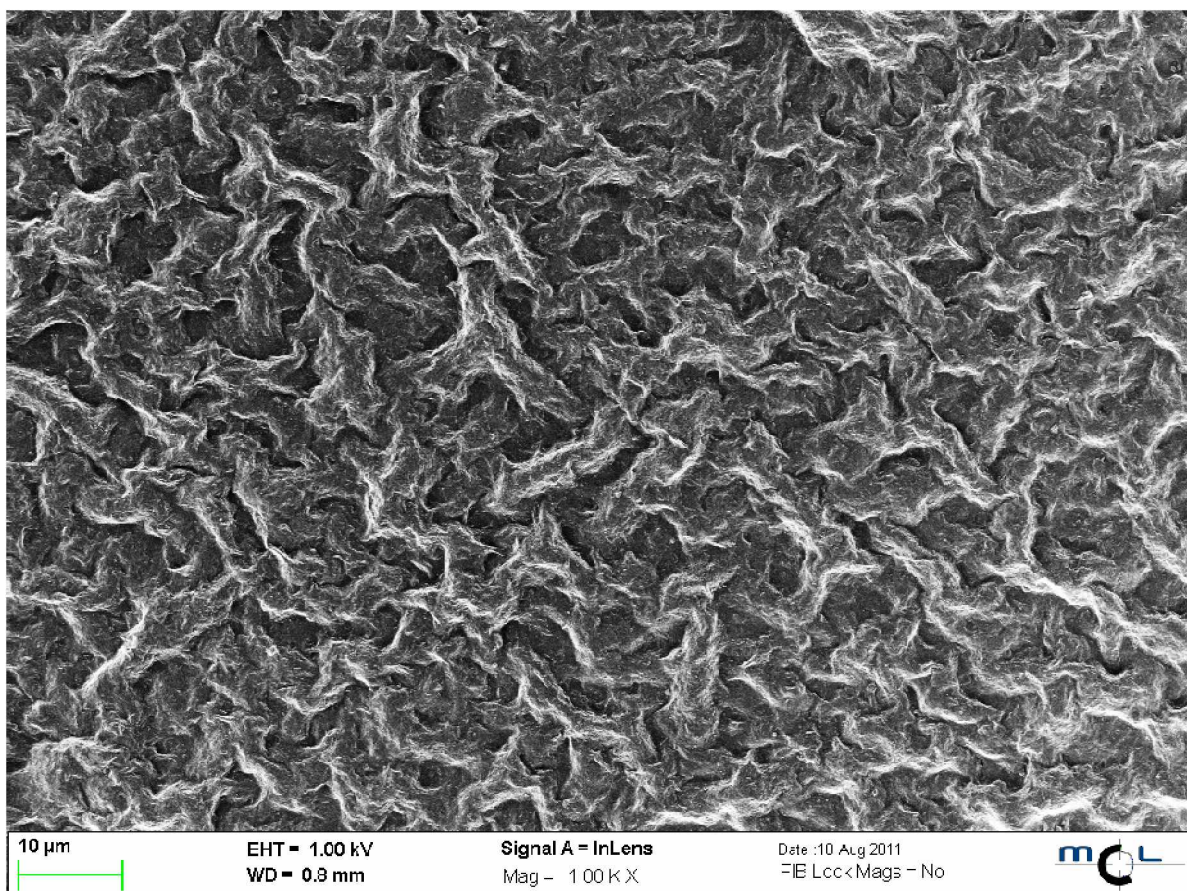


Fig. 3.42: Unmodified Cloisite-MMT at a magnification of 1k

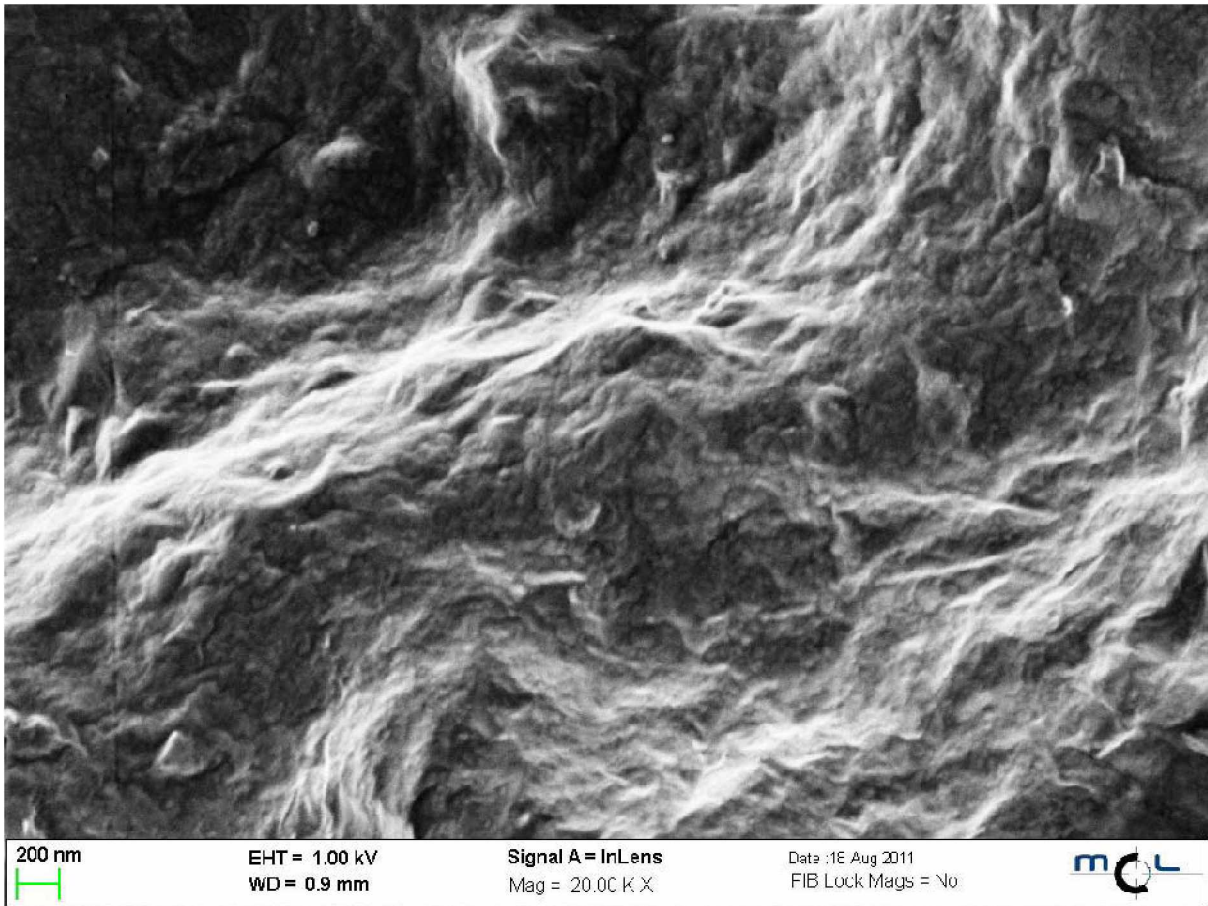


Fig. 3.43:Unmodified Cloisite-MMT at a magnification 20 k

Fig. 3.42 and Fig. 3.43 show the unmodified montmorillonite at a magnification of 1k and 20k. It is evident that the unmodified montmorillonite is present in a non exfoliated state. Especially Fig. 3.43 shows densely packed montmorillonite layers.

3.7.2 Cloisite_ODTAB/OA

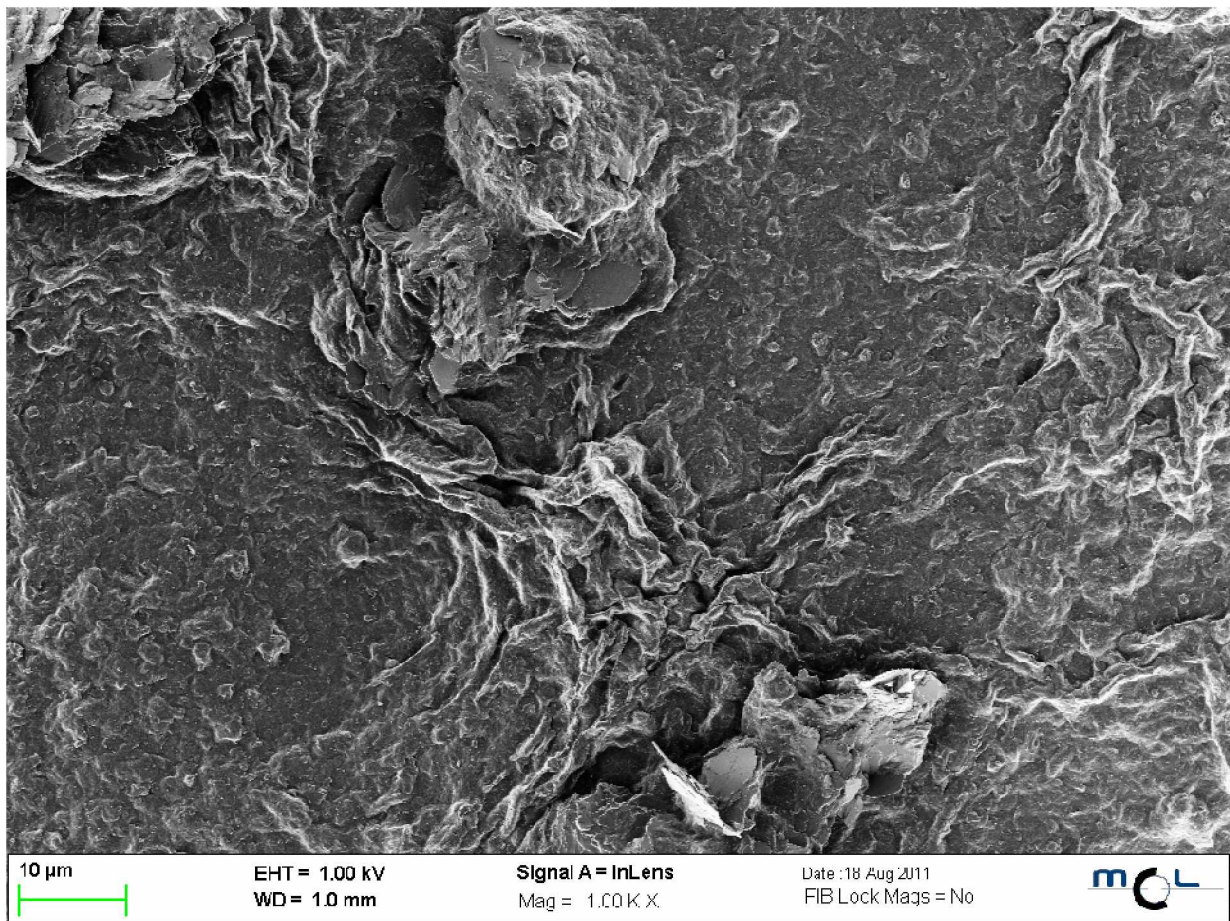


Fig. 3.44: Cloisite_ODTAB/OA at a magnification of 1 k

The comparison between the Cloisite-MMT and the Cloisite_ODTAB/OA samples under a magnification of 1k already shows a significant difference between the sample morphologies. In Fig. 3.44 many single platelets can be observed.

++

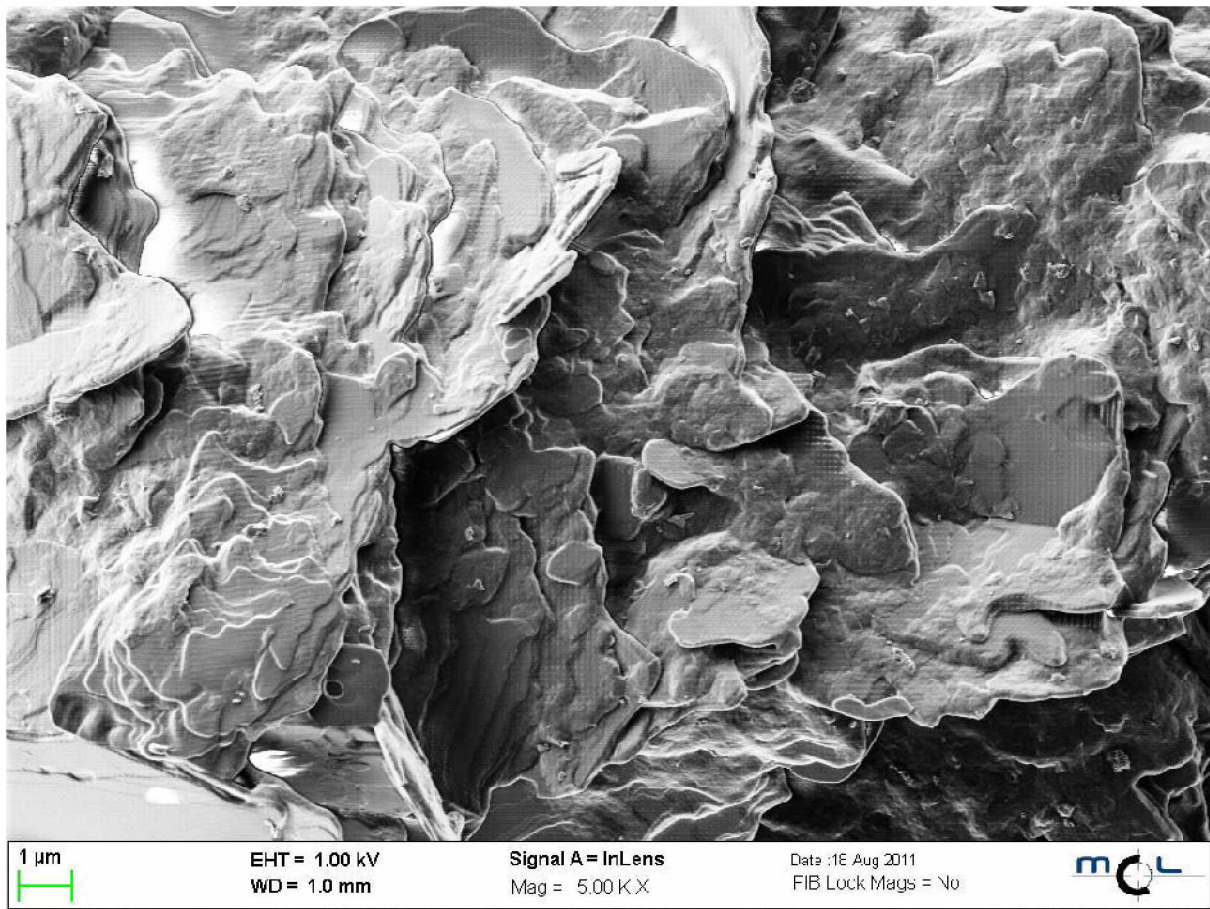


Fig. 3.45: Cloisite_ODTAB/OA at a magnification of 5 k

At a magnification of 5k more details of the structural change can be observed. Single platelets can be seen and an at least partially exfoliated state of the montmorillonite is evident.

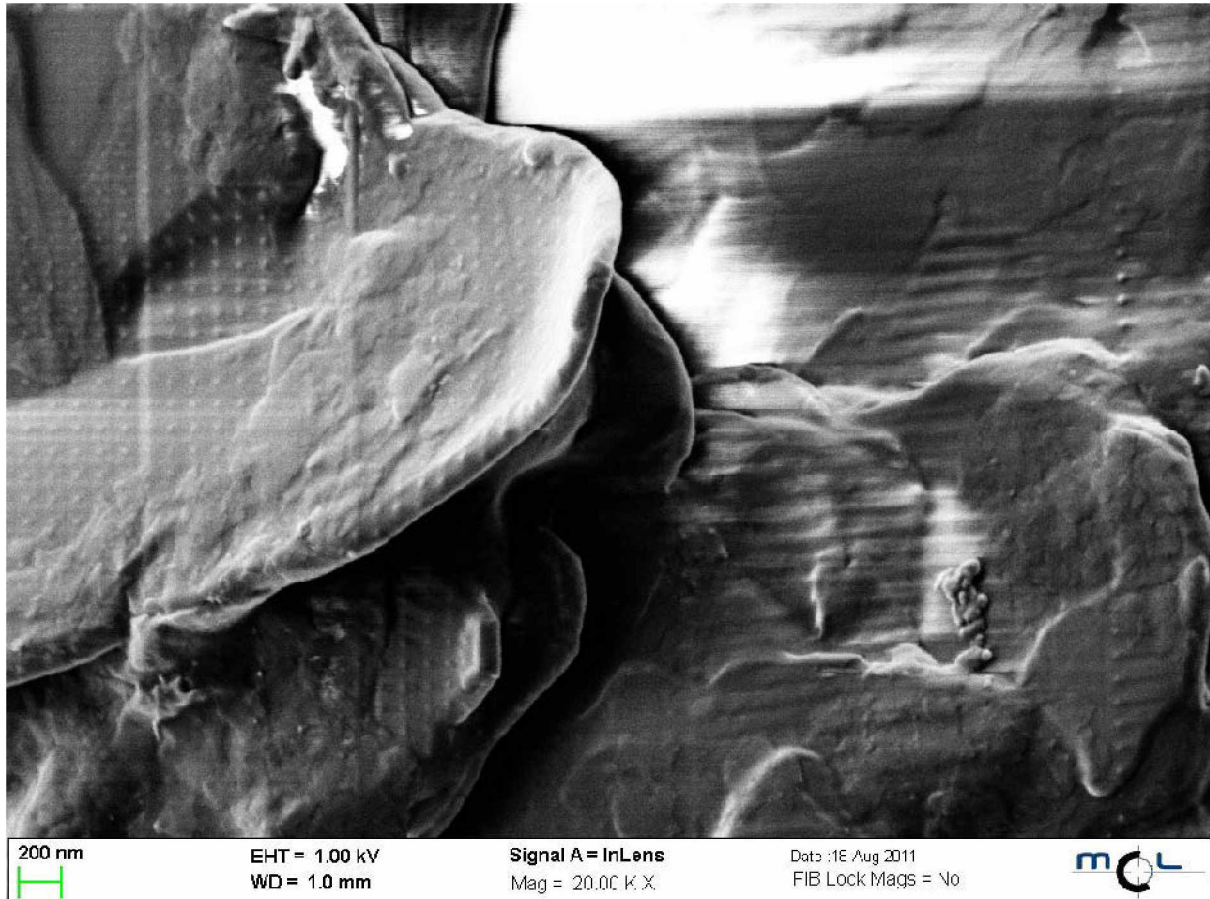


Fig. 3.46: Cloisite_ODTAB/OA under a magnification of 20 k

3.8 TEM-Evaluation

The TEM evaluation was used to verify the presence of exfoliated lamellas in a dispersed solution. (The TEM micrographs have been provided by DI. Hannelore Mattausch in cooperation with the University of Innsbruck.) The TEM measurements as well as the SEM measurements were only a qualitative indicator for the material morphology and only represent a small area of the samples. Nevertheless the insights gained by this method allow speculations regarding material properties like exfoliation and intercalation and are therefore used as a complementary method for the verification of the other characterization methods.

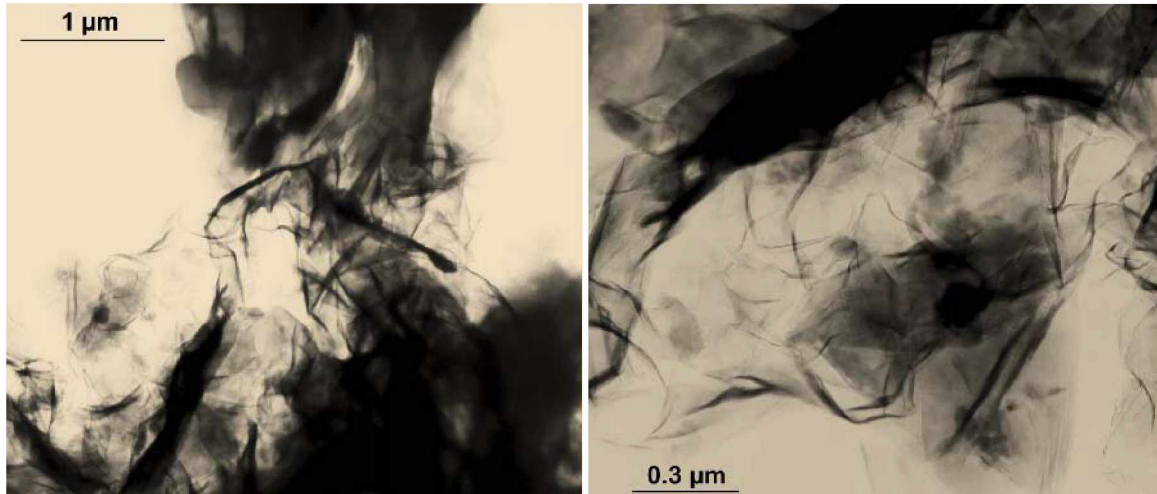


Fig. 3.47: Picture of a cluster of exfoliated lamella (Cloisite_ODTAB/OA)

For all the samples single exfoliated lamellas could be observed, which indicates that the samples were present in an at least partially exfoliated state. Fig. 3.47 shows a multitude of lamellas for a Cloisite_ODTAB/OA sample.

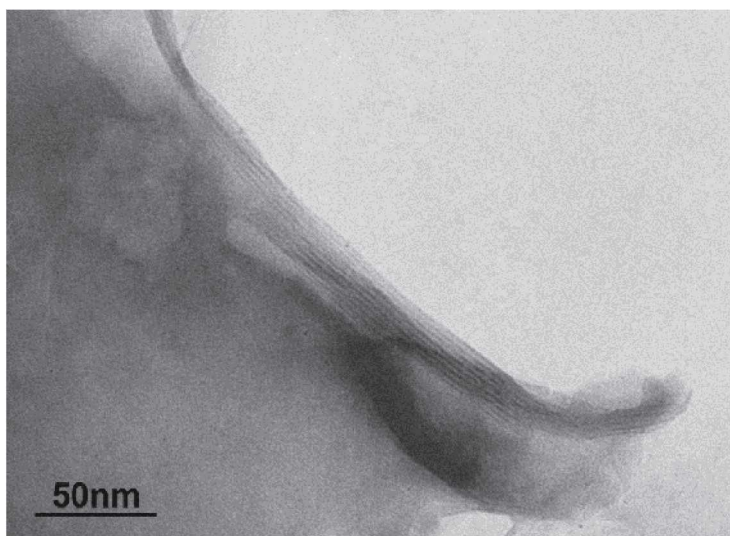


Fig. 3.48: Layer arrangement of Cloisite_ODTAB/OA

Fig. 3.48 shows a micrograph of an arrangement of montmorillonite layers for the sample Cloisite_ODTAB/OA. Such structures were also present in all samples, which leads to the conclusion that a possible exfoliation process has not been completed, as indicated by the presence of intact lamella structures.

4 Discussion

4.1 Results TGA

The thermogravimetric analysis of all organo-modified silicates showed, that the thermal degradation can be assigned to three distinct decomposition processes. From ambient temperature to 200°C the weight loss that had been observed for the unmodified montmorillonite was very weak or even not present. This weight loss was originally caused by the desorption and dehydration of water molecules. The absence of that weight loss indicates a successful ion exchange and hydrophobization of the clay material.

According to recent works with ammonium salt modified montmorillonite ([Vazquez, López et al. 2008](#)) the temperature range for the decomposition of the organic surfactants is located in a temperature range from 200 to 600°C. These findings could be verified in this work due to the fact that the unmodified montmorillonite does not show any thermally induced changes in that range, while the modified montmorillonite samples exhibited up to three distinct decomposition steps. Furthermore, the pure surfactants were tested and all showed a decomposition between 200 and 600°C, which also led to the conclusion that these decomposition processes were related to the organo-modification of the clays.

The first decomposition step can be roughly isolated in a temperature range from 200 to 350°C and can be either assigned to surfactant molecules which are adsorbed between pores and build up a “house-of-cards” structure such as proposed by ([He, Zhou et al. 2006](#)) or are adsorbed with their counterions ([Vazquez, López et al. 2008](#)). This is also the temperature range in which the maximum decomposition temperature of the fatty acids was found. Studies of montmorillonite modified with salts of fatty acids show similar decomposition peaks ([Sarier, Onder et al. 2010](#)). This weight loss is the most significant in the scanning range and amounts on the average to 49% of the total weight for Milos and 45% for Cloisite samples. This 4% difference will be discussed and clarified later.

The second weight loss that is related to the organo-modification can be confined to the temperature range of 350 to 460°C, but is not observable for all the samples. This weight loss is most probably the decomposition of surfactant molecules that are present in the interlayer space, but have not participated in the ion exchange process. The bonding of such molecules in the interlayer space has already been reported for ODTAB ([Xi, Martens et al. 2005](#)) and even for polycations ([Starodubtsev, Lavrentyeva et al. 2009](#)). According to ([Li and Jiang 2009](#)) the guest molecules are bound by Van der Waal forces on the intercalated surfactants which are in turn end tethered to the silica surface. These molecules can form bi- or multilayers on the existing monolayer of adsorbed surfactants ([Lee, Cho et al. 2005](#)). Thus the molecules which participated in the ion exchange built up an interface for more surfactant molecules that would have been limited by the theoretical CEC of the montmorillonite.

Not all of the tested samples exhibit this mass loss. The peak of the derivative weight loss is very weak for some samples or is overlapped by the broad first peak of the decomposition of the surface adsorbed surfactants. Especially for Milos samples this second peak is only visible for a combination of oleic acid and the ammonium salt.

In the temperature range between 450 to 630°C the thermally most stable molecules decompose. In various works this last organic degradation process is assigned to the decomposition of the intercalated surfactant ([Kozak and Domka 2004](#); [Cervantes-Uc, Cauch-Rodríguez et al. 2007](#)). This decomposition amounts to 7,5 wt.% for the modified montmorillonite samples. The absolute amount of molecules present in the interlayer space, however, is higher for Cloisite samples due to the fact that the most of the Milos samples have less “guest molecules” in the interlayer space. This could be an indicator for a difference of the molecule arrangement in the interlayer region or a difference in the interlayer distance.

The curve shapes of both the Milos and the Cloisite samples show a deviation for the combination of oleic acid and ODTAB as surfactants. The first decomposition peak related to the adsorbed molecules shifts to higher temperatures which can be attributed to a high loading rate of oleic acid. Those samples also exhibit a high amount of intercalated surfactant molecules which suggests a beneficial effect of the treatment with oleic acid on the intercalation of ODTAB and vice versa.

4.2 Results FT/IR

4.2.1 Band assignment

4.2.1.1 Vibrations of OH in montmorillonite

Water can be found in various forms in montmorillonite. It can be present as molecular water adsorbed on grain surfaces and pores or in the interlayer region. The character of this interlayer water is strongly dependent on the interlayer cations ([F. Cariatì 1981](#)). ([Janice L. Bishop 1994](#)) suggests that there are at least two different kinds of interlayer water present in montmorillonite. According to ([Farmer and Russell 1971](#)) tougher bound water molecules build up a hydration sphere around the cation. Timely removed molecules are located at the outer regions of this hydration sphere and can be evaporized by a drying or heating process at a temperature of ~105°C ([Janice L. Bishop 1994](#)). According to ([Russell 1964](#)) the bands, can be assigned as follows: Montmorillonite absorptions at ~918 cm⁻¹ can be assigned to the bending vibration of Al₂-OH. The bending vibration of AlFe-OH exhibits a peak at ~885cm⁻¹ ([Sposito 1983](#)) and AlMg-OH at ~840cm⁻¹. The broad signal at a wavenumber of 3415cm⁻¹ to 3450 cm⁻¹ can be assigned to the stretching vibration of H-O-H and are related to the timely removed weakly bound water. The stretching vibration of the firmly bound not hydrogen bonded water can be assigned to the ~3620cm⁻¹ peak and the bending vibration to the peak at a wavenumber of ~1635cm⁻¹. These modes can undergo slight shifts due to a

polarization of the water by the interlayer cations and cannot be seen as absolute values ([Janice L. Bishop 1994](#)).

4.2.1.2 FT/IR signals of the alkyl ammonium surfactants and fatty acids

The signals displayed by quaternary ammonium salts can be divided in the vibrations of the surfactant's head groups and $(\text{CH}_2)_n$ tail. The surfactant head group consisting of $-\text{N}(\text{CH}_3)$ exhibits an asymmetric stretching vibration of the CH_3 groups at 3040 cm^{-1} and a symmetric stretching vibration at 2985 cm^{-1} . The symmetric and asymmetric bending vibrations can be found at wavenumbers of $1480\text{-}1490$ and at 1405 cm^{-1} ([Scheuing David 1990](#)). For the methylene tails asymmetric stretching bands of the $\text{CH}_3\text{-R}$ groups can be located at 2956 cm^{-1} and at 2920 cm^{-1} for CH_2 . Symmetric stretching bands of $\text{CH}_3\text{-R}$ and CH_2 are usually observed at 2850 cm^{-1} . The bending vibrations of the CH_2 depend on the form of the subcell and can be found between 1468 and 1472 cm^{-1} . The symmetric and asymmetric bending vibration of the $\text{CH}_3\text{-R}$ can be assigned to 1490 , symmetric bending to 1480 and asymmetric bending can be assigned to 1380 cm^{-1} ([Li, Jiang et al. 2008](#)).

The characteristic stretching vibration of $\text{C}=\text{O}$ of the fatty acids carboxyl group can be found at 1710 cm^{-1} . The bands between 1241 and 1286 could be a combination band due to C-O stretch and O-H deformation vibration ([Socrates 2001](#)). The $\text{C}=\text{C}$ bonds of the unsaturated fatty acids also used exhibit characteristic bands. For terminal double bonds such as the vinyl group of undecylenic acid characteristic bands occur in the range of $995\text{-}980\text{ cm}^{-1}$ and $915\text{-}905\text{ cm}^{-1}$ as well as between $1645\text{-}1640\text{ cm}^{-1}$ and also a single band at $3095\text{-}3075\text{ cm}^{-1}$ ([Socrates 2001](#)). Commonly, carboxylic acids absorb in the region between 2700 to 2500 cm^{-1} as a result of the presence of hydrogen bonding. Hence, the occurring band in this region may be attributed to $\text{OH}\cdots\text{OH}$ interactions.

4.3 Conclusion

The results of the characterization lead to various conclusions regarding the modification process. In general, thermogravimetric measurements prove that a high weight percentage of the modified montmorillonite samples is related to organic substances and can therefore be assigned to the surfactants. These results are proven by infrared spectroscopy. The presence of various CH_2 related bands was observed and the characteristic bands for both the ammonium salts and the fatty acids could be ascertained. Although peaks like the characteristic $\text{C}=\text{O}$ vibration of the carboxylic acids or the $\text{R-N}(\text{CH}_3)_3$ related band of the ammonium salt heads prove the presence of the surfactants in the sample, but this does not clarify their exact location. To differentiate between adsorbed and intercalated molecules the decomposition maxima of the surfactants were evaluated. The tests showed that the loosely adsorbed molecules in the pores decompose at lower temperatures than their intercalated counterparts or the guest molecules also present in the interlayer space. Due to

these findings a schematic model of the molecules' arrangement in the interlayer space can be formulated.

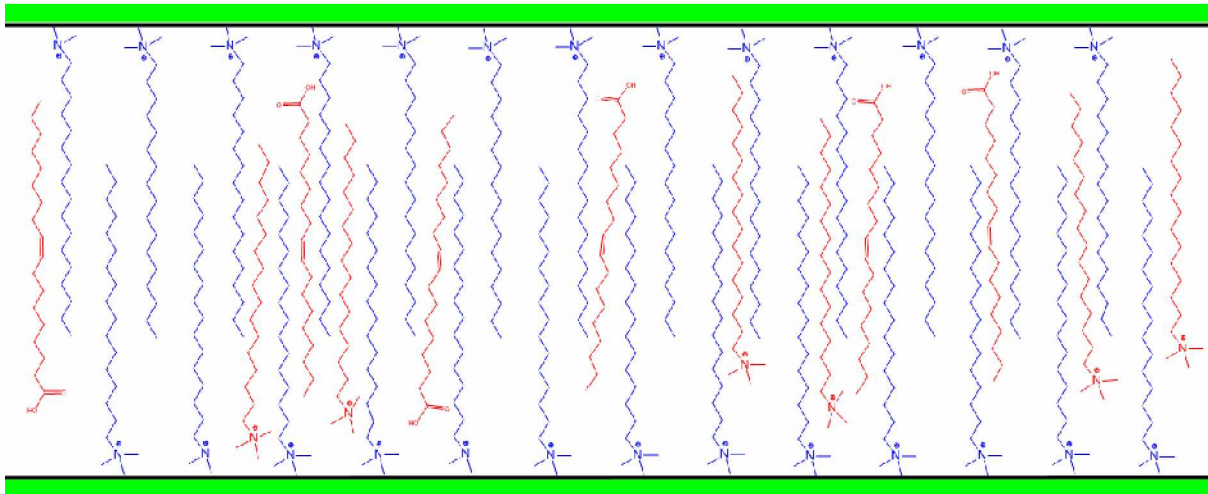


Fig. 4.1: Schematic model of a possible arrangement of the molecules in the interlayer space. Blue: Intercalated molecules; Red: "Guest molecules"

Fig. 4.1 shows a schematic model of the molecules' arrangement in the interlayer space. Due to the exchange of the sodium ions with the ammonium salt ions, a monolayer is built on the interlayer surfaces of the montmorillonite. In addition to this monolayer, TGA measurements suggest that there are two distinct groups of molecules present in the interlayer space. First the intercalated monolayer of ammonium salts and second ammonium salt molecules and fatty acid molecules which are bound by Van der Waal's interactions on the monolayer. This model is supported by the fact that two monolayers consisting of C18-chains with a length of 2618 pm and two $-N(CH_3)_3$ head groups, each with a length of 450 pm, would result in a theoretical spacing of 3518 pm. On the basis of the fact that the lowest spacing found by SAXS measurements is 4394 pm the schematic molecule arrangement in Fig. 4.1 could be a possible explanation. Similar results were also discovered by (Kozak and Domka 2004) for montmorillonite, and (Li and Jiang 2009) for rectorite. A successful intercalation can also be derived by a general evaluation of the SAXS data. The basal spacing of all the samples is significantly higher than the average spacing found for Sodium-MMT (Sarier, Onder et al. 2010)(Kozak and Domka 2004;He, Ma et al. 2010), especially for a combination of the surfactants ODTAB and oleic acid. For these surfactants the highest interlayer spacing and the highest percentage of intercalated molecules were found. Additionally, those findings were supported by the SEM measurements. Fig. 4.2 shows two pictures of montmorillonite samples at a magnification of 20k and the decisive difference that can be observed in the morphology of the samples.

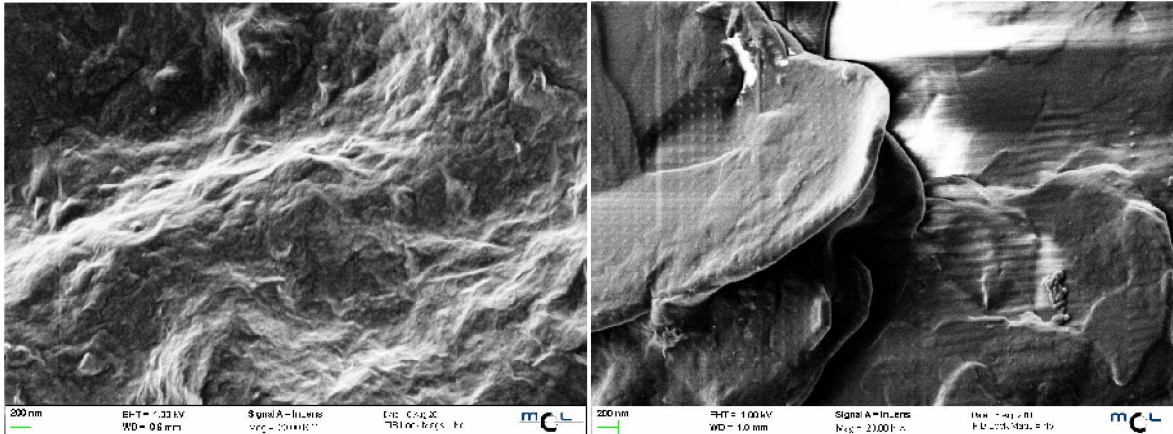


Fig. 4.2: Comparison of Cloisite-MMT (left) and Cloisite_ODTAB/OA (right) for a magnification of 20k

For all of the montmorillonite samples a platelet structure was observed. These SEM pictures suggest an intercalation and at least a partial exfoliation of the clay material, which has already been indicated by the SAXS and TGA measurements. In accordance to the other characterization methods the most significant difference in the morphology was observed for Cloisite_ODTAB/OA. The indication of an at least partial exfoliation (as derived from the SEM micrographs) could be substantiated by the results of the TEM pictures. For these measurements particle agglomerates up to a scale of 1000nm were observed but also a multitude of exfoliated particles. Fig. 4.3 shows two exfoliated lamellas.

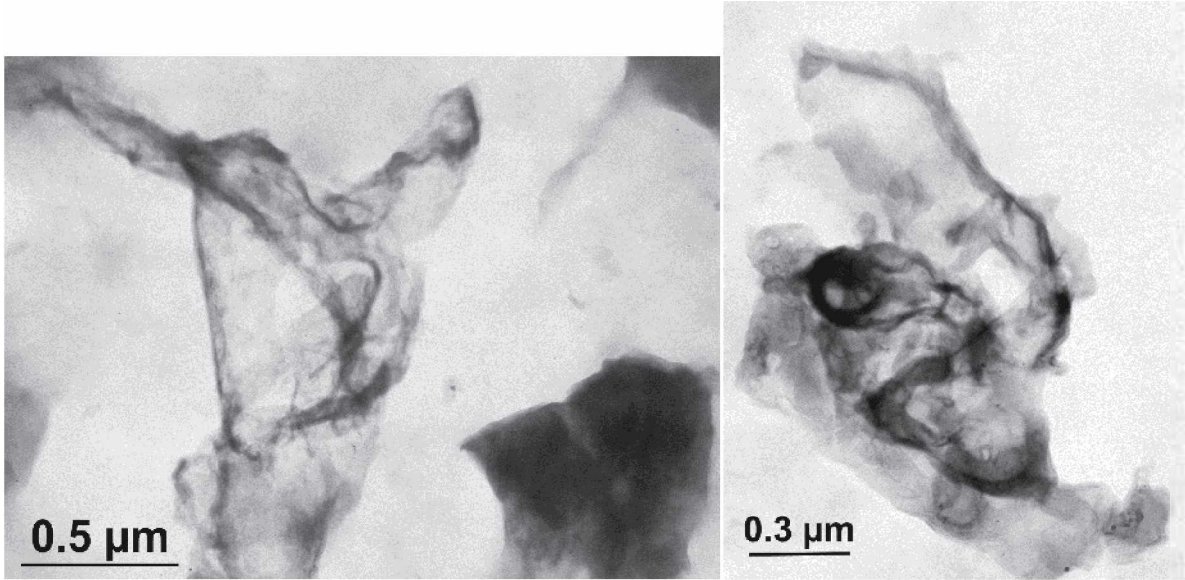


Fig. 4.3: Exfoliated montmorillonite lamellas, found for Milos_ODTAB/OA

4.4 Outline

The objective to obtain an intercalated and hydrophobized clay material can be, regarding the various measurement results, considered as successful. This objective has been achieved by applying a novel two-step modification process. The clay surface was coated with a fatty acid and the interlayer ions were exchanged with quaternary ammonium salts.

The material properties obtained by this method could be beneficial for further use of the clay as a filler material in polymer processing. In particular the change of the hydrophilic material behavior as well as the increase of the interlayer spacing could be important for the filler dispersion in a polymeric matrix.

5 Figures

- (1) http://www.univie.ac.at/Lewifak/kanon/Basics/Methoden_Spektroskopie.html, am 23. Juli 2009
- (2) http://books.google.at/books?id=X8YVhZ7LZ6cC&printsec=frontcover&dq=ir+spectroscopy&hl=de&ei=UGuUTb3AMNPb4Aau0ODPDA&sa=X&oi=book_result&ct=result&resnum=1&ved=0CEAQ6AEwAA#v=onepage&q=ir%20spectroscopy&f=false
- (3) <http://physics.schooltool.nl/irspectroscopy/method.php>
- (4) <http://www.google.at/imgres?q=SAXS&um=1&hl=de&client=opera&rls=de&channel=suggest&tbnm=isch&tbnid=48zo9ZFMUCjLXM:&imgrefurl=http://www.ipfdd.de/X-ray-Lab.197.0.html&docid=v5k3PdWtwk2eRM&w=500&h=300&ei=ukJFTpXBCMz1sGbQrb2zCQ&zoom=1&iact=hc&vpx=393&vpy=273&dur=982&hovh=174&hovw=290&tx=187&ty=86&page=1&tbnh=123&tbnw=205&start=0&ndsp=35&ved=1t:429,r:8,s:0&biw=1680&bih=967>
- (5) http://www.lkt.uni-erlangen.de/publikationen/buecher/Leseprobe_ptak.pdf
- (6) <http://www.mokkka.hu/drupal/en/node/8881>
- (7) Kern, W.: "Photochemie an Polymeren", Vorlesungsskripten, Lehrstuhl für Synthese von Spezial- und Funktionspolymeren, Montanuniversität Leoben, Österreich, 2008
- (8) http://www.netzsch-thermal-analysis.com/data/produkte/6_technische_daten_1.jpg
- (9) <http://upload.wikimedia.org/wikipedia/commons/0/0c/Montmorillonite-en.svg>
- (10) http://www.tno.nl/content.cfm?context=kennis&content=IP_patent&laag1=27&item_id=27&Taal=2
- (11) <http://www.californiaearthminerals.com/science/clay-minerals-research.php>
- (12) <http://www.chemistry.nmsu.edu>"Perkin-Elmer Spectrum One FTIR Spectrometer"

6 Literatur

- Avalos, F., J. C. Ortiz, et al. (2009). "Phosphonium salt intercalated montmorillonites." Applied Clay Science**43**(1): 27-32.
- Bober, P., J. Stejskal, et al. (2010). "Conducting polyaniline-montmorillonite composites." Synthetic Metals**160**(23-24): 2596-2604.
- Cervantes-Uc, J. M., J. V. Cauich-Rodríguez, et al. (2007). "Thermal degradation of commercially available organoclays studied by TGA-FTIR." Thermochimica Acta**457**(1-2): 92-102.
- Choi, Y. S. and I. J. Chung (2004). "An explanation of silicate exfoliation in polyacrylonitrile/silicate nanocomposites prepared by in situ polymerization using an initiator adsorbed on silicate." Polymer**45**(11): 3827-3834.
- Chu, C. C., M. L. Chiang, et al. (2005). "Exfoliation of montmorillonite clay by Mannich polyamines with multiple quaternary salts." Macromolecules**38**(15): 6240-6243.
- Domínguez, E. A., Mas fernanda Cravero, G.R. (2003). 2001. A Clay Odyssey, ELSEVIER SCIENCE B.V.
- F. Cariati, L. E., G. Micera, P. Piu, C. Gessa (1981). "Water Molecules and Hydroxyl Groups in Montmorillonites as Studied by Near Infrared Spectroscopy." Clays and Clay Minerals**29**(2): 157-159.
- Farmer, V. C. and J. D. Russell (1971). "Interlayer complexes in layer silicates. The structure of water in lamellar ionic solutions." Transactions of the Faraday Society**67**: 2737-2749.
- Fox, J. B., P. V. Ambuken, et al. (2010). "Organo-montmorillonite barrier layers formed by combustion: Nanostructure and permeability." Applied Clay Science**49**(3): 213-223.
- Gallego, R., D. García-López, et al. (2010). "The effect of montmorillonite and compatibilizer quantities on stiffness and toughness of polyamide nanoblends." Polymer International**59**(4): 472-478.
- Grim, R. E., Güven, N., (1978). Developements in Sedimentology 24: Bentonites: Geology, Mineralogy, Properties and Uses, Elsevier Scientific Publishing Company.
- Hatakeyama, T. Q., F.X. (1994). THERMAL ANALYSIS Fundamentals and Applications to Polymer Science, John Wiley & Sons, LTd.
- He, H., Y. Ma, et al. (2010). "Organoclays prepared from montmorillonites with different cation exchange capacity and surfactant configuration." Applied Clay Science**48**(1-2): 67-72.
- He, H. P., Q. Zhou, et al. (2006). "Microstructure of HDTMA(+)-modified montmorillonite and its influence on sorption characteristics." Clays and Clay Minerals**54**(6): 689-696.
- Hocine, O., M. Boufatit, et al. (2004). "Use of montmorillonite clays as adsorbents of hazardous pollutants." Desalination**167**: 141-145.
- Huang, G., Y. Li, et al. (2011). "A novel intumescent flame retardant-functionalized montmorillonite: Preparation, characterization, and flammability properties." Applied Clay Science**51**(3): 360-365.
- Janice L. Bishop, C. M. P. a. J. O. E. (1994). "Infrared Spectroscopic Analyses on the Nature of Water in Montmorillonite." Clays and Clay Minerals**42**(6): 702-716.

- Jiang, L., J. Zhang, et al. (2007). "Comparison of polylactide/nano-sized calcium carbonate and polylactide/montmorillonite composites: Reinforcing effects and toughening mechanisms." Polymer**48**(26): 7632-7644.
- Khalil, H. S. A. and A. A. Abdelhakim (2002). "Adsorption studies of fatty acids on montmorillonite-based filler clay." Journal of Applied Polymer Science**86**(10): 2574-2580.
- Kickelbick, G. (2007). Hybrid Materials: Synthesis, Characterization and Applications, WILEY-VCH Verlag GmbH & Co. KGaA, Weinheim.
- Koenig, J. L. (1999). Spectroscopy of Polymers, American Chemical Society.
- Koo, J. H. (2006). Polymer Nanocomposites: Processing, Characterization and Applications, The McGraw-Hill Companies, Inc.: 10-11.
- Kozak, M. and L. Domka (2004). "Adsorption of the quaternary ammonium salts on montmorillonite." Journal of Physics and Chemistry of Solids**65**(2-3): 441-445.
- Lee, S. Y., W. J. Cho, et al. (2005). "Microstructural changes of reference montmorillonites by cationic surfactants." Applied Clay Science**30**(3-4): 174-180.
- Li, Z. and W.-T. Jiang (2009). "A thermogravimetric investigation of alkylammonium intercalation into rectorite." Thermochimica Acta**483**(1-2): 58-65.
- Li, Z., W.-T. Jiang, et al. (2008). "An FTIR investigation of hexadecyltrimethylammonium intercalation into rectorite." Spectrochimica Acta Part A: Molecular and Biomolecular Spectroscopy**71**(4): 1525-1534.
- Lin, F.-H., C.-H. Chen, et al. (2006). "Modified montmorillonite as vector for gene delivery." Biomaterials**27**(17): 3333-3338.
- Ma, J., J. Xu, et al. (2003). "A new approach to polymer/montmorillonite nanocomposites." Polymer**44**(16): 4619-4624.
- Martin, Z., I. Jimenez, et al. (2009). "Spectromicroscopy Study of Intercalation and Exfoliation in Polypropylene/Montmorillonite Nanocomposites." Journal of Physical Chemistry B**113**(32): 11160-11165.
- Moreno, M., M. A. S. Ana, et al. (2010). "Poly(acrylonitrile)-montmorillonite nanocomposites: Effects of the intercalation of the filler on the conductivity of composite polymer electrolytes." Electrochimica Acta**55**(4): 1323-1327.
- Paus, J. H. (2007). PHYSIK in Experiment und Beispielen, Carl Hanser Verlag GmbH & Co. KG.
- Petzold, A. (1991). Physikalische Chemie der Silicate, Deutscher Verlag für Grundstoffindustrie GmbH.
- Russell, J. D. F., V.C. (1964). "Infra-red spectroscopic study of the dehydration of montmorillonite and saponite." Clay minerals bulletin**5**(32): 443-464.
- Saptari, V. (2004). Fourier-Transform Spectroscopy Instrumentation Engineering, The Society of Photo-Optical Instrumentation Engineers.
- Sarier, N., E. Onder, et al. (2010). "The modification of Na-montmorillonite by salts of fatty acids: An easy intercalation process." Colloids and Surfaces A: Physicochemical and Engineering Aspects**371**(1-3): 40-49.
- Scheuing David, R. (1990). Fourier Transform Infrared Spectroscopy in Colloid and Interface Science. Fourier Transform Infrared Spectroscopy in Colloid and Interface Science, American Chemical Society. **447**: 1-21.
- Singh, A. K. (2005). Advanced X-ray Techniques in Research and Industry, IOS Press.

- Socrates, G. (2001). Infrared and Raman characteristic group frequencies: tables and charts, Hohn Wiley & Sons Inc.
- Sposito, G., Prost, R., Gaultier, J.-P. (1983). "Infrared Spectroscopic Study of Adsorbed Water on Reduced-Charge Na/Li-Montmorillonites." Clays and Clay Minerals**31**(1).
- Starodubtsev, S. G., E. K. Lavrentyeva, et al. (2009). "Montmorillonite-polycation multilayers incorporated in polyacrylamide." Applied Clay Science**46**(1): 88-94.
- Vazquez, A., M. López, et al. (2008). "Modification of montmorillonite with cationic surfactants. Thermal and chemical analysis including CEC determination." Applied Clay Science**41**(1-2): 24-36.
- Xi, Y., W. Martens, et al. (2005). "Thermogravimetric analysis of organoclays intercalated with the surfactant octadecyltrimethylammonium bromide." Journal of Thermal Analysis and Calorimetry**81**(1): 91-97.